

GEMS & GEMOLOGY

SUMMER 2014

VOLUME L

THE QUARTERLY JOURNAL OF THE GEMOLOGICAL INSTITUTE OF AMERICA

The Future of Botswana's Diamond Industry

Determining Emerald Origin from Multi-phase Inclusions

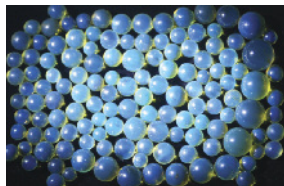
Cause of Color in Rare Blue Amber



pg. 109



pg. 115



pg. 135



pg. 167

EDITORIAL

95 Challenges and Opportunities

Duncan Pay

FEATURE ARTICLES

96 Botswana's Scintillating Moment

Robert Weldon and Russell Shor

Examines the history of diamond production in Botswana and the long-term outlook for beneficiation through value-added industries.

114 Three-Phase Inclusions in Emerald and Their Impact on Origin Determination

Sudarat Saeseaw, Vincent Pardieu, and Supharat Sangsawong

Discusses the role of three-phase inclusions in emerald, in combination with spectroscopy and trace-element analysis, in determining geographic origin.

NOTES AND NEW TECHNIQUES

134 Color Phenomena of Blue Amber

Yan Liu, Guanghai Shi, and Shen Wang

Investigates the presence of fluorescence, rather than iridescence, as the cause of color in blue amber from the Dominican Republic and Indonesia.

142 Experimental Studies on the Heat Treatment of Baltic Amber

Yamei Wang, Mingxing Yang, and Yiping Yang

Demonstrates the procedures for heating amber to achieve golden, red, "sun spark," and "beeswax" effects, and provides identification criteria for these products.

80TH ANNIVERSARY SPECIAL

170 Celebrating G&G's 80th Year and the Artistry of Harold and Erica Van Pelt

REGULAR FEATURES

141 Thank You, Donors

151 Lab Notes

Chameleon diamond with nickel absorption band • Long-term durability of CVD synthetic film on natural diamond • Star opal • Shell pearl as pearl imitation • Yellow CVD synthetic diamond • Flux-grown synthetic ruby with hydrothermal synthetic seed crystal • Rare faceted wurtzite • Tenebrescent zircon

158 Gem News International

Jadeite bangle with the appearance of polymer treatment • Prasiolite with inclusion influenced by Brazil-law twinning • Record-size natural moissanite crystals discovered in Israel • Unusual optical effect in blue sapphire • Assemblage of synthetic ruby in calcite matrix • Composite coral veneer glued to artificial matrix • Dyed bone as a red coral imitation • Bumble Bee "jasper" from Indonesia • Pyrex bracelets • Shattuckite from the DRC • Shanghai jewelry show • Museum exhibits at GIA New York

Editorial Staff

Editor-in-Chief

Duncan Pay
dpay@gia.edu

Managing Editor

Justin Hunter
justin.hunter@gia.edu

Editor

Stuart D. Overlin
soverlin@gia.edu

Technical Editors

Tao Z. Hsu
tao.hsu@gia.edu

Jennifer Stone-Sundberg

Associate Editors

Jennifer-Lynn Archuleta
jennifer.archuleta@gia.edu

Paula Bonilla
paula.bonilla@gia.edu

Editorial Assistants

Brooke Goedert
Nathan Renfro

Editors, Lab Notes

Thomas M. Moses
Shane F. McClure

Contributing Editors

James E. Shigley
Andy Lucas
Donna Beaton

Editor-in-Chief Emeritus

Alice S. Keller

Customer Service

Martha Erickson
(760) 603-4502
gandg@gia.edu

Production Staff

Creative Director

Faizah Bhatti

Image Specialist

Matt Hatch

Illustrators

Christopher Cruz
Larry Lavitt

Photographer

Robert Weldon

Production Supervisor

Richard Canedo

Video Production

Pedro Padua
Nancy Powers

Editorial Review Board

Ahmadjan Abduriyim
Tokyo, Japan

Shigeru Akamatsu
Tokyo, Japan

Edward W. Boehm
Chattanooga, Tennessee

James E. Butler
Washington, DC

Alan T. Collins
London, UK

John L. Emmett
Brush Prairie, Washington

Emmanuel Fritsch
Nantes, France

Eloïse Gaillou
Los Angeles, California

Jaroslav Hyršl
Prague, Czech Republic

A.J.A. (Bram) Janse
Perth, Australia

E. Alan Jobbins
Caterham, UK

Mary L. Johnson
San Diego, California

Anthony R. Kampf
Los Angeles, California

Robert E. Kane
Helena, Montana

Stefanos Karampelas
Lucerne, Switzerland

Lore Kiefert
Lucerne, Switzerland

Ren Lu
Wuhan, China

Thomas M. Moses
New York, New York

Mark Newton
Coventry, UK

Nathan Renfro
Carlsbad, California

Benjamin Rondeau
Nantes, France

George R. Rossman
Pasadena, California

Kenneth Scarratt
Bangkok, Thailand

Andy Shen
Wuhan, China

Guanghai Shi
Beijing, China

James E. Shigley
Carlsbad, California

Elisabeth Strack
Hamburg, Germany

Christopher P. Smith
New York, New York

Wuyi Wang
New York, New York

Christopher M. Welbourn
Reading, UK

GEMS & GEMOLOGY®

gia.edu/gems-gemology

Subscriptions

Copies of the current issue may be purchased for \$29.95 plus shipping. Subscriptions are \$79.99 for one year (4 issues) in the U.S. and \$99.99 elsewhere. Canadian subscribers should add GST. Discounts are available for group subscriptions, GIA alumni, and current GIA students. For institutional rates, contact Customer Service.

To purchase print subscriptions, visit store.gia.edu or contact Customer Service.

Database Coverage

Gems & Gemology is abstracted in Thomson Reuters products (Current Contents: Physical, Chemical & Earth Sciences and Science Citation Index—Expanded, including the Web of Knowledge) and other databases. For a complete list of sources abstracting *G&G*, go to gia.edu/gems-gemology.

Manuscript Submissions

Gems & Gemology welcomes the submission of articles on all aspects of the field. Please see the Guidelines for Authors at gia.edu/gandg or contact the Managing Editor. Letters on articles published in *Gems & Gemology* are also welcome.

Copyright and Reprint Permission

Abstracting is permitted with credit to the source. Libraries are permitted to photocopy beyond the limits of U.S. copyright law for private use of patrons. Instructors are permitted to photocopy isolated articles for noncommercial classroom use without fee. Copying of the photographs by any means other than traditional photocopying techniques (Xerox, etc.) is prohibited without the express permission of the photographer (where listed) or author of the article in which the photo appears (where no photographer is listed). For other copying, reprint, or republication permission, please contact the Managing Editor.

Gems & Gemology is published quarterly by the Gemological Institute of America, a nonprofit educational organization for the gem and jewelry industry.

Postmaster: Return undeliverable copies of *Gems & Gemology* to GIA, The Robert Mouawad Campus, 5345 Armada Drive, Carlsbad, CA 92008.

Our Canadian goods and service registration number is 126142892RT.

Any opinions expressed in signed articles are understood to be opinions of the authors and not of the publisher.

About the Cover

Botswana's diamond-based economy could continue to thrive even after the last rough has been extracted, thanks to the government's commitment to developing value-added industries such as polishing and jewelry manufacturing. The cover photo shows diamond cutter Mabedi Motlhasedi examining her work at Laurelton Diamonds, a manufacturing and retail subsidiary of Tiffany & Co. that opened a plant in Gaborone in 2011. Photo by Robert Weldon/GIA, courtesy of Tiffany & Co. and Laurelton Diamonds.

Printing is by L+L Printers, Carlsbad, CA.

GIA World Headquarters The Robert Mouawad Campus 5345 Armada Drive Carlsbad, CA 92008 USA

© 2014 Gemological Institute of America

All rights reserved.

ISSN 0016-626X



Challenges and Opportunities



Welcome to the second issue of our 80th year! In June, GIA held a reception at our Carlsbad headquarters to celebrate this anniversary and to honor the artistry of Harold and Erica Van Pelt. The reception marked the opening of a museum exhibit of their *G&G* cover shots, displayed alongside many of the fabulous pieces they photographed. The Van Pelt's beautiful images graced the covers of our journal for nearly 30 years and really symbolized the stature and quality of *G&G*.

Along with GIA president Susan Jacques, editor-in-chief emeritus Alice Keller, and frequent contributor John King, I was privileged to offer a few words to our guests. While the others spoke to *G&G*'s context, its place at the heart of GIA's mission, and the contributions that enriched the

journal over the years, my topic was the future.

Although there are undoubtedly challenges in living up to *G&G*'s 80-year legacy, there are corresponding opportunities to take our journal to a much wider audience. While technology and social media provide much of this new potential, it's also abundantly clear how well people respond to the print journal, and the importance of face-to-face contact in transforming ideas into reality. In the future, our strategy must incorporate both elements.

Although there are undoubtedly challenges in living up to G&G's 80-year legacy, there are corresponding opportunities to take our journal to a much wider audience.

Our lead article, by GIA's Robert Weldon and Russell Shor, examines Botswana's efforts to become a major diamond processing and jewelry manufacturing center, for the benefit of its people. The article draws from Weldon's 2013 visit to Botswana with GIA videographer Kevin Schumacher, whose extensive videos illuminate many of the locations and people described in the paper. We invite you to view them from your smartphone or tablet by using the quick reference (QR) code at the end of the article, or from your computer by visiting www.gia.edu/gems-gemology.

In the minds of many practicing gemologists, three-phase inclusions in emerald are inextricably linked to Colombian origin. Yet emeralds from Afghanistan, China, and Zambia can display strikingly similar inclusions. Sudarat Saeseaw, Supharat Sangsawong, and Vincent Pardieu, all from GIA's Bangkok lab, present detailed photomicrographs of samples from these localities combined with spectroscopy and trace-element analysis. The authors demonstrate that a combination of these techniques has significant potential for determining the geographic origin of emerald.

We also offer a fascinating paper examining the blue color phenomena seen in some Dominican and Indonesian amber. Yan Liu of Liu Research Laboratories and coauthors Guanghai Shi and Shen Wang provide the gemological basis for the surface-related blue fluorescence seen in such amber.

Our final feature article—also on amber—comes from Yamei Wang and Mingxing Yang, both of the China University of Geosciences in Wuhan, and Yiping Yang, a former postgraduate from the same institution. This paper documents their heat treatment experiments on a range of amber samples, which successfully reproduced some of the products found in today's jewelry marketplace. Along with the methods and results of their experiments, the authors present criteria for identifying heated amber.

One of our continuing priorities is to develop synergy with the GIA website. In this issue, we entreat you to visit—in case you missed them—our recent article posts and related videos. You'll hear the voices of researchers, miners, and gem professionals, and see inside research institutions, mines, museums, and the diverse locations where gems are bought and sold. Please visit page 172 for QR codes and links to this enhanced content.

We hope you enjoy the summer 2014 edition!

Duncan Pay | Editor-in-Chief | dpay@gia.edu

BOTSWANA'S SCINTILLATING MOMENT

Robert Weldon and Russell Shor

While South Africa's Nelson Mandela inspired the world with his vision of forgiveness and racial harmony, leaders in neighboring Botswana long ago sowed the seeds of cooperation and economic development. They also demonstrated a clear understanding of how to harness the country's natural resources—diamonds, primarily—for the good of its people. Botswana has now taken a bold step forward with a long-term plan for value-added industries that will keep the country vibrant long after its diamond reserves are spent. While Botswana's aspirations of becoming a major diamond center are great, so too are the challenges that lie ahead.

Just off Airport Road in Gaborone, Botswana, where the capital city's scrubby outskirts begin, a new complex erected in the open expanse might well be mistaken for the airport itself. The main building, a hulking structure surrounded by high fences and security cameras, is considerably larger than Sir Seretse Khama International's concourse. And for good reason: The Debswana complex, representing a fifty-fifty joint venture between De Beers and Botswana, includes a \$35 million state-of-the-art diamond sorting, valuing, and selling center, called DTC Botswana, the world's largest facility of its kind (Even-Zohar, 2002; De Beers, 2008). It has the capacity to make ready for market almost 45 million carats of rough per year, or about 40% of the world's total annual diamond supply. In value terms, it accounts for about \$6 billion worth of diamond rough annually (Spektorov et al., 2013; figures 1 and 2).

Behind this momentous change is the world's largest diamond producer, De Beers. As of November 2013, all of De Beers's mine production—from South Africa, Namibia, and Botswana, as well as Canada—is consolidated at DTC Botswana, in a pre-selling sorting and valuation process known as aggregation. While De Beers has fifty-fifty joint partnerships with

governments in other African countries such as Namibia and South Africa, Botswana is by far its largest and richest source of diamonds today. Through agreements with Botswana, the vast majority of the diamonds are purchased by De Beers for sale to the company's sightholders. Although De Beers was traditionally Debswana's only client, the renewal in 2006 of the 25-year mining lease for Jwaneng stipulated that as of 2013, 10–15% of production must be sold to the government-owned Okavango Diamond Company (ODC). This arrangement gives the government its own direct sales channel of rough diamond to clients around the world, bypassing the De Beers channel.

Figure 1. The Debswana complex in Gaborone includes DTC Botswana. Photo courtesy of DTC Botswana.



See end of article for About the Authors and Acknowledgments.

GEMS & GEMOLOGY, Vol. 50, No. 2, pp. 96–113,
<http://dx.doi.org/10.5741/GEMS.50.2.96>.

© 2014 Gemological Institute of America



Figure 2. These diamond octahedra rough in the 3 ct range are from Jwaneng in southern Botswana, the world's richest diamond mine by value. Photo by Robert Weldon/GIA, courtesy of DTC Botswana.

Perhaps even more importantly, a new 10-year sales contract, signed in 2011, included provisions for relocating the DTC—the De Beers sales arm—from London to Gaborone. This agreement essentially locks in the company's commitment to beneficiation ("Diamonds sparkle," 2011).

Aggregation of the diamonds at DTC Botswana precedes each of the so-called sights, where selected buyers from around the world convene to purchase rough allotments. The sights, held in London for close to a century, moved to Gaborone following reportedly intense mining lease renegotiations with Botswana's government that took place in 2004–2005 (Mokone et al., 2013). The move signals a historic change and a significant upheaval of De Beers's traditional business model, shedding a remnant of the control over diamond sales exerted by the company

since the colonial days of South Africa. As a result, more than 60% of its London-based staff relocated to Botswana in 2013. At a cost of over \$120 million, not to mention the loss of long-established power, it was surely not an easy decision (Ferreira-Marques, 2013).

But the die has been cast, and both De Beers and its parent company, Anglo American, have highlighted the positive aspects of the move. De Beers Group CEO Philippe Mellier (figure 3) says the efforts underscore the company's commitment to beneficiation. "As we make this move, Africa is once again at the forefront as De Beers and its partners lead the diamond industry into a sparkling new chapter in its illustrious history," Mellier noted (De Beers, 2013a). He added, "Africa was home to the diamond industry when it began in the late 19th century, and De Beers and its partners were central to that growth."



Figure 3. Philippe Mellier, CEO of De Beers Group. Courtesy of De Beers.

For the people of Botswana—the Batswana—the stakes are high: creating added value above and beyond the mining of resources. They expect the changes will stimulate the growth of diamond trading and rough diamond manufacturing, jewelry manufacture, related businesses, and other sectors of their economy. If the plan succeeds, this evolution will carry Botswana far beyond 2030, when the country's diamond reserves are expected to run out.

CHANGES DOWNSTREAM

The changes have required De Beers's 82 sightholders and their associates to alter their habits and travel schedules. Sightholders have begun to make the 10 treks a year to Gaborone instead of London (figure 4). Reports from the first DTC Botswana sight in November 2013 were largely positive, despite initial grumbling and some logistical challenges (Bates, 2013). For example, there are currently no direct flights to Gaborone from the United States, Asia, or Europe. The dearth of banking infrastructure, Internet service, hotels, restaurants that will accommodate special dietary considerations, taxis, theaters, and other amenities that sightholders were accustomed to in London is not making the transition easy. These challenges will have to be worked out over time.

"In a sense, this is exactly what it's all about," explains Kago Mmopi, communications and corporate affairs manager at DTC Botswana (figure 5). "Botswana is a developing country, and infrastructure is also developing, and needs to develop further. The move is inspiring the Batswana to do that. We have been speaking to local businessmen and alerting them of many opportunities that lie ahead. We also know that we need to fast-track this area."

The government is also pushing hard to create state-of-the-art infrastructure to facilitate diamond trading in Botswana. Jacob Thamage (figure 6) is the coordinator of the Diamond Innovation Hub, an organization set up in part by the government to coordinate banking, security, and transportation for the

Figure 4. Left: Keneilwe Dihutso, a diamond grader at DTC Botswana, displays a 54.29 ct rough octahedron from Jwaneng prior to a visit by De Beers sightholders. Right: The 54.29 ct crystal is shown next to a 3.00 ct octahedron from the same mine. Photo by Robert Weldon/GIA.





Figure 5. Kago Mmopi, DTC Botswana's communications and corporate affairs manager, says the new facility can process 45 million carats of diamond per year, about twice the capacity of Orapa House, the sorting facility used by De Beers until recent years. Photo by Robert Weldon/GIA.

diamond business, as well as to address the concerns of De Beers sightholders. But it also hopes to seize the opportunities that will arise for new diamond manufacturers in Botswana and the attendant businesses that will begin to grow as the diamond sector expands.

In Brief

- Botswana has emerged as a significant player in the diamond industry, with Gaborone becoming an increasingly important destination for sightholders and business interests.
- The government of Botswana, historically mindful of the country's importance to the world diamond market, has taken steps to partner with operations of different sizes to meet both industry demands and the needs of the Botswana.
- Future endeavors include moving beyond production and into value-added industries such as cutting and jewelry manufacturing, allowing for long-term economic growth.

“Our job at the Diamond Innovation Hub is to attract the kind of companies that will bring innovation to Botswana. The idea is to also be able to go into

partnerships with many of those companies,” Thamage explains. “We’ve always had aspirations and desires to benefit our people and add value to the country, for the various reasons that brings: skills building, employment, and the creation of ancillary services. In 1981, we had only one diamond-manufacturing factory. By 1992, we had two, and four in 1994. Between 2004 and 2006, we licensed 12 more factories to build.”

As of early 2014, 21 factories are licensed to facet diamonds in Botswana. One of them, the Indian-based Shrenuj Company, is manufacturing jewelry there as well (figure 7).

While the aspirations for Botswana and its people are great, the difficulties are equally so. Logistical challenges—simply the time and distance it takes buyers to get there—as well as the infrastructure needed to efficiently run the diamond industry after the end of mining, are the obvious barriers. More hotels and restaurants accommodating dietary needs of the diverse global business community will need to be built. International banking facilities and direct airline links to Gaborone need to be established, while unnecessary duplication of bureaucracy in the import and export sector must be eliminated.

Figure 6. Jacob Thamage, coordinator of the Diamond Innovation Hub, is responsible for attracting foreign investment in Botswana and helping provide impetus to beneficiation projects. Photo by Robert Weldon/GIA.





Figure 7. Shrenuj, a diamond and jewelry manufacturing firm based in India, became the first company to add value in Botswana beyond diamond manufacturing. This star motif in white and pink gold contains diamonds mined and manufactured in Botswana. Photo courtesy of Shrenuj.

Perhaps the biggest challenge for Botswana lies in the competitive strength of diamond centers around the world, which have been cutting diamonds for decades, if not centuries. Diamonds flow naturally toward Antwerp, Tel Aviv, Mumbai, and New York. Even though none of these manufacturing centers have their own diamond mines (as Botswana does) they have the necessary infrastructure and skills base, and they are generally located closer to end consumers. This is not yet the case for Botswana. Today, almost a million people are employed in the Indian diamond industry, which commands almost 60% of the polished market (Mbayi, 2011), compared to the 3,200 cutters in Botswana. Yet the Botswana are confident that this number will grow, as competencies are developed downstream.

“A lot of our youth have come into the diamond business and excelled, and that has been a pleasant surprise,” explains Thamage. “But as we all know, it is an expensive industry that requires a lot of cash. The schemes we have in terms of funding our youth are not enough now for them to be able to buy diamonds for themselves. What we hope to see, as a beginning, is that a lot of those workers will someday open an office, just like this one, become diamond-taires, and start contract polishing.”

Growth in African manufacturing, however small, is not going unnoticed in other cutting centers. *The Hindu Business Line* cited beneficiation programs in Africa as one of the reasons why the Indian market is “losing its sparkle” (Ashok, 2013).

Those concerns are premature, given Botswana’s minor role in manufacturing. What the country needs is a critical mass of talent, manufacturing efficiencies, and an infrastructure that supports a cutting industry. For consumers of such goods, inevitable questions arise: Are the diamonds well cut? Is there an understanding of proper yield? Can African labor costs compete with those of India? Can the world do business in Africa? Will consumers around the world, heeding a call to contribute to beneficiation in Africa, demand diamonds that are both mined *and* cut there? To illuminate these questions requires a basic understanding of the country, its people, and its diamond richness (figure 8).

BOTSWANA’S DIAMOND BUSINESS

Botswana remains a landlocked, sparsely populated territory comprising some 600,000 square kilometers, composed chiefly of arid savannah (figure 9). What Botswana lacks in agricultural capacity it makes up for with the world’s richest diamond reserves and production—four major mines and other deposits identified through exploration—as well as a relatively stable democratic government, and a hardworking, well-ed-

Figure 8. At Laurelton Diamonds Botswana, a cutting subsidiary of Tiffany & Co., skills transfer brings much-needed jobs to the local Botswana. Photo by Robert Weldon/GIA.





Figure 9. Map of Botswana's diamond mines.

ucated population. Its 2013 GDP per capita of approximately \$16,400 is among the highest on the continent and closing in on neighboring South Africa's, which is declining (CIA World Factbook, 2013).

At the time of its independence in 1966, Botswana was one of Africa's poorest countries, with only a few miles of paved road and a largely agrarian and illiterate population. The average GDP per capita was \$80. A Harvard study written in 2005 noted that the country's future in the early 1960s was "inesestimably bleak." Even Seretse Khama, Botswana's first president (1966–1980), conceded that his country was "beyond doubt one of the poorest nations in Africa" (Alfaro et al., 2005). Relations between Great Britain and Botswana remained cordial through the transition, in part because Botswana offered so little strategic importance. In 1966, Queen Elizabeth II knighted Khama, who had studied at Oxford and married an Englishwoman, Ruth Williams (figure 10).

Just one year later, Botswana's fortunes radically improved. The country's diamond reserves, unknown at the time of independence, became evident when the first diamond-rich kimberlite pipe was discovered by De Beers prospectors at Orapa in 1967 (De Beers, 2014). Diamond production began in 1970 (Janse, 2007). The sudden windfall could have taken the poverty-stricken new country in any number of directions, but a dedication to democracy and ethical governance prevailed. So did the understanding that the diamond riches could not be achieved without

technical assistance. In a 1978 speech, Khama declared, "We will have to learn how to share aspirations and hopes as one people, united by a common belief in the unity of the human race. Here rests our past, our present, and, most importantly of all, our future."

Khama's foresight appears particularly prescient today. Following his inauguration, he proposed the controversial 1967 Mineral Rights Act, aimed at vesting all mineral resources in the central government rather than in the hands of tribal leaders. Khama's delicate negotiations, and his appeal for tribal elders to consider the good of the nation rather than the good of the tribe, ultimately led to passage of the act. His skills as a negotiator and leader were now cemented (Alfaro et al., 2005). This agreement, as well as a progressive and open attitude toward foreign investment, would lay the foundation for Botswana's extraordinary growth, and ultimately for future negotiations with De Beers.

No other mining groups existed in Botswana. In 1968, a jointly owned company called Debswana (85% owned by De Beers and 15% by the government) was formed. For Khama and the democratic rulers who succeeded him, Debswana became the model for Botswana's negotiations with other diamond and metal mining companies. By 1975, the discovery of additional diamond-rich pipes—such as the spectacu-

Figure 10. In 1948, Seretse Khama caused a considerable stir, both in England and in Botswana, when he married an Englishwoman, Ruth Williams. Their son Ian Khama, far left, has been Botswana's president since 2008. Photo by Brian Seed, © Time & Life Pictures/Getty Images.



lar Jwaneng deposit—truly changed the equation. Two decades later, Botswana had become the most important diamond producer, supplying one quarter of the world's diamonds by value (Janse, 1996). Although the government could have chosen to nationalize the mines, as neighboring countries were doing (Alfaro et al., 2005), Botswana's leadership chose to negotiate terms that were extremely favorable to the country while acknowledging that it lacked the capacity to build the mining operations. Renegotiation with De Beers in 1969 led to a new agreement, essentially resulting in fifty-fifty joint ownership (Hazelton, 2002). That, combined with revenues from taxation of its resources, has given Botswana the lion's share of the profits from diamond mining. Conversely, for De Beers, Botswana became a sort of insurance policy against growing competitors, particularly in Russia and Australia (Shor, 1990).

As much as the partnership between government and private enterprise has been lauded, it has also faced opposition. Critics contend that the partnership is too lopsided to be efficient and suggest that in recent economic downturns, as in the mining contraction of 2009 and 2010, many Botswana have been left without a safety net. Diversification of the economy and less reliance on a single "cash crop" would serve as a hedge against downturns, it is believed, particularly as diamond mining reaches an end in Botswana. Some suggest that the partnership is in fact counterproductive, for that very reason. "The... relationship serves as a disincentive to economic diversification and political accountability," wrote Kenneth Good, an Australian professor in global studies at the University of Botswana who was expelled from the country in 2005 for writing a book critical of its politics (van Wyk, 2009).

The relationship has not always been smooth, and some historians note that Botswana has struggled, at times contentiously, to diversify its economy and to make De Beers its partner in the manufacturing aspect of the diamond business as well. According to industry journalist Chaim Even-Zohar (2007), De Beers was initially against bringing facilities to Botswana. Even-Zohar notes that the company "did everything in its power to prevent the establishment of more than two or three token manufacturing units."

Shortly before the Jwaneng contract renewal, President Festus Mogae (1998–2008) expressed his country's objective: "We are looking for some improvement in the sharing of benefit. The resource is ours, which is very important, but the investor is also

entitled to a fair return" (Idex, 2004). Clearly much has changed since 2006, when the new agreements came into play. Today, beneficiation is a word that ostensibly holds equal weight with De Beers and Botswana. Mellier often singles out Botswana in speeches dealing with the company's portfolio, noting the country's role as a manufacturer and its rising profile as a rough diamond trading destination (Mellier, 2014).

Seretse Khama and subsequent presidents have all played significant roles in harnessing the country's natural wealth and building institutions of good governance, education (the current literacy rate is almost 85%), and anticorruption. As in several preceding years, Botswana was rated the least corrupt African country in 2013 by Transparency International. But it was not only the rich diamond reserves that affected Botswana's destiny; more recently, copper, gold, nickel, uranium, and other resources have been discovered. A focus on bolstering secondary and higher education, and a commitment to steering the economy away from total dependence on diamond revenue, began in earnest in 2008, when Ian Khama was voted into office. The fruits of an educated populace, good governance, and skillful negotiation for the extraction of its wealthy natural resources—particularly diamonds—have kept Botswana on track as one of the world's fastest-growing countries, averaging 10% annual growth for almost three decades (Sanchez, 2006; Farah, 2013; figure 11).

While building the framework for its people, the government is equally committed to responding to business needs. "I've had the chance to observe what's happening in mining in plenty of other countries," says Jim Gowans, outgoing managing director for Debswana. "Government officials in Botswana may not get enough credit for having done a good job. They have an idea about what they need to do, and they're pretty quick to do it. Another big benefit for Botswana is to have a democratic system and only four presidents in their history." Certainly these factors have led to stability.

From the late 1970s into the early 21st century, well over half of the country's GDP was from diamonds, but a consistent policy to make the country less dependent on mining has emerged. In 2013, the diamond business alone—not counting copper, nickel and gold, or other industries—contributed to over a third of the country's revenues. Over the years, Botswana has been lucrative for De Beers as well. In 2000 alone, over 80% of the company's revenue came from its Botswana portfolio—53% of that from



Figure 11. The Three Dikgosi, a frequently visited monument in Gaborone, depicts the tribal elders who traveled to Great Britain in 1885 to request the creation of the Bechuanaland Protectorate, the precursor to the modern state of Botswana. Photo by Robert Weldon/GIA.

the Jwaneng mine alone (Even-Zohar, 2002). For De Beers, reliance on Botswana's riches—and some might argue overreliance—is also evident.

Of course, there are still enormous challenges Botswana must contend with. In the 1990s, the scourge of HIV/AIDS virus hit hard in the sub-Saharan country (Weldon, 2001). Today, approximately 24% of the population is infected with the virus, according to the World Health Organization. Botswana's relatively tiny population and workforce can ill afford such a devastating blow. Nevertheless, Botswana's leaders have met the challenge with education programs on HIV prevention, partnerships and grants with pharmaceutical companies such as Bristol-Myers Squibb, and the construction of hospitals and treatment centers. Grants from the Bill & Melinda Gates Foundation are aimed at managing the symptoms of the disease or preventing its progression. Over 80% of Botswana infected with HIV/AIDS are covered by free antiretroviral medication, and 100% have access to it. President Quett Masire (1980–1998) was the first Botswana leader to face the problem at the turn of the century, and in 2009 he declared it a national imperative to wipe out the disease. He established 2016 as the target year when no new infections would occur. In 2011 alone, the Botswana government spent some \$385.5 million on AIDS prevention, care, and treatment, with a special focus on children stricken with AIDS or orphaned by the disease. The results have been dramatic in terms of life expectancy through earlier detection and treatment, and reductions of HIV transmission from mother to child (figure 12). In 2012, President Khama

noted in a state of the nation address that the country was on track to achieve a less than 1% transmission from mother to child by 2015. Botswana's example has been lauded throughout Africa and the rest of the world. The expenditures "come at a considerable cost," according to Khama, though they are universally considered utterly necessary for Botswana to move forward economically and socially.

Another challenge was the attempted relocation of indigenous peoples in the Kalahari Desert to make room for a potential new mine at Gope. Survival International, a UK-based non-governmental organization, campaigned for several years against developing the mine and, in late 2010, attempted to block its licensing. According to reports, a lawsuit ended the crisis by allowing the Kalahari Bushmen to return to their land ("Botswana outraged...," 2011).

In 2012, De Beers produced less than 30 million carats worldwide—another year of retrenchment from a high of 34 million carats in 2006—due mainly to flagging global diamond demand, a lingering after-effect of the 2008 global recession. The following year saw major changes at the sources, such as the sale of the Finsch mine and a slope failure at Jwaneng (Greve, 2013). Liquidity problems for many Indian manufacturers, which still cut most of Botswana's diamonds, also slowed the momentum. For Debswana, a company dedicated to addressing safety concerns, it was also a difficult year. The slope failure at Jwaneng in June 2012 killed an employee, and investigations into its cause shuttered the mine for several months. Debswana has since taken an even more aggressive stance

Figure 12. The government of Botswana ensures that its citizens are eligible for free antiretroviral medications to treat HIV infection. Additionally, a series of programs aimed at reducing transmission of HIV from mother to child have been instituted. Photo by Lucian Coman, © Shutterstock.





on safety, promulgating a “zero harm culture” while improving its production figures (J. Gowans, pers. comm., 2013).

In tandem with declining production, 2012 sales totaled \$5.5 billion, a billion less than 2011 (De Beers, 2013b). Nevertheless, the goal of transferring De Beers’s sales arm to Botswana was accomplished in 2013. The business lull may have been advantageous by allowing a more gradual buildup of Gaborone as a diamond sorting, valuing, and selling center. Debswana is poised for growth, particularly as new dia-

mond customers emerge in India, China, and other developing markets. De Beers estimates 5% growth in China, Hong Kong, and India by 2017, while the U.S. market—which now represents over a third of global diamond sales—will slip by about a third of its present portion.

“Beyond mining, the creation of long-term, value-added products, training, and employment for Botswana is beginning to take effect, though there is still a ways to go,” says Pauline Paledi, the executive director of the Botswana Diamond Manufacturers Association (figure 13). The organization, established in 2007, consists of some 17 full members who actually manufacture diamonds in the country today, plus recent applications for an additional four members at the time of this writing. The association lobbies the Botswana government “as a single voice,” explains Paledi, and works out compliance matters regarding labor laws and visa and residency issues for foreign manufacturing companies. The goal is to attract more foreign investment, and eventually homegrown diamond manufacturing as well. “We see growth ahead,” says Paledi. “The market is getting stronger for manufacturing, and it is diversified, as we can all see.”

The notion that diamonds mined on African soil could also be manufactured and sold there, bringing long-term sustainability to Africans, has largely eluded the continent since South African diamonds were discovered in 1867. For the Botswana, such dreams now appear enticingly possible.

DIAMOND MINES OF BOTSWANA

From Gaborone, a car can reach the front gate of Jwaneng, the world’s richest diamond mine, in about

Figure 13. Pauline Paledi, executive director of the Botswana Diamond Manufacturers Association. Photo by Robert Weldon/GIA.





Figure 14. This panoramic view of the Jwaneng mine, Botswana's largest and most lucrative, shows a manmade pit—visible from outer space—that covers approximately 520,000 square meters at the surface and is more than 400 meters deep. Photo by Robert Weldon/GIA.

two and a half hours, a ride straight through a desolate, hilly region of savannah and occasional cattle ranches. For those lucky enough to receive an invitation to visit the mine and proceed through security checks and briefings, the overwhelming desire is to peer over the edge into this open pit, a gigantic man-made hole visible from outer space (figure 14).

Jwaneng—whose name means “place of small stones” in Setswana—was discovered in 1973. The pit currently descends nearly 400 meters into three separate kimberlite pipes. It is expected to reach almost 700 meters in depth by 2017, as new cuts dig into the kimberlitic ore in the search for diamonds. The latest is Cut 8, which extends laterally into the kimberlite pipes at Jwaneng and is expected to produce over 100 million carats and extend the life of the mine until 2028. A bird’s-eye view of this massive removal of earth reveals the rugged face of Botswana’s principal mine by value, which has the capacity to produce some 2.5 million carats of diamond on a monthly basis. During the recession, and because of the 2012 slope failure, production dropped to about half of that (Mmopi, pers. comm., 2013). Once fully operational, Cut 8 will transform Jwaneng into one of the world’s super-pit mines.

Jwaneng employs over 2,500 people, though they are rarely visible, partly due to the pit’s immense size and partly for security and safety reasons. Cut 8 is expected to expand the workforce by at least 50%. At the bottom of the pit, kimberlitic ore is broken up through dynamite blasting on a regular basis. Miners are also busy maneuvering the massive Komatsu 930 trucks, each the size of a house and designed to cart out 250 tons of kimberlitic ore per haul (figure 15). A

staggering 60 million tons of earth are thus removed in a high production year; on any given workday, traffic from the trucks forms a constant stream into and out of the mine. Where the earth goes after processing is another logistical and engineering feat.

First, the ore is crushed into much smaller particles at a plant on the surface. The clay and mud are removed, and the diamonds are separated from the ore by X-ray at a completely automated recovery plant (CARP) where, as a theft countermeasure, no human hands touch the ore. After that, the diamonds

Figure 15. A Komatsu 930 truck can remove up to 250 tons of diamond-bearing rock and earth in a single haul. Photo by Robert Weldon/GIA.





Figure 16. Mixed rough from Debswana's mines must be collected and sorted into categories by size, color, and clarity. Photo by Robert Weldon/GIA.

are presorted, cleaned, and packaged using laser technology (again with no hands touching the rough). The diamonds are then ready for transport to Gaborone for sorting and valuing, and ultimately for sale. The rough is classified by weight, shape, clarity, and color, regardless of source. According to Kago Mmopi, Debswana's mines alone supply between 200,000 and 500,000 carats to DTC Botswana on a weekly basis (figure 16).

A similar procedure takes place at Debswana's other mines, all of which are open pit. The Orapa mine is Botswana's oldest, established in 1971, a few years after diamonds were first discovered in a dry northeastern part of the country. As with all De Beers projects, the mine is owned fifty-fifty with the government. Orapa has the capacity to produce almost 20 million carats a year; in 2012, however, production slowed to 11 million carats due to global economic conditions. Letlhakane and Damtshaa are both much smaller-capacity mines, producing less than a million carats annually. Combined, Debswana's four mines

produced 20.22 million carats in 2012 and treated 21.87 million tons of earth—just over a carat per ton (De Beers, 2013b). In 2013, Debswana produced over 22 million carats; these numbers are expected to increase as global economic recovery takes hold.

Botswana's other diamond mines are independently owned rather than joint ventures between De Beers and the government. One of these is the Lerala mine, owned by DiamonEx, which has been stalled due to restructuring and is expected to reopen in 2014. Others such as the Karowe mine, operated by Lucara Diamond Corporation, are selling diamonds through auctions. Karowe made news by yielding 26,196 carats for auction ("Lucara completes first sale of Botswana diamonds," 2012) and announcing the find of a 4.77 ct blue diamond as well as several large diamonds (Golan, 2013). Auctions are also the government's preferred method of selling diamonds, at least for now.

THE OKAVANGO DIAMOND COMPANY: THE MARKET EXPERIMENT

De Beers was traditionally the sole purchaser of diamonds mined in Botswana. A renegotiation in September 2011 changed that, with the government obtaining the right to purchase a progressive 10–15% allotment of the rough to sell through its own channels over the next few years. To that end, the government established the ODC (figure 17) in 2012 and

Figure 17. The Okavango Diamond Company, a wholly owned government company that derives its name from Botswana's rich Okavango Delta, purchases over 10% of the rough diamonds produced by Debswana for sale to clients around the world. This margin will increase gradually to 15%. Photo by Robert Weldon/GIA.





Figure 18. Marcus Terhaar, deputy managing director of the Okavango Diamond Company. Photo by Robert Weldon/GIA.

appointed Toby Frears as its managing director that same year.

As diamonds arrive weekly at Debswana, De Beers and government negotiators settle on a value for the goods. After the purchases are made, De Beers aggregates Botswana's goods with its allotments from Namibia, South Africa, and Canada.

The 10%-plus that the ODC buys on a weekly basis is gathered and sold to clients around the world via auction. Sales occur about 10 times a year and include parcels and single stones 10 ct or larger. It is thus a different system from the fixed allocation contracts implemented by De Beers and its sightholders. As would be expected, ODC clients must be properly vetted and comply with strict guidelines to register and qualify as buyers. Details about each company's role in the diamond value chain, top personnel, and compliance with all diamond sector regulations are required by ODC.

For all its advantages, the auction system tends to be risky: volatile during good economic times, and slow to nonproductive during bearish economies. Under such conditions, fixed contracts make it easier to fine-tune and control the market. Marcus Terhaar (figure 18), ODC's deputy managing director, explains that the auctions help the government derive current market value for the products.

"Auctions are going to be far more volatile than other selling mechanisms. But that's not necessarily a bad thing, because over a consolidated period of time, you will find that they do very well despite the boom-and-bust cycle."

Jacob Thamage, who also serves on the board of the ODC, agrees, alluding to current economic cli-

mate. "For ODC to launch under these conditions is actually very good, because, like they say, 'Rough seas make the best sailors.' It is conditions such as these that will really teach us what the market is, and what it could be."

ODC officials seem open to the idea of a dual selling system that incorporates both ideologies. "A lot of companies use dual systems—meaning that they have options *and* contracts. That tends to mitigate the risk," Thamage explains. "By the middle of 2014, we will have completed a full cycle of selling and understood the possibilities of auctions and contracts."

Terhaar highlights the beneficiation aspects that are already taking place through the ODC: "What we have in Botswana, insofar as the diamond sector is concerned, is a very strong diamond mining industry. We have a very well-established sorting and valuing operation in Debswana, and we have a good five to seven years into diamond manufacturing. Rough trading is clearly the missing link for Botswana, and that is the primary focus of the ODC. It will bring jobs. This means that 150 people are coming to our premises every five weeks or so. That means 150 more hotel accommodations, 150 more seats on local airlines, and 150 more customers looking for taxis, making dinner reservations at restaurants. It will foster the growth of ancillary services: diamond reports, banking, rough valuing, and marketing services, and so many other types of related services."

For now, ODC is busy establishing its operation, conducting sales, and promoting itself as a viable separate channel for rough diamond buying. "This is a big feather in Botswana's cap," says Terhaar. "Ten years ago this was all bush country. Botswana has proven that it can be done. And while there is a lot of learning to capture, there is certainly the motivation, and the will, for Botswana to perform as a benchmark diamond center—as efficiently as Antwerp, Israel, or any other diamond center in the world."

CAN A CUTTING INDUSTRY BE SUSTAINED IN BOTSWANA?

While Botswana prospered by carefully redirecting its diamond wealth into nation-building, establishing a domestic diamond manufacturing industry remained an elusive goal until recently. Neighboring South Africa benefited from a well-established diamond cutting industry that employed several thousand workers. Even so, much of this industry survived because De Beers subsidized local cutting operations by providing rough at a 10% discount (actually sparing

buyers export taxes on rough). Some of these operations existed mainly as a means for their owners to obtain rough allocations from De Beers. They performed minimal work on stones in the local plants before exporting them to Israel, Antwerp, or India for actual manufacturing (Shor, 1990; figure 19).

In the past, De Beers actively discouraged diamond manufacturing in Botswana, claiming the costs of doing business there were not low enough to compete with India and China. In addition, De Beers noted, the country was too far removed from major consumer markets (Grynberg, 2013).

De Beers's opposition began to crumble in 1990 when the company entered negotiations to renew its five-year contract with the government to sell rough mined by Debswana. With De Beers owning 50% of Debswana, such contracts would seem to be a routine matter, but in 1989 the government had raised the issue of starting a domestic manufacturing operation. At the same time, a number of major rough diamond dealers were lobbying Botswana's parliament to sell 20% of the company's production outside De Beers's network, claiming they would be willing to pay 5–7% higher prices than De Beers. One of those dealers, Maurice Tempelman of Lazare Kaplan International (LKI), offered to build a polishing factory if the government was willing to supply diamonds to the operation (Shor, 1990). The government made no such promise, but LKI built the factory anyway.

De Beers, which already employed 5,000 workers at its three mines in Botswana, eventually agreed to develop a cutting factory, mainly to forestall the parliament from considering this 20% "market window" (Shor, 1990). The operation, named Teemane, opened in 1993, but a decade later only three others had been built, the largest being the Lazare Kaplan International operation (J. Thamage, pers. comm., 2013).

Botswana assumed a much greater role in De Beers's operations after 2001 when, as part of the company's reorganization, it assumed a 15% stake in the firm's ownership. Botswana also captured a much greater strategic role after De Beers began phasing out its agreement with Alrosa, the Russian diamond mining company, to market its production—accounting for about 25% of De Beers's rough sales—and sold off its aging South African mines and its \$5 billion diamond stockpile (Even-Zohar, 2007). By 2005, Botswana was by far the largest and most profitable part of De Beers's operations, accounting for 70% of its earnings (Grynberg, 2013). This fact was not lost on the country's leadership, which leveraged



Figure 19. Laurelton, a joint venture manufacturing branch of Tiffany & Co., has set up shop close to the DTC Botswana complex and the Diamond Technology Park. Today, it works with Indian cutting experts to bring about a transfer of skills to the Botswana. The manufacturing plant has ample room for growth, which it clearly expects. Photo by Robert Weldon/GIA.

an aggressive series of beneficiation measures in its negotiations for both the sales contract with Debswana and the renewal of the 25-year lease at Jwaneng (Even-Zohar, 2007).

The agreements, reached in 2006, covered a thousand pages but contained three main requirements that would transform operations for both sides:

- De Beers would directly supply local firms that qualified for a diamond manufacturing license.
- De Beers would relocate all of its sorting and rough sales operations from London to Gaborone by 2009.
- A certain percentage of De Beers sight goods would be reserved for local polishing operations.

In short, the government of Botswana, which had owned a 15% stake in De Beers since 2000, now had sufficient clout to force the company to supply local polishing operations, and to require large diamond manufacturers to develop factories on its soil if they wanted to obtain supplies of rough diamonds (Grynberg, 2013).

While the 2006 agreement provided for supplies to 10 factories, as selected by De Beers, Botswana

moved aggressively beyond De Beers's plans and issued licenses to 16 companies, which began taking rough supplies through separate sights domestically in January 2007. By fall of that year, six had gone into production (Golan, 2007). On the second point, the 2008–2009 world financial crisis hit De Beers hard, requiring the company to borrow \$500 million from shareholders (including \$200 million from the Oppenheimer Trust, which owned 40% of the company). The crisis also forced De Beers to postpone its relocation plans until 2013 (Krawitz, 2008; Anglo American, 2009).

In 2008, in preparation for De Beers's arrival and the growth of a domestic cutting industry, the diamond industry, led by South African manufacturer Safdico with the Botswanan government's cooperation, commissioned the Diamond Technology Park. The secure 35,000-square-meter facility was located next to the new De Beers building and just four kilometers from Sir Seretse Khama International Airport. It was designed to house about 15 medium-size manufacturing operations in two buildings, plus industry services such as banking, manufacturing equipment, and diamond grading—GIA's Gaborone laboratory was one of the first tenants—in a third building. The Diamond Technology Park website notes that by 2012, these operations had outgrown the complex, causing a number of manufacturers to locate in the industrial parks nearby.

Statistics for 2013 indicate that Botswana's drive to create a local diamond manufacturing industry has been a success. More than 3,000 workers are employed in polishing operations (compared to fewer than 500 in 2006) and several thousand more through ancillary businesses serving the diamond sector. Polished diamond exports neared \$800 million and were forecast to top \$1 billion by 2015, compared to \$100 million in 2008. The Diamond Technology Park was fully rented, and the government commissioned plans for a fourth building of 4,000 square meters to be completed by the end of 2014 (Grynberg, 2013; Shor, 2013). By the end of 2013, 24 manufacturers were operating in Botswana, 21 of them receiving rough from Debswana through local sights (figure 20).

One reason for this success is that even before De Beers transferred all of its sorting and sales operations to Gaborone, the Botswana sights consisted primarily of higher-value rough that could be profitably polished (Grynberg, 2013). But the rush to open diamond manufacturing operations in Botswana rekindled the debate over whether diamond manufacturing there



Figure 20. A cutter at Diacore Botswana examines the initial facets made on a fancy yellow diamond. Photo by Robert Weldon/GIA.

was economically sustainable, particularly in light of Canada's unsuccessful attempts to develop large-scale cutting operations ("Yellowknife diamond-cutting plant's future in limbo," 2009; Danylchuk, 2013).

MANUFACTURING COSTS

Diamond manufacturing costs in Botswana range from just under \$40 to \$60 per carat, depending on the efficiency and technological capabilities of a given operation. These costs include labor, utilities, maintenance and technology support, and transportation. This cost range is much lower than Canada's (\$80 per carat) but still more than double that of China (\$17 per carat) and four to six times that of India (\$10 per carat), which polishes 92% of world production by volume (Gregorian, 2013; figure 21).

Visits to nearly all of Botswana's large manufacturing facilities found them fully committed to developing sustainably profitable operations. These operations began between 2006 and 2010, using expatriates from India, China, South Africa, and Israel to train local polishers. Each operation had to be started from scratch because no skilled workers, equipment, or financing were available locally (R. Moses, pers. comm., 2013). Over the next four to five years, however, local polishers largely replaced foreign workers at the wheels, and now comprise 80–90% of the workforce (figure 22). For many local Botswana, the employment opportunities have helped them extricate themselves from poverty. In some cases, the salaries have helped feed entire families.

The country's largest diamond factory is run by Eurostar, an Antwerp firm that has its roots in India. The company now employs 520 workers; 485 of these are locals who received a minimum of six

DIAMOND MANUFACTURING COSTS, BY COUNTRY

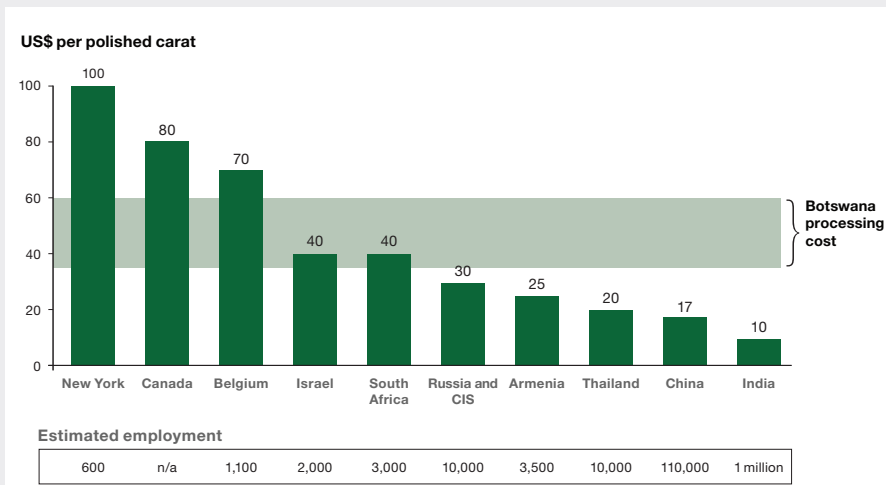


Figure 21. This chart, prepared for the World Bank, analyzes the per-carat costs of diamond manufacturing (including labor and operating charges) in diamond centers worldwide against Botswana's costs (Grigorian, 2012).

months of training and are polishing precision-cut round and princess diamonds 0.25 ct and up. The company recently spent \$7.5 million to upgrade its high-tech processing equipment.

Expatriates still dominate the highly technical aspects of the cutting process: rough planning, bruting and laser sawing, and shaping. Here, too, Botswana trainees work beside the technicians, learning how to use advanced equipment (figure 23).

Another large operation, employing 300 workers, is Shrenuj, which produces half-carat and larger rounds and has also begun a jewelry manufacturing

operation. The company has a program to hire hearing-impaired workers, who now comprise one-quarter of its labor force—but is still working to match the productivity of its Indian operations (K. Lanny, pers. comm., 2013). Nevertheless, the operation has become profitable as performance improves.

Labor costs are less of an issue with Safdico and Diacore Botswana (formerly Steinmetz), which specialize in large, high-quality diamonds. Both companies have developed rigorous training programs because each diamond must meet very high, exacting standards. Safdico and Diacore both added that they are in Botswana for the long term (K. Teichman and R. Moses, pers. comms., 2013).

The government has been diligently auditing companies to ensure that diamond factories provide full training and employ Botswana to perform all of the work necessary to produce finished stones (R. Moses, pers. comm., 2013). Diamond executives give the government high marks for introducing regulations and policies that support equipment imports, funds transfer, building licenses, and transparency.

Several diamond firms have taken their beneficent role beyond offering training and employment to local workers. Safdico supports programs that train computer technicians, schoolteachers, and other community-building professionals in villages outside the capital. Diacore Botswana provides microloans to employees for school fees and conducts events for community improvement projects. They have also supported sporting events and employ prominent local athletes (figure 24).

Figure 22. Diacore Botswana offers diamond manufacturing jobs to hundreds of Botswana. Photo by Robert Weldon/GIA.



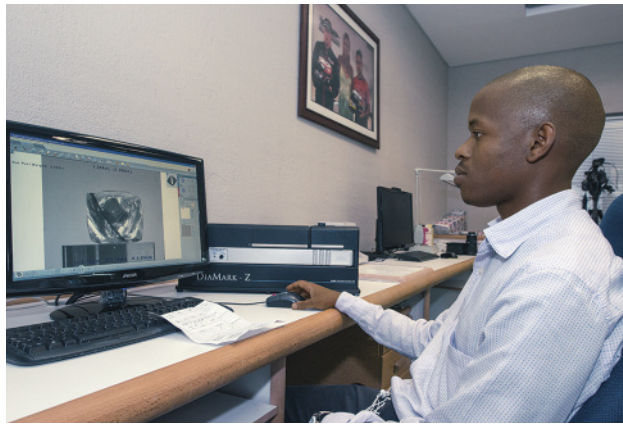


Figure 23. The use of highly sophisticated planning, sawing, and polishing technology is prevalent at the new manufacturing plants in Gaborone. Photo by Robert Weldon/GIA.

Beyond the high cost of labor, significant challenges to sustaining a diamond processing industry remain. Infrastructure is still lacking. Power outages are common, Internet service remains sluggish, and importing or repairing equipment is still very costly and inefficient.

Executives of manufacturing facilities in Botswana, while acknowledging the economics and challenges, are divided over whether the country's diamond industry can become fully self-sufficient. But even the most skeptical see significant potential for improving Botswana's competitive position so that it may become a successful niche producer, like New York or Antwerp. "It is still early days, initial stages," said Erik

Figure 24. Diacore Botswana manager Kefir Teichman (right) poses with gemologist Monica Alfred, a five-year veteran of the company and a member of Botswana's national volleyball team. Photo by Robert Weldon/GIA.



van Pul, manager of Eurostar in Botswana. "We are seeing improvements all the time as workers gain more expertise and government services and infrastructure improves."

In 2010, for example, most Botswana diamond operations could not profitably produce polished diamonds below one carat because training and high-tech processing equipment were not fully in place. By 2012, the more advanced operations were producing 0.40 ct stones—at a profit, according to van Pul. At least 10 factories were producing precision "triple-excellent" cuts comparable to any diamond polishing operation in the world. While that represents true progress, one analyst believes that the ability to polish melee (0.10–0.20 ct) profitably is necessary to create a manufacturing industry that sustains large-scale employment (M. van den Brande, pers. comm., 2013).

THE FUTURE

The year 2027 is the government's benchmark for developing a diamond-polishing industry that does not depend on domestic rough (figure 25). Jwaneng is scheduled to be redeveloped into an underground mine that same year, which will sharply reduce production. By comparison, Australia's Argyle mine fell from a peak annual output of 42 million carats as an open pit to 20 million carats as an underground mine (Argyle Diamond Mine, 2013). Production will likely continue 30 to 40 years beyond this date, but with much smaller volume and higher cost.

Both the Botswana government and the diamond community anticipate that rough auctions by Okavango Diamond Company will stimulate manufacturing and help build the country's trading base. Okavango is a government-affiliated company that has begun selling between 12% and 15% of the country's diamond production through monthly tender sales. Existing diamond manufacturers say the tenders will cut costs and provide greater access to supplies (R. Moses, pers. comm., 2013). Another goal, according to Terhaar, is attracting smaller diamond companies and rough traders to set up business in the country. Okavango sales have much lower purchase requirements than De Beers sights, plus a fairly simple application process that will enable such firms to participate. Building this trading environment will be critical, and the government understands that it needs to work with the diamond industry to lower infrastructure costs and improve services for the country's diamond polishing industry to survive beyond supplies from its mines (Grynberg, 2013).

Indeed, one World Bank study (Grigorian, 2013) noted that “[diamond] producing countries hoping to establish a viable cutting industry are squeezed by competition from two directions: one from low-cost economies such as India and China, another from high-skills economies such as the United States, Belgium, Israel, and Canada. For any latecomer, the challenge is plain: Either be cheaper (and work harder) than the former, or be more knowledgeable and skills-intensive than the latter.” The way through this competition, the study concluded, was for these countries to achieve a manufacturing niche by branding to provide added value to their products.

It remains to be seen whether Botswana-branded cut diamonds will captivate consumer attention globally. Buyers are increasingly conscious of the products they purchase and the supply chain involved. The storyline for a Botswana brand is undoubtedly strong. Consumers, drawn to African diamonds for well over a century, could find assurance in knowing that the diamonds they purchase

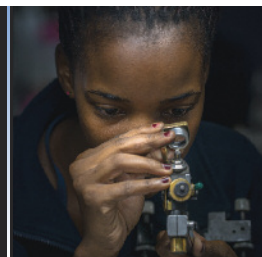


Figure 25. Botswana is capitalizing on its diamond resource riches by adding value through diamond manufacturing. Though not yet large by global standards, the cutting industry in this sub-Saharan country shows considerable promise. De Beers now holds its rough diamond sales in Gaborone and has encouraged large diamantaires to set up manufacturing plants there. Photo by Robert Weldon/GIA.

today have contributed to skills transfer in Africa, poverty alleviation, and the dignity of employment for Botswana’s people.

For More on Botswana’s Diamond Industry

Discover more about Botswana’s strategies and challenges as it develops a thriving diamond industry. *G&G’s* exclusive online content provides access to video interviews and additional resources to enhance your knowledge of this country’s importance to the diamond and jewelry markets.



Visit www.gia.edu/gems-gemology, or scan the QR code on the right.

ABOUT THE AUTHORS

Mr. Weldon is manager of photography and visual communications, and Mr. Shor is senior industry analyst, at GIA in Carlsbad, California.

ACKNOWLEDGMENTS

The authors wish to thank DTC Botswana for kindly allowing GIA to interview staff and take photos on the diamond floor. Warm thanks to Alan Bronstein for his encouragement, insights, and introductions. Thanks also to Marc van den Brande for his invaluable assistance, Drs. Roman Grynberg and Bram Janse for their insights, and the executives of Botswana’s diamond-manufacturing facilities who opened the doors to their operations to the authors. Claudia D’Andrea, director of GIA’s Bangkok campus, and Anthony Licht of GIA’s Johannesburg lab provided firsthand

knowledge of the Botswana diamond industry. Many thanks to Kevin Schumacher, GIA’s digital resources specialist, who provided video expertise during the interviews in Botswana.

We dedicate this article to our colleague and friend, Tawfic Farah, GIA’s vice president of international operations until his untimely death in 2013. Tawfic had a passion for Botswana, and he nurtured a strong desire to help the people of Africa by providing educational opportunities. “We need to find a way to be on the right side of history,” he would often advise us. Tawfic wrote a scholarly paper on Botswana that was not published but served as the seed for this story.

REFERENCES

- Alfaro L., Spar D., Allibhooy F. (2005) Botswana: A diamond in the rough. HBS case no. 9-703-027. Harvard Business School Publishing, Boston, <http://altongp.com/currentprojects/Zimbabwe%20Diamond/Botswana%20Diamonds.pdf>.
- Anglo American (2009) Annual report 2009. http://ar09.angloamerican.solutions.investis.com/financial_statements/notes/note38.html.
- Argyle Diamond Mine (2013) The future: Argyle as an underground operation. http://www.argylediamonds.com.au/index_operations.html.
- Ashok T. (2013) Indian diamond industry losing sparkle. *The Hindu Business Line*, Jan. 29, <http://www.thehindubusinessline.com/opinion/indian-diamond-industry-losing-sparkle/article4357705.ece>.
- Bates R. (2013) What sightholders really think about De Beers' move to Botswana. *JCK*, Oct. 15, <http://www.jckonline.com/blogs/cutting-remarks/2013/10/15/what-sightholders-really-think-about-de-beers-move-to-botswana>.
- Botswana looking to raise rent on Jwaneng mining lease. (2004) *Idex*, No. 174, pp. 75–76, http://www.idexonline.com/portal_Full-MazalUbracha.asp?id=23157.
- Botswana outraged over boycott of diamonds, tourism (2011) *Bangkok Gems & Jewellery*, Vol. 24, No. 6, p. 47.
- Danylchuk J. (2013) Yellowknife diamond row factory deal still not iced. *Northern Journal*, Feb. 26, <http://norj.ca/2013/02/yellowknife-diamond-row-factory-deal-still-not-iced>.
- De Beers (2008) Largest, most sophisticated sorting facility in the world begins operations in Botswana. March 18, http://www.debeersgroup.com/ImageVaultFiles/id_686/cf_5/8-03.PDF.
- (2013a) De Beers holds inaugural international sight in Botswana. Nov. 11, http://www.debeersgroup.com/ImageVaultFiles/id_2126/cf_5/De_Beers_holds_inaugural_sight_in_Gaborone.PDF.
- (2013b) Operating and financial review 2012. http://www.debeersgroup.com/ImageVaultFiles/id_2064/cf_5/2012_OFRR.PDF.
- (2014) Debswana. <http://www.debeersgroup.com/operations/mining/mining-operations/debswana>.
- Diamonds sparkle (2011) *African Mining*, Vol. 16, No. 6, November–December, p. 66.
- Even-Zohar C. (2007) *From Mine to Mistress: Corporate Strategies and Government Policies in the International Diamond Industry*. Mining Communications Ltd., London.
- Farah T. (2013) The politics of development in Africa: Botswana as a case study. Working paper, GIA Library, Carlsbad, California.
- Ferreira-Marques C. (2013) Goodbye London, hello Gaborone: De Beers sales head to Africa. *Reuters*, Oct. 3, <http://www.reuters.com/article/2013/10/03/us-debeers-idUSBRE99204C20131003>.
- Golan E. (2007) DTC sightholders list: Who's on and what now? *Idex Online*, Dec. 20, http://www.idexonline.com/portal_FullNews.asp?TextSearch=&KeyMatch=0&id=29129.
- (2013) Lucara recovers 4.77 ct blue diamond. *Idex*, Vol. 28, No. 274, p. 125, http://www.idexonline.com/portal_FullNews.asp?id=37641.
- Greve N. (2013) De Beers 2012 gem production dips to 27.9m, sales down 16%. *Mining Weekly*, Feb. 15, <http://www.mining-weekly.com/article/de-beers-2012-gem-production-dips-to-279m-2013-02-15>.
- Grigorian K. (2012) Diamond production and processing: What Armenia can learn from an intra-regional exchange on the diamond trade. World Bank, http://siteresources.worldbank.org/INTECALEA/Resources/1040211-1251905880790/KB47_ArmeniaDiamond.pdf.
- Grynberg R. (2013) Some like them rough. Botswana Institute for Development Policy. Discussion Paper 142.
- Hazelton R. (2002) Diamonds: Forever or for good? The Diamonds and Human Security Project, Partnership Africa Canada, Occasional Paper #3, March, http://pacweb.org/Documents/diamonds_KP/3_diamonds_Forever_Eng_March2002.pdf.
- Janse A.J.A. (1996) History of diamond sources in Africa, Part II. *G&G*, Vol. 32, No. 1, pp. 2–30, <http://www.gia.edu/gems-gemology/spring-1996-diamond-history-africa-janse>.
- (2007) Global rough diamond production since 1870. *G&G*, Vol. 43, No. 2, pp. 98–119, <http://www.gia.edu/gems-gemology/summer-2007-global-rough-diamond-production-janse>.
- Krawitz A. (2008) De Beers postpones setting up aggregation in Botswana. *Diamonds.net*, Dec. 9, <http://www.diamonds.net/news/NewsItem.aspx?ArticleID=24441>.
- Lucara completes first sale of Botswana diamonds (2012) *Solitaire*, No. 61, September, p. 28.
- Mbayi L. (2011) Linkages in Botswana's diamond cutting and polishing industry. MMCP Discussion Paper No. 6, http://www.prism.uct.ac.za/Papers/MMCP%20Paper%206_0.pdf.
- Mellier P. (2014) We cannot lose consumer trust in diamonds. *Professional Jeweller*, Jan. 28, <http://www.professionaljeweller.com/article-14143-we-cannot-lose-consumer-trust-in-diamonds/>.
- Mokone O., Mogapi S. (2013) The treacherous home coming journey of Botswana diamonds. *Sunday Standard Online*, Nov. 25, <http://www.sundaystandard.info/article.php?NewsID=18502&GroupID=4>.
- Sanchez L. (2006) Botswana: A rags to riches story. *Jewellery News Asia*, No. 256, January, pp 141–152.
- Shor R. (1990) Prosperity & politics. *JCK*, Vol. 161, No. 6, June, pp. 56–72.
- (2013a) Botswana: Making beneficiation work. *GIA Research & News*, June 24, <http://www.gia.edu/research-news-botswana-making-beneficiation-work>.
- (2013b) Industry Analysis: Demand improves after slow autumn, but challenges remain. *GIA Insider*, <http://www.gia.edu/gia-news-research-march-2013-demand-improves-slow-autumn>.
- Spektorov Y., Linde O., Cornelissen B., Khomenko R. (2013) The global diamond report 2013: Journey through the value chain. Bain & Company Insights, Aug. 27, <http://www.bain.com/publications/articles/global-diamond-report-2013.aspx>.
- Transparency International (2013) Botswana. <http://www.transparency.org/country/#BWA>
- Weldon R. (2001) Diamonds for good. *Professional Jeweler*, January, <http://www.professionaljeweler.com/archives/articles/2001/jan01/0101dn1.html>.
- Yellowknife diamond-cutting plant's future in limbo (2009) CBC News, June 11, <http://www.cbc.ca/news/canada/north/yellowknife-diamond-cutting-plant-s-future-in-limbo-1.800202>.

THREE-PHASE INCLUSIONS IN EMERALD AND THEIR IMPACT ON ORIGIN DETERMINATION

Sudarat Saeseaw, Vincent Pardieu, and Supharat Sangsawong

Until now, the observation of three-phase inclusions in emeralds has been considered a potential indicator of Colombian origin. Nevertheless, emeralds from Afghanistan (Panjshir Valley), China (Davdar), and Zambia (Kafubu and a new deposit at Musakashi) may contain three-phase inclusions resembling those often found in specimens from Colombian deposits (Muzo, Chivor, La Pita, Coscuez, and Peñas Blancas). This article presents detailed photomicrographs of samples from these localities, with a focus on their multiphase inclusions. Also investigated are spectroscopic features and trace-element data. For the gemologist studying the origin of emeralds hosting three-phase inclusions, a powerful set of tools to aid in this determination comes from the combination of detailed microscopic examination, UV-Vis-NIR and FTIR spectroscopy, and LA-ICP-MS trace-element analysis.

The traditional practice of assigning Colombian origin to emeralds exhibiting three-phase inclusions (Giuliani et al., 1993) is in need of updating, as we now know that such inclusions are often seen in emeralds from other locations, including China, Zambia (Schwarz and Pardieu, 2009), and Afghanistan (Hammarstrom, 1989; Bowersox et al., 1991). The characterization of these inclusions using spectroscopy and chemical composition has not been documented until now.

A new Zambian deposit at Musakashi was first reported in 2005 (Zwaan et al., 2005), and field trip reports were subsequently published (Klemm, 2009 and 2010). These articles presented historical and geological information about the mine (see box A), examined the gemological properties of these new emeralds, and presented chemical analysis using electron microprobe (Zwaan et al., 2005).

The present study characterizes emeralds containing multiphase inclusions from all of the localities above by using microscopy, spectroscopy, and trace-element analysis to create a framework for geographic origin determination.

See end of article for About the Authors and Acknowledgments.

GEMS & GEMOLOGY, Vol. 50, No. 2, pp. 114–132,
<http://dx.doi.org/10.5741/GEMS.50.2.114>.

© 2014 Gemological Institute of America

MATERIALS AND METHODS

A total of 84 emeralds were studied, gathered from the GIA Field Gemology Collection and from gem merchants of Zambian and Colombian emeralds. Color ranged from light to deep green. The samples were studied in three forms: 55 were rough samples with one or two polished surface windows, 28 were fabricated as optical wafers oriented either perpendicular or parallel to the crystal's c-axis, and one was faceted. After fabrication, the samples ranged from 0.18 to 4.85 ct. The group consisted of:

- Eleven samples reportedly from Musakashi (figure 1), acquired from gem dealer Guy Clutterbuck, who visited the mines several times. Weight range: 0.57–4.85 ct.
- Ten samples collected from the Kagem mine in the Kafubu area of Zambia by author VP in the summer of 2013. Weight range: 0.29–2.22 ct.
- Fifteen samples collected from Afghanistan's Panjshir Valley by author VP in 2011. Weight range: 0.18–1.80 ct.
- Thirteen samples collected from Davdar, China, by author VP in 2005 and 2009. Weight range: 0.16–1.77 ct.
- Thirty-five Colombian samples from Muzo (12), Coscuez (12), La Pita (3), Peñas Blancas (2), and Chivor (6), acquired from Flavie Isatelle, a



Figure 1. These emeralds from Musakashi, Zambia, range from 0.57 to 4.85 ct. The rough samples were polished with one window on each. The faceted sample measures $6.29 \times 5.35 \times 3.53$ mm and weighs 0.97 ct. Photo by N. Kitdee.

field gemologist/geologist who visited in May 2010, and gem merchant Ron Ringsrud. Weight range: 0.12–4.14 ct.

Standard gemological properties were measured with a Rayner refractometer (yttrium-aluminum-garnet prism) equipped with a near sodium-equivalent light source to measure refractive index and birefringence, a Chelsea filter, and four-watt long-wave (365 nm) and short-wave (254 nm) UV lamps to observe fluorescence. Due to fracturing in the samples, coupled with their relatively small sizes, no useful specific gravity measurement was acquired. The wafers' optical path lengths were measured using a Mitutoyo Series 395 spherical micrometer with an accuracy of 2 microns. Microscopic examination was performed with GIA binocular microscopes at $10\times$ – $70\times$ magnification, using both darkfield and brightfield illumination. Other lighting techniques, including fiber-optic illumination, were employed to investigate internal characteristics. Photomicrographs were captured at up to $180\times$ magnification with a Nikon SMZ 1500 sys-

tem using darkfield, brightfield, and oblique illumination with a fiber-optic light.

Ultraviolet through visible and near-infrared (UV-Vis-NIR) spectra were collected with a Hitachi U-2900 spectrophotometer (for polarized ordinary ray spectra) at 1 nm resolution and a PerkinElmer Lambda 950 spectrophotometer at 0.3 nm resolution, operating with a 60 mm integrating sphere accessory and a Lambda polarizer accessory. Fourier-transform infrared (FTIR) spectroscopy was performed using a Thermo Nicolet 6700 FTIR spectrometer operating with a $4\times$ beam condenser accessory at 4 cm^{-1} resolution. A Renishaw inVia Raman microscope fitted with a 514 nm argon ion laser was used for identifying inclusions.

For laser ablation-inductively coupled plasma-mass spectrometry (LA-ICP-MS) chemical analysis, we used a Thermo Scientific X Series II ICP-MS combined with a Nd:YAG-based laser ablation device operating at a wavelength of 213 nm. For the ICP-MS operations, the forward power was set at 1300 W and the typical nebulizer gas flow was approximately

BOX A: EMERALDS FROM MUSAKASHI, ZAMBIA

Little information is available about the Musakashi deposit (figure A-1) reportedly discovered in 2002, and much of it is conflicting. It appears to have originally been worked by local miners from 2002 to 2004. Emeralds from Musakashi were first reported in 2005 by Antonin Seifert, Stanislav Vrána, Björn Anckar, and Jaroslav Hyršl (Zwaan et al., 2005). Seifert and his colleagues reported that these emeralds had a significantly different color from those found in the Kafubu area. The Musakashi stones were said to show an intense bluish green reminiscent of emeralds from Muzo, Colombia. The similarity did not end there:

The most interesting characteristic was the presence in all the stones of three-phase inclusions, consisting of a bubble and a cube-shaped crystal in a liquid, almost identical to those commonly seen in Colombian emeralds.

Zwaan et al. also identified sphene, iron oxides, feldspar, and quartz as mineral inclusions.

Production reportedly resumed in 2006, starting with hand tools and progressing to the use of an excavator for a few months in 2009 (Klemm, 2009 and 2010). These reports, published after visits to Musakashi in July 2009 and August 2010, provide details adding to the history of emerald mining there.

Location and Access

During the dry season, the Musakashi area is accessible by a five-hour, 165 km (102 mile) drive from Ndola, mainly on the poorly maintained Kasempa road (Klemm, 2009 and 2010).

Production and Distribution

According to the mine director, the area produced about 15–20 kg of emeralds from its discovery through late 2010 (Klemm, 2010). Gem merchant Guy Clutterbuck, who supplied some of the samples for this study, reported to one of the authors in 2013 and 2014 that limited emerald mining was still taking place near Musakashi.



Figure A-1. This map shows the location of the Kafubu and the Musakashi emerald deposits.

0.90 L/min. The carrier gas used in the laser ablation unit was He, set at approximately 0.78 L/min. The alignment and tuning sequences were set to maximize Be counts and keep the ThO/Th ratio below 2%. Laser ablation conditions consisted of a 40 μm diameter laser spot size, a fluence of $10 \pm 1 \text{ J/cm}^2$, and a 7 Hz repetition rate. For quantitative analysis, samples must be calibrated against an external standard of known composition, which meant measuring the signals for the elements of interest in the sample and comparing them to the signals for a standard with known concentrations of those elements. Generally, NIST 610 and 612 glasses were used for calibration standards. All elemental concentrations were calculated by applying ^{29}Si as an internal standard, with Si concentration calculated from the theoretical value of beryl (31.35 wt. %). Laser spots were applied in the same area where UV-Vis spectra were collected, which was usually clean and had an even color dis-

tribution, though color-zoned areas were also sampled (figure 2).

RESULTS

Gemological Properties. The samples' gemological properties are summarized in table 1. The refractive indices varied from 1.570 to 1.588 for n_e and 1.576 to 1.593 for n_w , with birefringence between 0.006 and 0.010. Emeralds from Musakashi, Davdar, and all the Colombian deposits had lower RI than the samples from Kafubu and Panjshir. The Musakashi emeralds displayed a particularly strong pink reaction in the Chelsea color filter, while a pink to strong pink display was typical in samples from all other localities except for Kafubu, in which there was no reaction.

Microscopic Characteristics. *Musakashi, Zambia.* In the 11 samples reportedly from Musakashi, the most common inclusions were three-phase, usually con-

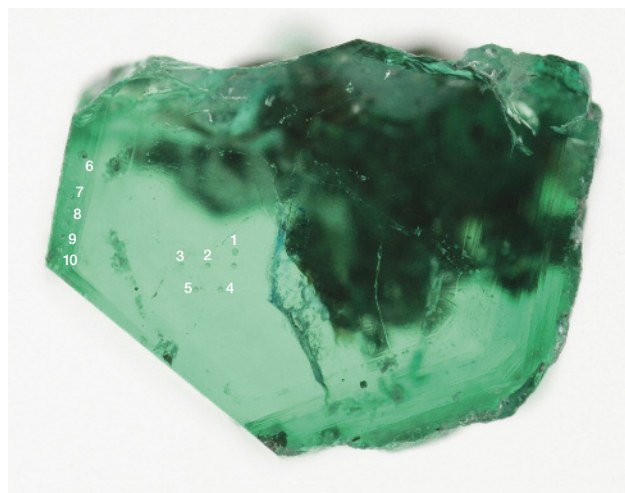


Figure 2. This optical wafer from a Muzo emerald provides an example of the LA-ICP-MS sample points selected in this study. Heavily included areas were avoided in favor of well-crystallized zones in the sample that best represent the chemical composition of that emerald. Photo by S. Engniwat.

taining at least two colorless transparent crystals and a rather small gas bubble suspended in a fluid (figures 3 and 4). Such inclusions were found in every sample we studied. The gas bubble always measured within the size range of the two crystals in the multiphase inclusion. In those inclusions containing two crystals, both crystals appeared to be singly refractive under cross-polarized illumination. The larger crystal was essentially cubic and bright, while the smaller one was rounded and faint (figure 3, A and B). In many samples, the multiphase inclusions also hosted one or more small dark to black crystals, and occasionally tiny colorless or whitish crystals (figures 3 and 4). Some of these inclusions were identified by Raman spectroscopy (figure 4); the gas phase was identified as CO₂ (peaks at 1284 and 1387 cm⁻¹). The singly refractive cubic crystals displayed only the emerald spectrum and no Raman lines, suggesting they could be halides (Venkateswaran, 1935). Daughter crystals

were identified as calcite (peaks at 283, 713, and 1085 cm⁻¹). An additional peak at 2328 cm⁻¹ was assigned to N₂. These results match those for fluid inclusions found in Colombian emeralds (Giuliani et al., 1994), but SEM is needed to identify the different complex mixed salts and daughter minerals. The shape of the inclusions was usually irregular, with numerous branches. In rare cases they appeared needle-like (figure 3C) or jagged (figure 3D).

Under darkfield illumination, tube-like growth features (figure 5) were found in 10 of the 11 Musakashi samples. The tubes were oriented parallel to the prism faces of the crystal, a common feature in emeralds. Each sample had an evenly distributed green color except for one that displayed color banding ranging from strong green to colorless perpendicular to the c-axis and the growth tubes.

Solid inclusions were quite rare. Of the 11 emeralds, only four hosted mineral inclusions that were not part of multiphase inclusions. The most common

In Brief

- Three-phase inclusions in emerald, once considered a reliable indicator of Colombian origin, have also been observed in specimens from Zambia, Afghanistan, and China.
- Microscopy, spectroscopy, and trace-elemental analysis were used to characterize 84 emeralds with multiphase inclusions.
- A promising basis for determining the geographic origin of emeralds comes from a combination of these methods.

crystal inclusions identified using Raman spectroscopy were colorless and transparent euhedral calcite crystals (figure 6, left). Also found were several opaque and metallic euhedral inclusions resembling

TABLE 1. Gemological properties of emeralds from various sources.

Property	Musakashi, Zambia	Kafubu, Zambia	All Colombia	Davdar, China	Panjshir, Afghanistan
Refractive indices					
n _e	1.572–1.578	1.582–1.588	1.570–1.573	1.577–1.580	1.572–1.580
n _ω	1.580–1.582	1.590–1.593	1.576–1.580	1.583–1.588	1.580–1.590
Birefringence	0.006–0.008	0.005–0.008	0.006–0.008	0.005–0.008	0.007–0.010
Chelsea filter	Strong pink	Inert	Pink to strong pink	Pink	Inert to pink

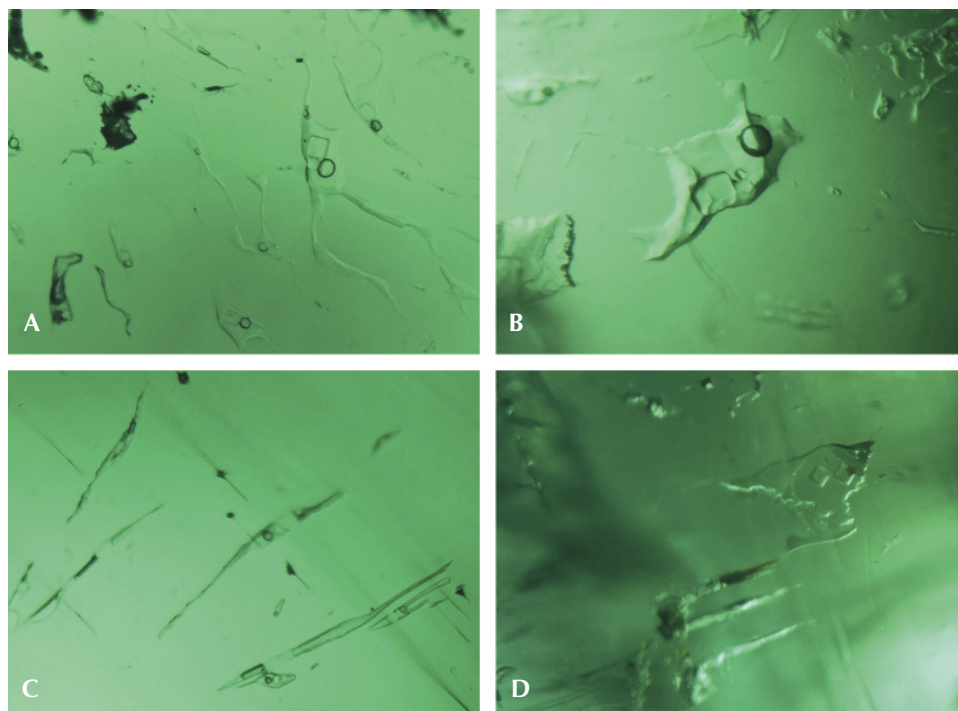


Figure 3. Three-phase inclusions in Musakashi emeralds. A: The larger multi-phase inclusion displays several crystals and a small gas bubble. B: Along with the gas bubble, at least three colorless crystals and one or two tiny dark crystals are visible. C: Two colorless transparent crystals and a small gas bubble in elongated multiphase inclusions. D: Two colorless transparent crystals with a small gas bubble and a tiny black crystal in irregularly shaped multiphase inclusions. Photomicrographs by S. Saeseaw, brightfield illumination. Image widths 9 mm (A) and 7 mm (B–D).

iron oxide, possibly hematite or the martite variety of hematite (figure 6, center), and some whitish translucent crystals identified as cryolite (figure 6, right). The iron oxide minerals identified usually occur in granitic pegmatites, but here they appeared in an emerald that also hosted pyrite and calcite inclusions.

Kafubu, Zambia. Most of the inclusions in the Kafubu samples were multiphase and rectangular in shape (figure 7), but some were quite irregular in outline (figures 8 and 9). These inclusions typically hosted some liquid and a gas bubble, but in several cases it was possible to see a solid third phase. Usu-

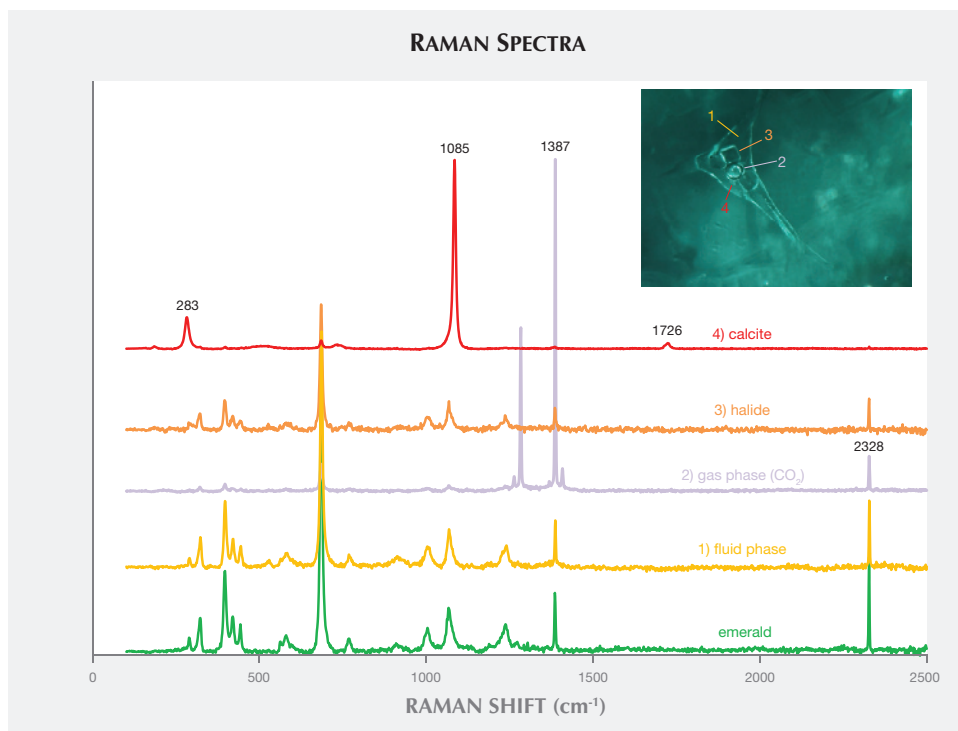


Figure 4. This Musakashi emerald clearly displays a gas bubble, a cubic crystal, two rounded colorless crystals, a tiny black crystal, and two tiny whitish rhombohedra. Raman spectroscopy was used to identify the host emerald (green), the CO₂ gas bubble (purple), the square halide crystal (orange), and the smaller carbonate crystal (red). Photomicrograph by S. Saeseaw; brightfield illumination.



Figure 5. Growth tubes parallel to the prism faces of the crystal are visible in this Musakashi emerald. Photomicrograph by S. Saeseaw, brightfield illumination. Image width 27 mm.

ally the associated crystal had very low relief. When the inclusions were studied between crossed polarizers, the crystal showed evidence of being doubly refractive (figure 9). This was very different from our observations of the Musakashi emeralds, which had at least two singly refractive crystals (halides) trapped within the multiphase inclusions.

Another interesting observation of the Kafubu emeralds was that when the inclusion and the gas bubble were flat, we could estimate the size ratio between them. In these samples, the gas bubble appeared to contain one-third to one-half the volume of the multiphase inclusion at room temperature. This was much larger than the gas bubble observed in emeralds from Musakashi, which indicates considerably different temperature and pressure conditions of formation and possibly very different fluid composition. These observations suggest a different geologic background.

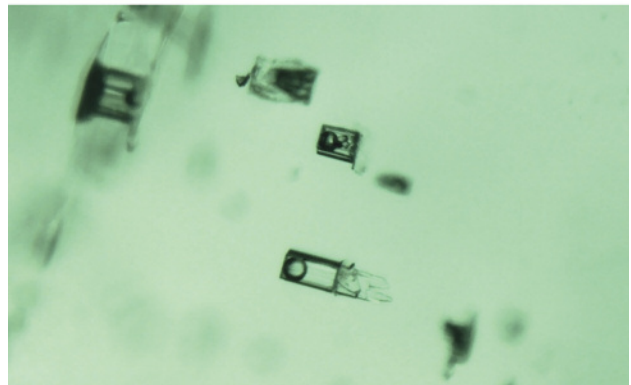
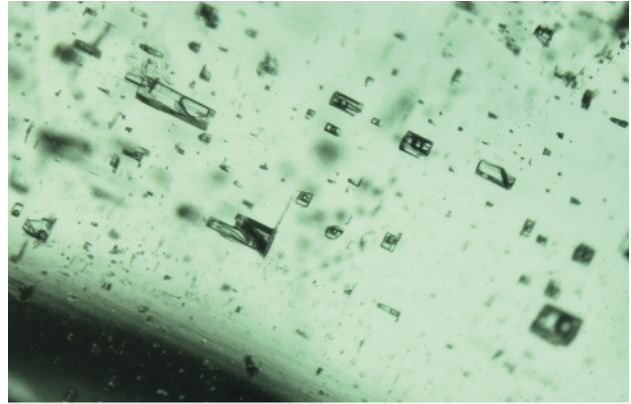
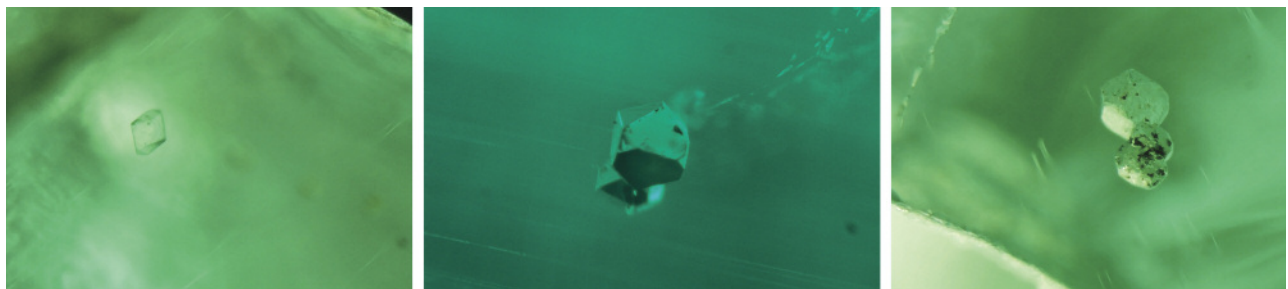


Figure 7. Top: Rectangular multiphase inclusions were visible in emeralds from Kafubu. Bottom: Detail of rectangular multiphase inclusions in an emerald from the Kagem mine reveals relatively large gas bubbles, with and without solid inclusions. Photomicrographs by V. Pardieu, brightfield illumination. Image widths 27 mm (top) and 11 mm (bottom).

Solid inclusions with no associated liquid or gas inclusions were quite common in all the samples from Kafubu. One of the authors (VP) visited Kagem

Figure 6. Single-phase solid inclusions found in the emeralds from Musakashi vary significantly and consist of: a colorless transparent crystal identified by Raman spectroscopy as calcite (left); a metallic opaque crystal, possibly hematite or martite (center); and whitish translucent crystals identified using Raman spectroscopy as cryolite (right). Photomicrographs by S. Saeseaw, darkfield illumination. Image widths 13 mm (left), 11 mm (center), and 10 mm (right).



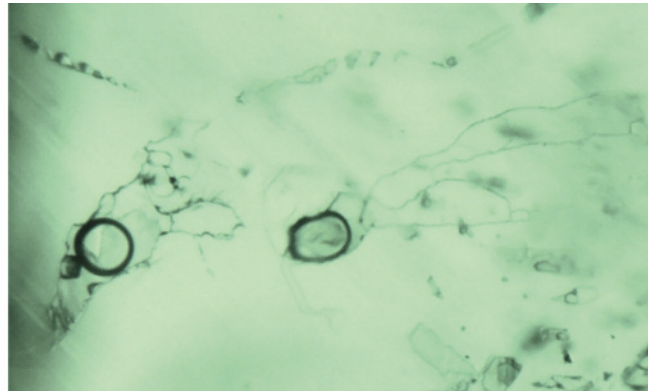
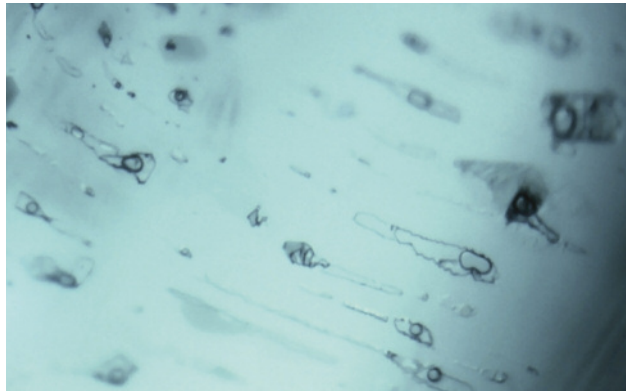


Figure 8. Irregularly shaped multiphase inclusions in emeralds from Kafubu showed liquid containing a gas bubble and in some cases a solid third phase. Photomicrographs by V. Pardieu, brightfield illumination. Image widths 13 mm (left) and 10 mm (right).

in 2011 and 2012 and found that the emeralds there were commonly associated with quartz, pyrite, dark brown to black tourmaline, mica, and chlorite (figure 10). The most common crystal inclusions found had dark, opaque, and dendritic features, identified by Raman spectroscopy as pyrolusite, amphibole, and tourmaline (figure 11), as well as chlorite and mica. These inclusions offer telltale features that reflect the mineral associations found at the site.

Panjshir Valley, Afghanistan. Most of the inclusions in emeralds from the Panjshir Valley are multiphase. These typically have an elongated needle-like shape (figures 12 and 13), but they may also display an irregular (figure 14) or even jagged aspect (figure 12). These inclusions often host several cubic to rounded

transparent crystals, and sometimes small, dark opaque crystals. Examined under crossed polarizers, the cubic crystals appeared to be singly refractive and the small rounded crystals appeared doubly refractive (again, see figure 12). These observations were identical to those previously reported (Bowersox et al., 1991). The gas bubble appeared to be smaller than the main crystal inclusion (which was usually cubic).

Davdar, China. Most of the inclusions in the samples from Davdar were multiphase. These were often jagged or irregular in shape (figures 15–17) and occasionally needle-like (figure 16). Some fluid inclusions contained two halide cubes (figure 16), as reported previously

Figure 9. Irregular multiphase inclusions in emeralds from Kafubu. Under cross-polarized illumination, a small doubly refractive crystal inclusion becomes visible as a bright spot (see red arrow). Photomicrograph by V. Pardieu; image width 13 mm.

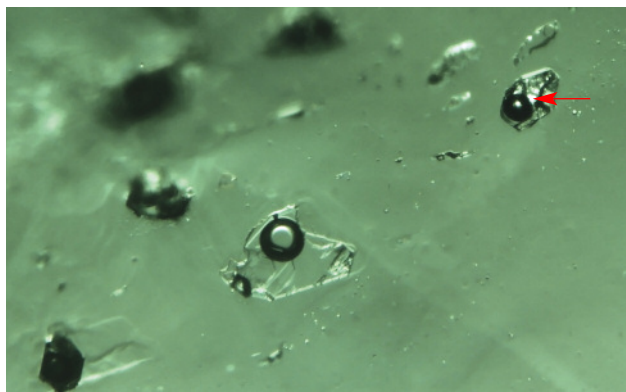
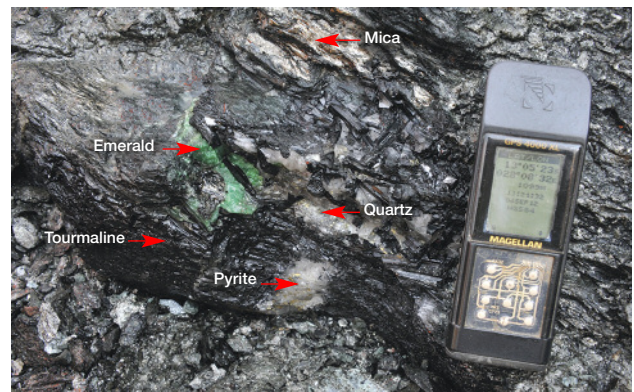


Figure 10. An interesting scene observed at the Kagem mine: an emerald crystal associated with black tourmaline, quartz, mica, and pyrite. It was not surprising to see this mineral association at the site, as it can also be seen inside the gem. This offers a fine example of the direct association between the geological background and the internal world of a gemstone. Photo by V. Pardieu.



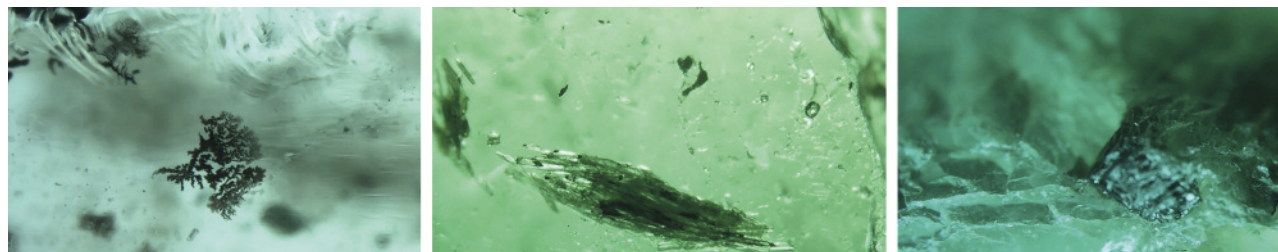


Figure 11. Various single-phase solid inclusions were observed in emeralds from the Kagem mine. Left: A dendritic black opaque mineral inclusion (probably pyrolusite). Center: A dark brownish transparent mineral inclusion identified by Raman spectroscopy as amphibole. Right: A dark brownish mineral inclusion identified as tourmaline with Raman. Photomicrographs by V. Pardieu, brightfield illumination. Image widths 20 mm (left) and 40 mm (center and right).

(Marshall et al., 2012). In these emeralds, the gas bubble was smaller than the whole inclusion and usually somewhat smaller than the associated cubic crystals.

Colombia. The most common inclusion in the Colombian emeralds was a jagged multiphase inclusion hosting a gas bubble and one or more cubic crystals (figures 18–20). In these stones, the gas bubble was usually smaller than the whole inclusion and no larger than the associated cubic crystal. Many of these emeralds also contained a tiny dark opaque crystal (figures 18 and 20, right) and clusters of daughter crystals, usually irregularly shaped (figures 19, bottom, and 20, left).

These daughter crystals are related to various carbonate compounds (Giuliani et al., 1994). Most of the multiphase inclusions had the classic jagged shape associated with Colombian emeralds. In several cases the shape was more elongated, like a blade (figure 20, center), and occasionally irregular (figure 20, right).

UV-Vis-NIR Spectroscopy. The samples collected for UV-Vis-NIR spectroscopy were fabricated as optical wafers oriented either perpendicular or parallel to the crystal's c-axis—with the exception of emeralds from Musakashi, which were either faceted or contained a single polished window. In this study, UV-Vis-NIR

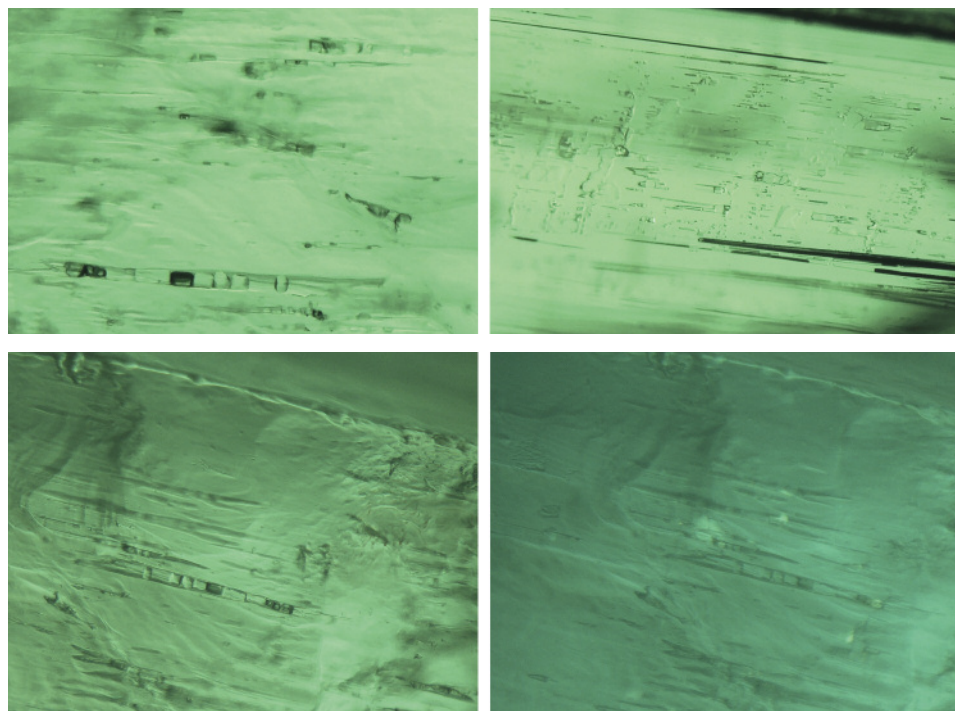


Figure 12. These Panjshir emeralds contain a needle-like multiphase inclusion hosting crystals and gas bubbles (left), and jagged, irregularly shaped multiphase inclusions hosting crystals and gas bubbles (right). Photomicrographs by V. Pardieu, brightfield illumination. Image widths 8 mm (left) and 13 mm (right).

Figure 13. Elongated needle-like multiphase inclusions, hosting several crystals and gas bubbles, in emeralds from the Kamar Safeed area near Khenj in the Panjshir Valley. Photomicrographs by S. Saeseaw, brightfield illumination (left) and crossed polarizers (right). Image widths 9 mm.

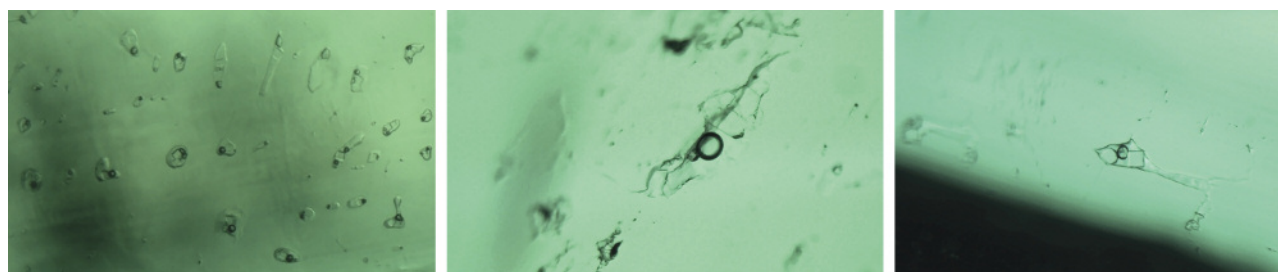


Figure 14. Left: This emerald from the Kamar Safeed area in the Panjshir Valley of Afghanistan contains an irregular blocky multiphase inclusion hosting gas bubbles, a liquid phase, and several crystals. Center: Irregularly shaped multiphase inclusion hosting a gas bubble and several crystals, from the Koskanda area near Khenj. Right: Irregularly shaped multiphase inclusion hosting a small gas bubble and several crystals (one cubic and one more rounded), from Kamar Safeed. Photomicrographs by V. Pardieu, brightfield illumination. Image widths 9 mm (left and center) and 7 mm (right).

spectra characterized the following chromophores for emerald (Wood and Nassau, 1968):

Cation	Identifying absorption characteristic	Possible geographic origin
Cr ³⁺	Bands at approximately 430 and 600 nm (ω), and at approximately 420 and 630 nm (ϵ) Lines at 476, 680, and 683 nm	Musakashi, Kafubu, Davdar, Panjshir, Colombia
Fe ²⁺	A band at 620 nm (ϵ), and a broad band at approximately 810 nm (ω , ϵ)	Strong: Kafubu Moderate: Davdar, Panjshir
Fe ³⁺	Narrow bands at 372 (ω) and 465 nm (ω , ϵ), and a band at approximately 400 nm (ω , ϵ)	Kafubu, Panjshir
V ³⁺	Bands at approximately 400 nm (ω) and 654 nm (ϵ)	Strong: Davdar, Colombia

Zambia. In the 11 unoriented samples from Musakashi, the UV-Vis spectra displayed minimum absorptions at about 348 and 510 nm for the ordinary ray. For octahedral Al³⁺ in emeralds, substituted Cr³⁺ exhibited bands at 430 and 600 nm for the ordinary ray and lines at 476, 680, and 683 nm. These emeralds showed no significant Fe²⁺-related absorption features in the NIR region, and no Fe³⁺ was observed (figure 21A).

The nine fabricated samples from Kafubu all displayed the same absorptions: UV-Vis minima at 367 and 514 nm for the ordinary ray, and at 390 and 500 nm for the extraordinary ray. Moreover, a narrow Fe³⁺ band was observed at 372 nm in the ordinary ray but not the extraordinary ray, and a strong Fe²⁺ band at around at 810 nm was recorded (figure 21B).

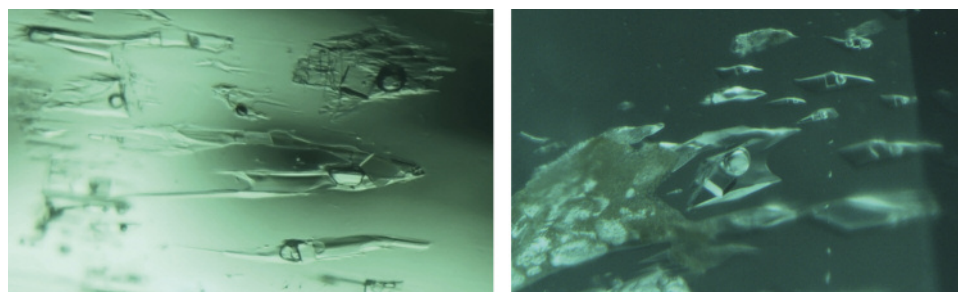


Figure 15. Jagged multiphase inclusions hosting gas bubbles and several crystals in emeralds from Davdar, China. Photomicrographs by S. Saeseaw, brightfield illumination. Image widths 7 mm.

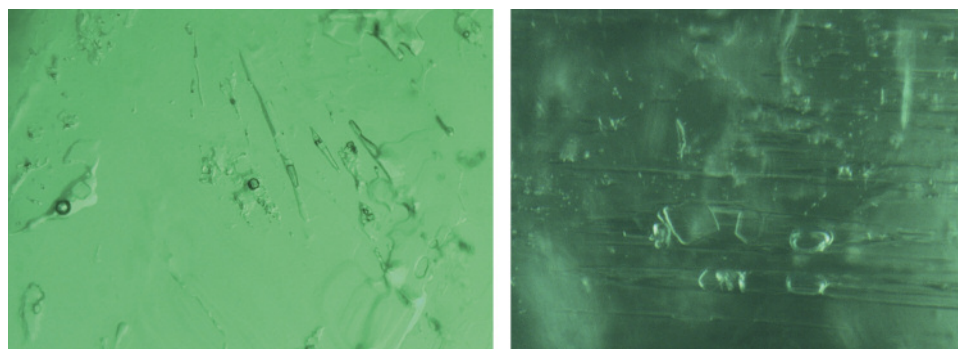


Figure 16. Irregular and needle-shaped multiphase inclusions found in emeralds from Davdar, hosting single gas bubbles, multiple cubic crystals, rounded transparent crystals, and tiny black opaque solids. Photomicrographs by S. Saeseaw, brightfield illumination. Image widths 8 mm (left) and 7 mm (right).

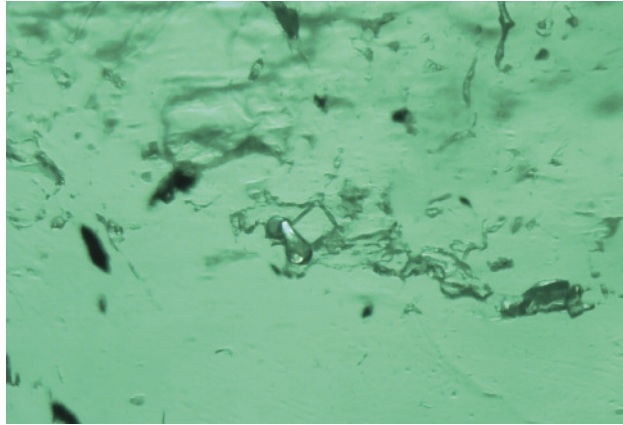


Figure 17. Irregular multiphase inclusions with a gas bubble and a cubic crystal in an emerald from Davdar. Photomicrograph by S. Saeseaw, brightfield illumination. Image width 8 mm.

Afghanistan. Nine fabricated samples were studied. Their UV-Vis spectra showed the Fe^{3+} peak at 372 nm for the ordinary ray and moderate Fe^{2+} absorption at 810 nm, similar to Kafubu emeralds. Yet some of the Panjshir samples appeared to contain no Fe^{3+} , due to a low iron concentration, and they also exhibited peak heights at 810 nm that were lower than in the Kafubu samples (figure 21C).

China. Ten samples were measured, but only three were fabricated perpendicular or parallel to the c-axis. A representative UV-Vis spectrum is displayed in figure 21D. Davdar and Musakashi emeralds presented similar spectra, but with higher Fe^{2+} absorption in the NIR region of the former. But no Fe^{3+} features were observed, and strong V^{3+} absorptions were detected.

Colombia. The eight fabricated samples from Chivor, Coscuez, and Muzo exhibited UV-Vis spectra similar to those of Musakashi emeralds. Neither Fe^{2+} nor Fe^{3+}

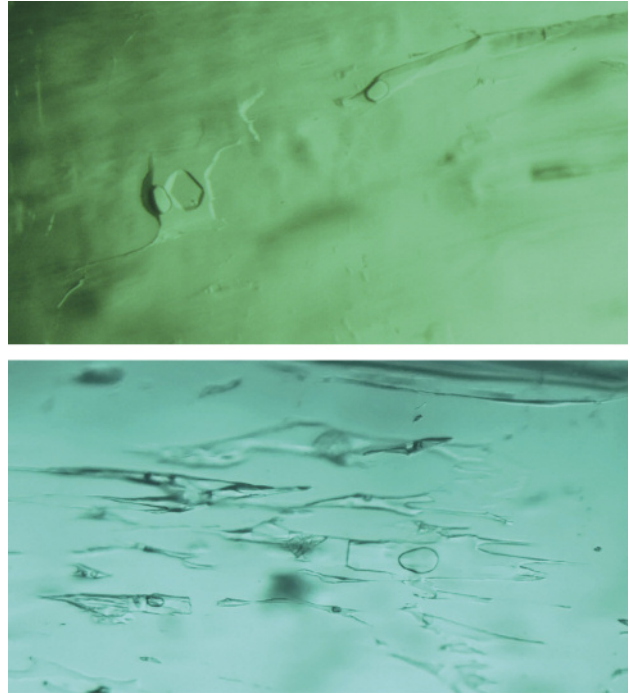


Figure 19. Examples of multiphase inclusions in emeralds from Colombia. Top: This multiphase inclusion hosting a gas bubble and a large colorless cubic crystal with barely visible edges, which appears larger than the bubble, is seen in an emerald from the La Pita area. Bottom: Another example of jagged multiphase inclusions hosting a gas bubble, a large colorless cubic crystal (larger than the bubble), and possibly a smaller cluster of daughter crystals. This sample was from the Coscuez area. Photomicrographs by S. Saeseaw, brightfield illumination. Image widths 9 mm (top) and 10 mm (bottom).

were observed. Absorptions corresponding to V^{3+} were present at about 400 and 654 nm (figure 21E).

FTIR Spectroscopy. FTIR spectra were recorded in the 400–7800 cm^{-1} region, with the major area of

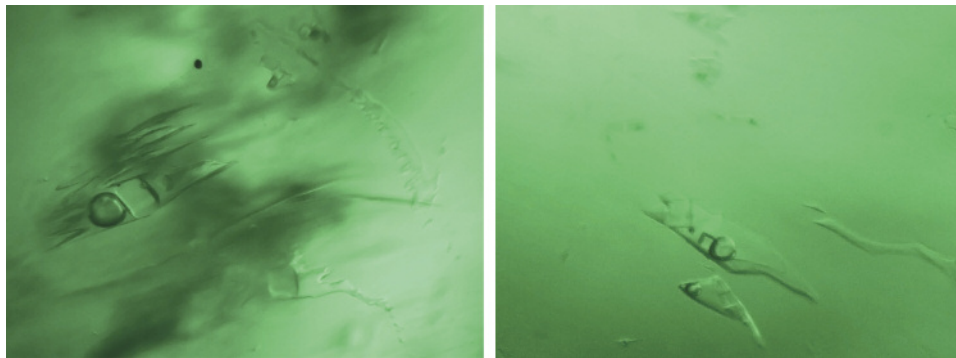


Figure 18. Two classic jagged multiphase inclusions in emeralds from Muzo, Colombia, hosting a gas bubble with two cubic crystals and a tiny dark opaque crystal. Photomicrographs by S. Saeseaw, brightfield illumination. Image widths 9 mm (left) and 7 mm (right).



Figure 20. Left: In Colombian emeralds such as this one from Muzo, liquid was often associated with a gas bubble as well as a large colorless cubic crystal. In this sample, some smaller colorless and dark crystals are also visible. Center: Elongated blade-like multiphase inclusions hosting a gas bubble and a large colorless cubic crystal (slightly larger than the bubble) in an emerald from Coscuez. Right: In some cases, the multiphase inclusions were not jagged or elongated blades but irregularly shaped. Here the multiphase inclusions from a Coscuez emerald host a gas bubble, a large colorless cubic crystal (about the same size as the bubble), and some smaller crystals. Photomicrographs by S. Saeseaw, brightfield illumination. Image widths 13 mm (left) and 8 mm (center and right).

interest between 4500 and 7500 cm^{-1} —specifically, the area related to water molecule vibrations. The resulting spectra indicated that the emeralds could be divided according to type I and II water molecule assignments (Wood and Nassau, 1968; Schwarz and Henn, 1992). Type I water molecules are oriented in the channels, not linking to other alkali metal ions, and their H-H direction is parallel to the c-axis. Type II molecules are located adjacent to alkali metal ions in the channel, and their H-H direction is perpendicular to the c-axis.

All of the emeralds contained type I water molecules except the samples from Kafubu (figure 22). The extraordinary ray plots of type I emeralds each exhibited a 7140 cm^{-1} peak that was more intense than the peaks found at 7095 and 7072 cm^{-1} . The plots from type II emeralds displayed their highest-intensity peak at 7095 cm^{-1} . These results matched previous reports (Wood and Nassau, 1968; Schwarz and Henn, 1992) that assigned the 7140 cm^{-1} peak to type I water molecules and the 7095 cm^{-1} peak to type II water molecules.

Trace-Element Analysis. All 84 emeralds from the five different localities were analyzed using LA-ICP-MS (table 2).

Zambia. The Musakashi emeralds shared similar trace-element chemistry with the Colombian samples. They contained low concentrations of alkali metals (Li, Na, K, Rb, and Cs); Mg, and Fe, as well as minor traces of Ni. Total alkali ion concentrations averaged 4250 ppmw. In terms of chromophore elements, the concentrations of Cr were greater than V, and the Cr/V ratio ranged between 1.7 and 5.3. Fe

content varied from 680 to 1,490 ppmw. Trace amounts of Ni were also present.

The samples from Kafubu were rich in the trace elements Li, Na, K, Rb, Cs, Mg, and Fe, as well as Ti, Sc, Mn, Ni, and Zn. Total alkali ion concentration was as high as 34,747 ppmw; Mg and Fe contents averaged 15,004 and 8,621 ppmw, respectively. The chromophore elements Cr and V varied from 733 to 4,330 ppmw for Cr and from 71 to 180 ppmw for V; the Cr/V ratio was between 8 and 40. Small amounts of Sc were detected, from 12 to 75 ppmw. Significant traces of Mn, Ni, and Zn were also present.

Afghanistan. Afghan emeralds from Panjshir contained on average 10,780 ppmw of alkali ions. The chromophore elements Cr and V ranged from 118 to 4,730 ppmw and from 255 to 3,680 ppmw, respectively. The Cr/V ratio was 0.3 to 3.3. Iron contents ranged from 1,010 to 9,820 ppmw. Scandium contents were detected up to 2,290 ppmw, the highest concentration for this element in our study.

China. The emeralds from Davdar contained relatively lower amounts of combined alkali ions, 8,835 ppmw on average. Their green color was caused by the presence of both Cr and V, which varied from 146 to 5,630 ppmw for Cr and from 657 to 6,960 ppmw for V. The ratio for Cr/V was 0.1 to 1.0. Iron concentrations ranged up to 4,350 ppmw.

Colombia. All the Colombian emeralds contained low concentrations of alkali metals (Li, Na, K, Rb, and Cs), as well as Mg and Fe. Total alkali ion concentrations averaged 4,725 ppmw. The chromophore elements Cr and V ranged from 172 to 10,700 ppmw for

UV-VIS-NIR ABSORPTION SPECTRA

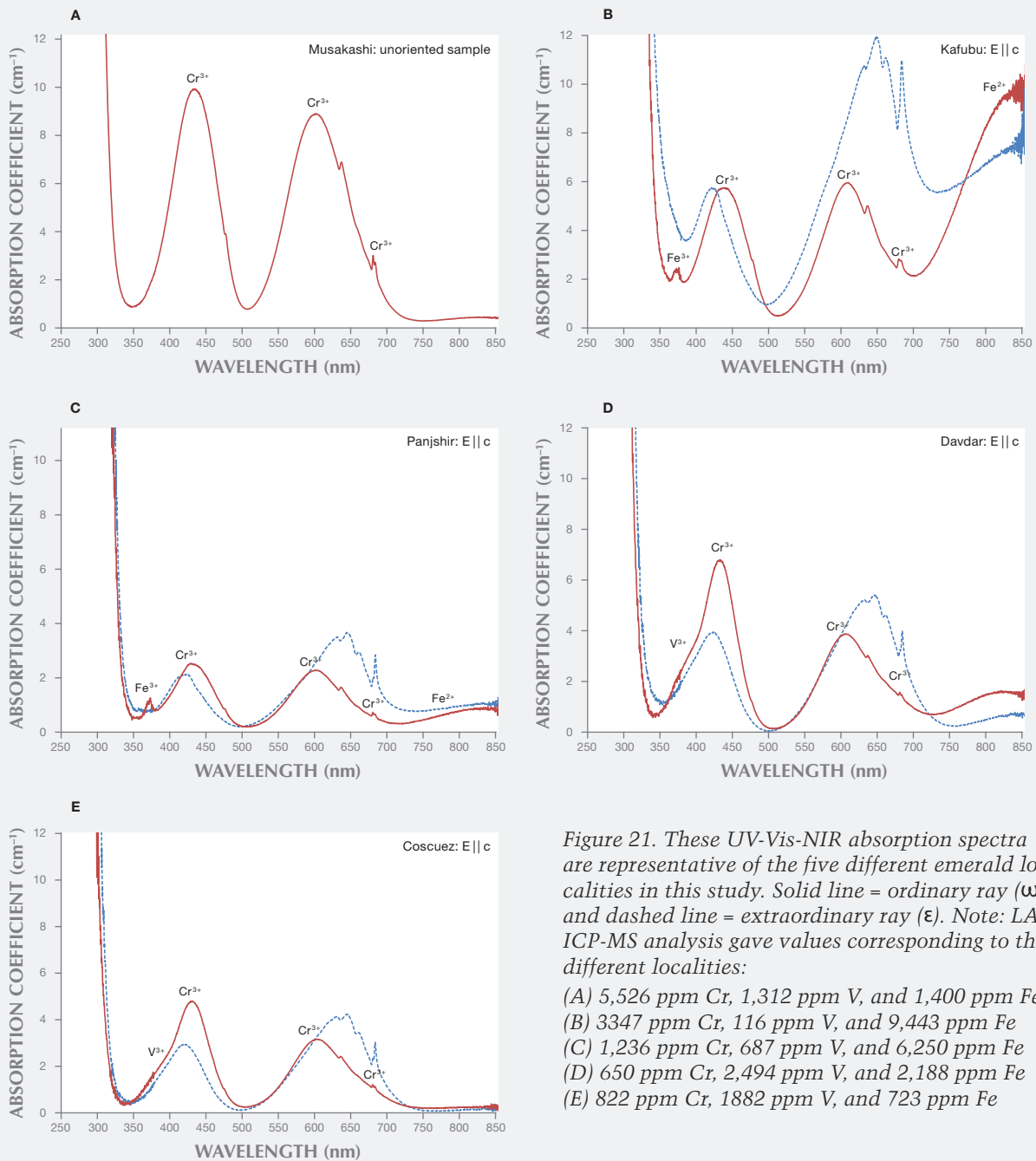


Figure 21. These UV-Vis-NIR absorption spectra are representative of the five different emerald localities in this study. Solid line = ordinary ray (ω) and dashed line = extraordinary ray (ϵ). Note: LA-ICP-MS analysis gave values corresponding to the different localities:

- (A) 5,526 ppm Cr, 1,312 ppm V, and 1,400 ppm Fe
- (B) 3347 ppm Cr, 116 ppm V, and 9,443 ppm Fe
- (C) 1,236 ppm Cr, 687 ppm V, and 6,250 ppm Fe
- (D) 650 ppm Cr, 2,494 ppm V, and 2,188 ppm Fe
- (E) 822 ppm Cr, 1882 ppm V, and 723 ppm Fe

Cr and from 218 to 10,100 ppmw for V; the Cr/V ratio was between 0.04 and 3.5. La Pita contained higher Cr and V than the other Colombian mines. Overall, the Colombian emeralds contained the lowest Fe concentrations in this study, from 117 to 2,030 ppmw.

DISCUSSION

Geology. Several summaries describing the geology of major emerald deposits are available in the gemological and geological literature (Giard, 1998; Behmenburg, 2002; Groat et al., 2008), but very few have dealt

TABLE 2. Chemical composition (average ppmw) of 84 emerald samples by LA-ICP-MS.^a

Element	Musakashi, Zambia	Kafubu, Zambia	Panjshir, Afghanistan	Davdar, China	Coscuez, Colombia	Muzo, Colombia
	11 samples, 55 spots	10 samples, 165 spots	15 samples, 205 spots	13 samples, 103 spots	12 samples, 100 spots	12 samples, 89 spots
⁷ Li	55–97 (73)	360–872 (576)	78–254 (113)	72–332 (109)	52–139 (83)	28–92 (45)
⁹ Be	40,700–55,6000 (47,260)	40,600–59,000 (49,630)	44,500–57,900 (51,578)	45,800–71,400 (54,515)	45,200–57,100 (50,448)	43,400–56,800 (51,053)
²³ Na	1,150–5,900 (4,109)	14,200–20,100 (17,204)	2,470–15,600 (9,822)	4,200–12,500 (8,356)	2,530–6,500 (4,885)	1,890–9,860 (4,527)
²⁴ Mg	928–5,740 (3,652)	12,600–17,400 (15,004)	1,790–15,700 (9,197)	3,420–11,700 (7,366)	2,100–5,840 (4,176)	1,720–6,590 (3,869)
²⁷ Al	75,6000–108,000 (90,895)	64,100–92,400 (77,865)	71,900–110,000 (90,390)	81,200–153,000 (101,220)	83,400–112,000 (94,655)	81,300–109,000 (97,888)
³⁹ K	25–102 (59)	305–890 (506)	52–1,590 (670)	102–609 (340)	6–46 (14)	7–49 (26)
⁴⁵ Sc	40–240 (119)	12–75 (31)	49–2,290 (580)	54–916 (372)	2–258 (41)	34–706 (224)
⁵¹ V	588–2,100 (1,165)	71–180 (109)	255–3,680 (1,444)	657–6,960 (2,867)	656–6,210 (2,204)	673–6,920 (2,062)
⁵³ Cr	1,340–6,170 (4,211)	733–4,330 (2,287)	118–4,730 (1,832)	146–5,630 (1,333)	172–6,330 (1,156)	208–4,890 (1,620)
⁵⁷ Fe	680–1,490 (1,224)	5,900–11,600 (8,621)	1,010–9,820 (3,890)	1,230–4,350 (2,440)	285–1,130 (650)	188–2,030 (588)
⁶⁹ Ga	13–29 (20)	9–19 (15)	12–38 (24)	10–43 (23)	13–54 (28)	17–44 (30)
⁸⁵ Rb	1–5 (3)	17–105 (65)	4–110 (50)	3–29 (15)	0.7–3 (2)	0.8–5 (3)
¹³³ Cs	3–10 (6)	527–2,210 (1,391)	11–97 (49)	6–41 (15)	7–19 (12)	4–19 (11)
⁴⁷ Ti	bdl–30 (6)	6–25 (12)	bdl–67 (14)	bdl–63 (7)	bdl–27 (6)	bdl–14 (4)
⁶⁰ Ni	bdl–12 (6)	7–38 (20)	bdl–14 (2)	bdl	bdl–3 (2)	bdl–3 (1)
⁶⁶ Zn	bdl–2 (1)	12–44 (29)	bdl–5 (1)	bdl–8 (2)	bdl–2 (1)	bdl–5 (1)

^aData reported in minimum and maximum values, with average concentration in parentheses; ppmw = parts per million by weight; bdl = below detection limit.

with the newer deposits such as Davdar or Musakashi. The mention by Klemm (2010) of sandstone as a possible host rock for Musakashi emeralds is quite interesting, as calcareous sandstone was also identified as the main host rock of the emeralds from Davdar (Pardieu and Soubiraa, 2006; Michelou and Pardieu, 2009; Schwarz and Pardieu, 2009; Marshall et al., 2012). It is

very intriguing to observe similar multiphase inclusions in the stones from these two deposits.

Multiphase Inclusions. The discovery of three-phase inclusions in samples reportedly from Musakashi was rather surprising. While these inclusions are similar to those in emeralds from Colombia, Afghan-

Peñas Blancas, Colombia	La Pita, Colombia	Chivor, Colombia	Detection limit
2 samples, 10 spots 30–65 (48)	3 samples, 15 spots 24–80 (44)	6 samples, 35 spots 40–113 (67)	0.2
49,900–54,700 (52,480)	52,900–70,700 (58,666)	46,900–56,000 (50,365)	2.3
2,390–4,100 (3,226)	1,980–7,000 (4,677)	1,340–6,090 (3,448)	8.8
2,280–3,740 (2,888)	1,840–6,830 (4,475)	1,100–5,280 (2,859)	0.4
96,600–109,000 (102,750)	92,300–129,000 (105,493)	84,600–110,000 (97,188)	3.6
8–11 (10)	bdl–40 (24)	bdl–30 (14)	3.0
36–82 (57)	94–344 (248)	6–173 (87)	0.8
317–3,960 (2,000)	6,000–10,100 (8,004)	218–2,020 (846)	0.3
1,810–2,540 (2,183)	2,940–10,700 (5,645)	671–2,880 (1,334)	2.5
164–656 (400)	200–383 (280)	117–862 (366)	18.4
12–30 (20)	32–36 (34)	7–40 (19)	0.1
0.6–1	bdl–4 (3)	0.5–3 (2)	0.1
3–10	5–12	6–16 (11)	0.1
4–7 (4)	bdl–5 (4)	bdl–7 (4)	2.1
bdl	bdl	bdl	0.5
bdl	bdl	bdl	0.4

istan, and China (Xin Jiang), specimens from the neighboring Kafubu area of Zambia contain two-phase inclusions or three-phase inclusions with crystals that are only visible under cross-polarized light (Zwaan et al., 2005). The stones reportedly from Musakashi had multiphase inclusions hosting not only liquid and gas bubbles but also several solid

phases. Usually at least two crystals could be seen: one cubic, one more rounded, and often several smaller ones ranging from transparent colorless to opaque black. This was not typically observed in our Colombian samples. The cubic crystals, the gas phase, and the daughter crystals were identified by Raman spectroscopy as a halide, CO₂, and carbonate, respectively. These results are identical to those reported for fluid inclusions in Colombian emerald (Giuliani et al., 1994). The shape of the cavity housing the multiphase inclusions in our Musakashi samples was usually quite irregular, not unlike those seen in those from Colombia, Afghanistan, and China. In some cases the cavity's shape was similar to the jagged form commonly found in Colombian emeralds or the elongated needle shape typical of Panjshir emeralds. But for the most part, the cavities in the Musakashi samples were similar to those associated with Davdar.

Unlike the Kafubu emeralds, the multiphase inclusions in our Musakashi samples also contained more crystals with single refraction than double refraction. The gas bubbles in Musakashi multiphase inclusions were smaller than those found in Kafubu material. These results reflect the possibility that different temperature and pressure conditions, geologic backgrounds, and fluid compositions existed when the emeralds from these two neighboring locations formed.

Spectroscopy. *UV-Vis-NIR.* The UV-Vis-NIR spectra were characterized by absorptions that resulted from the presence of the chromophores chromium, vanadium, and iron, illustrated in figure 21. The Musakashi emeralds shared similar absorption characteristics with those from Colombia and Davdar, but with lower V³⁺ absorption. Furthermore, the Musakashi samples showed no significant Fe²⁺-related absorption features at about 810 nm, and no Fe³⁺ absorption at about 372 nm, which distinguished them from Davdar and most of the Kafubu material. Kafubu and Panjshir samples showed a strong narrow absorption band at 372 nm corresponding to Fe³⁺, as well as a broad band around 810 nm corresponding to Fe²⁺. The Davdar emeralds displayed only the Fe²⁺-related broad band. The 810 nm peak is related to Fe content, though their relationship has not been clearly established yet. With higher iron concentration, the peak intensity at 810 nm increased, along with the peak at 372 nm. In this study, we measured the 810 nm peak height of the ordinary ray, which ranged from 7 to 11 cm⁻¹ (Kafubu) and from 1 to 5 cm⁻¹ (Panjshir).

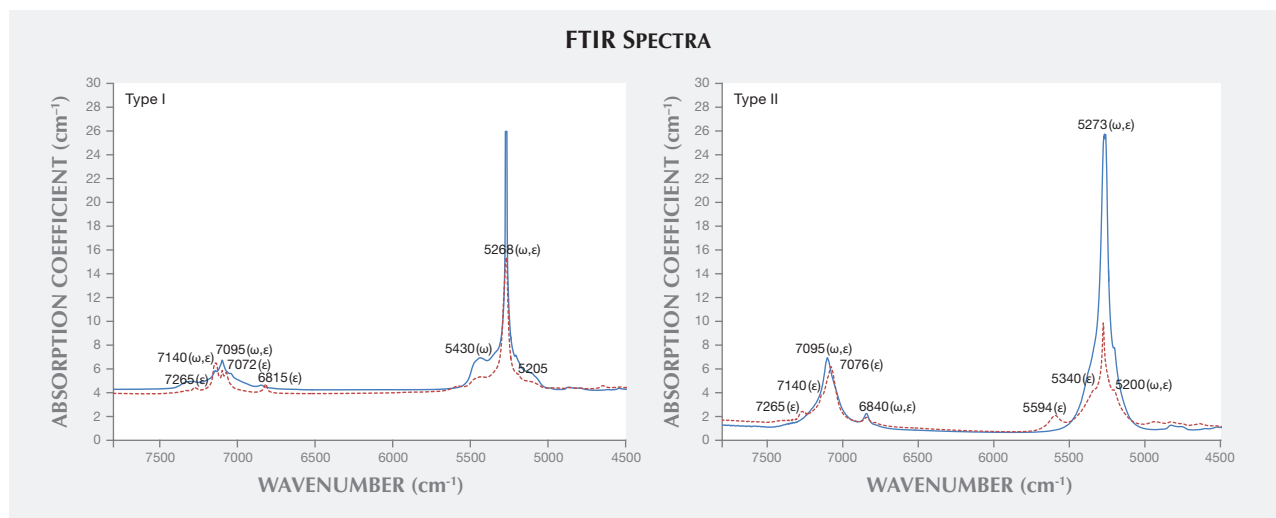


Figure 22. Representative FTIR spectra (solid line = ordinary ray ω , dashed line = extraordinary ray ϵ) illustrating the type I and II water observed in emeralds from each origin. Type I samples showed peaks at 7140 (ϵ , ω), 7095 (ϵ , ω), 7072 (ϵ), 7042 (ω), 6843 (ω), 6815 (ϵ), 5430 (ω), 5268 (ω , ϵ), and 5205 (ω , ϵ) cm^{-1} . Type II samples (which were only from Kafubu) showed peaks at 7265 (ϵ), 7140 (ϵ), 7095 (ω , ϵ), 7076 (ϵ), 6840 (ω , ϵ), 5594 (ϵ), 5340 (ϵ), 5273 (ω , ϵ), and 5200 (ω , ϵ) cm^{-1} .

FTIR. The FTIR spectra recorded for the type I emerald samples all showed a 7140 cm^{-1} peak, higher than those at 7095 and 7072 cm^{-1} for the extraordinary ray, related to low alkali metals contents in the channels of the beryl structure. (Again, Kafubu was the only locality that yielded type II samples.) Total alkaline ion concentration, determined using LA-ICP-MS, showed no relationship with the peak at 7140 cm^{-1} . This was because some of the alkali metals may exist in sites other than those that influence the water spectrum. For example, Li may occur in Be or Si sites, depending on ion sizes.

Trace-Element Variations. The samples from Musakashi were characterized by LA-ICP-MS as having low concentrations of alkali metals and Mg, and high Al content. Most of the Kafubu emeralds seemed to have an abundance of the alkali metals Li, Na, K, Rb, and Cs. Various log-log population fields generated from the trace-element data collected (with multiphase inclusions) showed great potential in distinguishing geographic origin (figures 23–25). To explore this further, we added published data for Brazilian emeralds from Rio Grande do Norte (Zwaan et al., 2012), which confirmed the usefulness of this separation criterion. A log-log plot of Li versus Cs content can easily separate the two Zambian deposits (figure 23). The same type of plot can generally distinguish Panjshir and Davdar from Musakashi and Colombian emeralds, even with a small overlapping

area. This plot may also help differentiate between Davdar and Panjshir, as the areas overlap only slightly. We compare this to Schwarz and Pardieu (2009), whose diagram of Ga versus Fe showed nearly complete overlapping between Davdar and Panjshir, rendering it impossible to distinguish between the two locations. As the population fields in the log-log plot of Li vs. Cs overlap for Musakashi and all Colombian emeralds, a plot of Fe vs. K and Fe vs. Ga proved useful in separating between these two origins (figures 24 and 25). In addition, the recorded Ni content was just above the detection limit in emeralds from Musakashi but below the detection limit in most Colombian samples. Average Fe concentrations were highest in samples from Kafubu. Moreover, the Panjshir emeralds contained higher Sc, which was very useful in distinguishing them.

CONCLUSIONS

For many years, the observation of three-phase inclusions in emeralds was considered a reliable indicator of Colombian origin. But with the arrival in the market of emeralds from Panjshir (Afghanistan), Davdar (China), and Kafubu and Musakashi (Zambia) that may also display three-phase inclusions, origin determination became more complicated. There are some notable differences, however.

Emeralds from the Musakashi deposit are of particular interest, as their internal features are quite different from those found in the well-known deposits

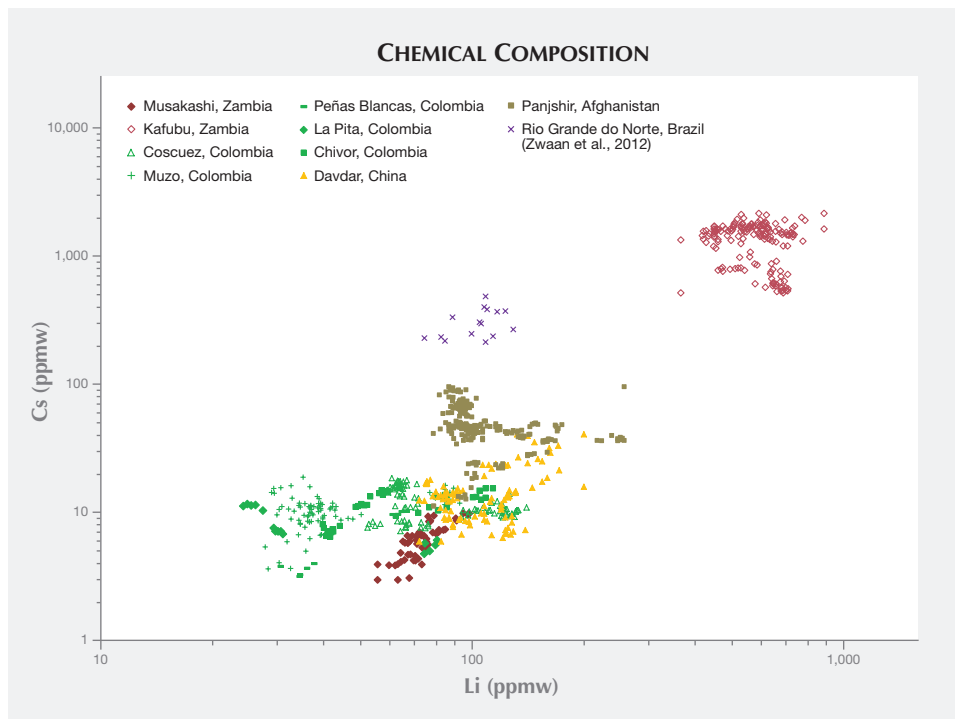


Figure 23. Log-log plot of lithium (Li) versus cesium (Cs) concentrations in emeralds from the five different localities.

in the neighboring Kafubu area. The inclusion scene within the Musakashi emeralds is indeed dominated by multiphase inclusions that are commonly associated with Colombian origin. Nevertheless, the outline and make-up of these multiphase inclusions may be more irregular than those typical of Colombian de-

posits. Furthermore, the tendency of Musakashi emeralds to have at least two crystals associated with a gas bubble may raise questions about a possible Zambian origin.

Emeralds from Panjshir, Afghanistan, are often characterized by elongated needle-shaped multiphase

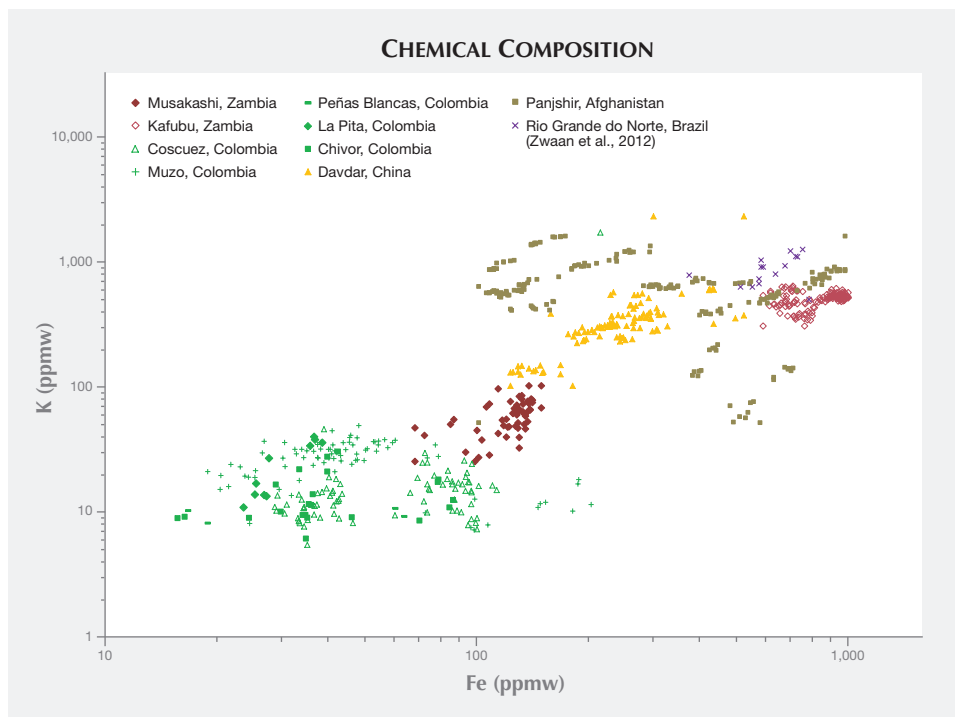


Figure 24. Log-log plot of iron (Fe) versus potassium (K) concentrations in emeralds from the five different localities.

TABLE 3. Summary of physical properties, UV-Vis-NIR absorption data, and trace-element chemistry of emeralds from five different localities.

Locality	Refractive index	Color filter reaction	Microscopic characteristics	UV-Vis spectroscopy (cations in addition to Cr ³⁺)	Trace-element analysis (84 samples)
Musakashi, Zambia	1.572–1.582	Strong pink	Multiphase inclusions tend to be more irregular than those in Colombian gems; multiphase inclusions with at least two crystals associated with a gas bubble may indicate Zambian rather than Colombian origin	No significant Fe ²⁺ -related absorption features in the NIR region, and no Fe ³⁺ observed	Low alkali metal concentrations (1,530–6,060 ppmw) Cr > V; Cr/V ratio 1.7–5.3 Fe concentration: 680–1,490 ppmw Li vs. Cs log-log plot can help separate Musakashi from Kafubu and slightly separate from Colombia Fe vs. K log-log plot can help separate Musakashi from Colombia
Kafubu, Zambia	1.582–1.593 (RI values typically higher than other localities)	Inert	Multiphase inclusions are usually rectangular in shape, but may be irregular in outline; solid crystals of pyrolusite, chlorite, mica, amphibole, and tourmaline	Strong broad Fe ²⁺ band at approximately 810 nm O-ray: narrow Fe ³⁺ band at approximately 372 nm	High alkali metal concentrations (15,834–23,294 ppmw) Cr >> V; Cr/V ratio 8–40 Fe concentration: 5,900–11,600 ppmw Li vs. Cs log-log plot can help separate Kafubu from others
Panjshir Valley, Afghanistan	1.572–1.590	Inert to pink	Multiphase inclusions tend to be more elongated or needle-shaped than other localities; each may host several cubic to rounded transparent crystals, and sometimes small, dark opaque crystals	Medium broad Fe ²⁺ band at approximately 810 nm O-ray: Fe ³⁺ peak at 372 nm in some samples	Moderate to high alkali metal concentrations (3,946–17,505 ppmw) Cr and V concentrations may be similar: Cr/V ratio 0.3–3.3 Fe concentration: 1,010–9,820 ppmw Li vs. Cs log-log plot can help separate Panjshir from Kafubu, Musakashi, and Colombia (and Davdar, to a lesser extent)
Davdar, China	1.577–1.588	Pink	Multiphase inclusions are usually jagged or irregular in outline, and some are needle-like	Similar to Musakashi: Small broad Fe ²⁺ band at approximately 810 nm Similar to Colombia: Strong V ³⁺ bands at approximately 400 and 654 nm	Low to moderate alkali metal concentrations (5,190–12,620 ppmw) Slightly more V than Cr; Cr/V ratio 0.1–1.0 Fe concentration: 1,230–4,350 ppmw Fe vs. K log-log plot can help separate Davdar from Musakashi and Colombia Li vs. Cs log-log plot can help separate Davdar from Panjshir, to a lesser extent
Colombia (Muzo, Coscuez, La Pita, Peñas Blancas, and Chivor)	1.570–1.580 (typically lower than other localities)	Pink to strong pink	Classic jagged multiphase inclusions host a gas bubble and one or more cubic crystals; gas bubbles are usually smaller than the whole inclusion, and also smaller or about the same size as the associated cubic crystal	No Fe ²⁺ or Fe ³⁺ observed Weak to medium V ³⁺ bands at approximately 400 and 654 nm	Low alkali metal concentrations (1,515–8,115 ppmw) Cr and V concentrations may be similar: Cr/V ratio 0.04 and 3.5 Fe concentration: 117–2,030 ppmw Fe vs. Ga and Fe vs. K log-log plot can help separate Colombia from others

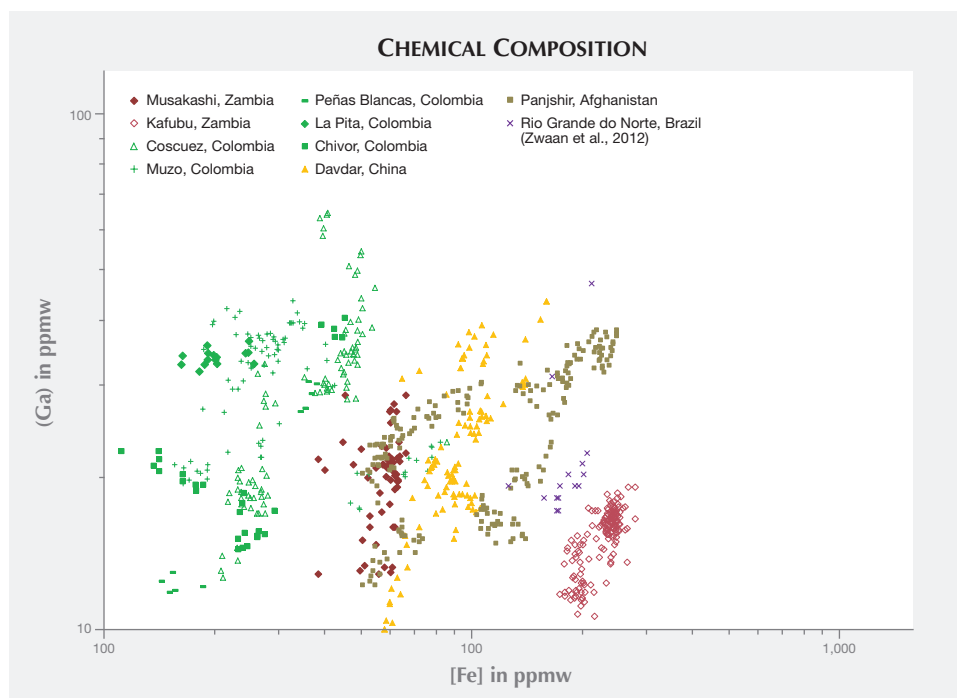


Figure 25. Log-log plot of iron (Fe) versus gallium (Ga) concentrations in emeralds from the five different localities.

inclusions rather than the traditional jagged type often seen in Colombian material. Furthermore, Afghan emeralds often host up to 10 cubic to rounded transparent crystals, and sometimes small dark, opaque crystals. When examined between crossed polarizers, the cubic crystals appeared to be singly refractive and the small rounded crystals appeared doubly refractive. Such features are not typical of Colombian emeralds.

The multiphase inclusions in emeralds from Davdar, China, can be very similar to those in emeralds from Colombian deposits. Many of the multiphase inclusions found in Davdar specimens are jagged and have only one cubic crystal. But the shape of these multiphase inclusions is usually more irregular (sometimes needle-like) than the jagged outline typically observed in Colombian emeralds.

Studying the inclusion scene in these emeralds can be quite confusing, but spectroscopy and trace-element chemistry can provide additional valuable tools to distinguish between them. The presence or absence of Fe^{2+} and Fe^{3+} and the varying intensity of V^{3+} absorption may suggest different countries of origin. More generally, plotting the log-log results from the LA-ICP-MS data for Cs, Li, K, Ga, and Fe resulted in population fields that also appear very promising as a tool in determining the origin of emeralds.

In many cases, the combination of the inclusion scene, UV-Vis-NIR absorption data, and trace-element chemistry (summarized in table 3) can help the gemologist determine the origin of emeralds with three-phase or multiphase inclusions.

ABOUT THE AUTHORS

Ms. Saeseaw is a senior manager of colored stones, Mr. Pardieu is a senior manager of field gemology, and Dr. Sangsawong is a research scientist, all at GIA in Bangkok.

ACKNOWLEDGMENTS

The authors thank Mr. Guy Clutterbuck for providing Musakashi emeralds. We also thank GIA's Jonathan Moyal for lapidary assis-

tance. John Emmett, Kenneth Scarratt, Emily Dubinsky, and Nathan Renfro provided many helpful discussions. Assistance from Nattida Ng-Pooresatien and Charuwan Khowpong with data collection is also greatly appreciated.

REFERENCES

- Behmenburg C. (2002) Beryl and emerald: History and myth. In *Extralapis: Emeralds of the World, extraLapis English No. 2*, Lapis International, East Hampton, CT.
- Bowersox G., Snee L.W., Foord E.E., Seal II R.R. (1991) Emeralds of the Panjshir Valley, Afghanistan. *G&G*, Vol. 27, No. 1, pp. 26–39.
- Giard D., Ed. (1998) *L'éméraude*. Association Française de Gemnologie, Paris.
- Giuliani G., Cheilletz A., Dubessy J., Rodriguez C.T. (1993) Chemical composition of fluid inclusions in Colombian emerald deposits. *8th Quadrennial IAGOD Symposium*, pp. 159–168.
- Groat L.A., Giuliani G., Marshall D.D., Turner D. (2008) Emerald deposits and occurrences: A review. *Ore Geology Reviews*, Vol. 34, No. 1-2, pp. 87–112, <http://dx.doi.org/10.1016/j.oregeorev.2007.09.003>.
- Hammarstrom J.M. (1989) Mineral chemistry of emeralds and some associated minerals from Pakistan and Afghanistan: An electron microprobe study. In A.H. Kazmi and L.W. Snee, Eds., *Emeralds of Pakistan: Geology, Gemology & Genesis*. pp. 125–150.
- Klemm L. (2009) Fieldtrip to emerald mines in Zambia, summer 2009. From http://www.gubelingemlab.ch/PDF/Fieldtrips/2009_Field_report_LK_Zambia_forInternetx.pdf.
- (2010) Fieldtrip to emerald mines in Zambia, summer 2010. From http://www.gubelingemlab.ch/PDF/Fieldtrips/2010_Field_report_LK_Zambia_Internet.docx.pdf.
- Marshall D., Pardieu V., Loughrey L., Jones P., Xue G. (2012) Conditions for emerald formation at Davdar, China: Fluid inclusion, trace element and stable isotope studies. *Mineralogical Magazine*, Vol. 76, No. 1, pp. 213–226, <http://dx.doi.org/10.1180/minmag.2012.076.1.213>.
- Michelou J.-C., Pardieu V. (2009) A glimpse of the new fine emerald deposit at Xinjiang's Davdar Mine. *InColor*, No. 10, Spring, pp. 26–28, 30.
- Pardieu V., Soubiraa G. (2006) From Kashmir to Pamir, Summer 2006: Gemmological expedition report to ruby, emerald and spinel mining areas in Central Asia. Part 4: China (Xin Jiang): Emeralds from the silk roads. <http://www.fieldgemology.org/gemology%20china%20emerald%20davdar.php>.
- Schwarz D., Henn U. (1992) Emeralds from Madagascar. *Journal of Gemmology*, Vol. 23, No. 3, pp. 140–149.
- Schwarz D., Pardieu V. (2009) Emeralds from the Silk Road countries – A comparison with emeralds from Colombia. *InColor*, No. 12, Fall/Winter, pp. 38–43.
- Schwarz D., Mendes J.C., Klemm L., Lopes P.H.S. (2011) Emeralds from South America – Brazil and Colombia. *InColor*, No. 16, Spring, pp. 36–46.
- Venkateswaran C.S. (1935) The Raman spectra of some metallic halides. *Proceedings of the Indian Academy of Sciences – Section A*, Vol. 1, No. 11, pp. 850–858.
- Wood D.L., Nassau K. (1968) The characterization of beryl and emerald by visible and infrared absorption spectroscopy. *American Mineralogist*, Vol. 53, May-June, pp. 777–799.
- Zwaan J.C., Seifert A.V., Vrána S., Laurs B.M., Anckar B., Simmons W.B., Falster A.U., Lustenhouwer W.J., Muhlmeister S., Koivula J.I., Garcia-Guillerminet H. (2005) Emeralds from the Kafubu area, Zambia. *G&G*, Vol. 41, No. 2, pp. 116–148.
- Zwaan J.C., Jacob D.E., Häger T., Cavalcanti Neto M.T.O., Kanis J. (2012) Emeralds from the Fazenda Bonfim region, Rio Grande do Norte, Brazil. *G&G*, Vol. 48, No. 1, pp. 2–17, <http://dx.doi.org/10.5741/GEMS.48.1.2>

For online access to all issues of GEMS & GEMOLOGY from 1934 to the present, visit:

gia.edu/gems-gemology

COLOR PHENOMENA OF BLUE AMBER

Yan Liu, Guanghai Shi, and Shen Wang

The greenish blue color observed in some amber from the Dominican Republic and Indonesia is actually fluorescence stimulated by ultraviolet (UV) light. A previous study described the color as iridescence over a yellow background, but it is in fact a surface fluorescence. Since this amber can be considered a long-wavelength pass filter with a half-pass wavelength at about 530 nm in its spectral transmittance, it does not transmit either UV or short-wave visible light. As this material completely absorbs light in the UV range and strongly absorbs light in the short-wave visible range, the stimulated blue color is confined exclusively to the surface. The amber from this study also showed the Usambara effect, the phenomenon in which color varies with the path length of light through a sample.

Amber is fossilized tree resin used for jewelry, decoration, medicine, and perfume. Specimens with inclusions of insects and plants are of great scientific significance and highly esteemed by collectors. Amber is usually yellow to brown, and some specimens display red to brownish red or reddish brown colors. Blue amber is rare, found mainly in the Dominican Republic with some production from Indonesia and Mexico. This variety comes from the resin of the extinct tree species *Hymenaea protera* (Iturralde-Vinent and MacPhee, 1996; Poinar and Poinar, 1999). According to Iturralde-Vinent and MacPhee (1996), most Dominican amber occurs in two zones: north of Santiago de los Caballeros (the “northern area”) and northeast of Santo Domingo (the “eastern area”).

Although resinites of different ages exist, available biostratigraphic and paleogeographic data suggest that the main amber deposits in the Dominican Republic (including those famous for yielding biological inclusions) were formed in a single sedimentary basin during the late Early Miocene through early Middle Miocene (15 to 20 million years ago). There is little evidence of extensive reworking or redeposition of the ambers. Before the studies of Iturralde-Vinent and MacPhee (1996), amber from the northern area was thought to have formed during the Early Eocene to Early Miocene epochs (Baroni-Urbani and Saunders, 1982; Lambert et al., 1985; Poinar and Cannatella, 1987; Grimaldi, 1996), while published estimates for the eastern area ranged from the Cretaceous to Holocene epochs (Burleigh and Whalley, 1983; Poinar and Cannatella, 1987; Grimaldi, 1996).

Bellani et al. (2005) studied blue amber from the Dominican Republic and identified the aromatic hydrocarbon component perylene as the source of the UV-stimulated fluorescence emission in the visible wavelength range from 430 to 530 nm, resulting in the observed greenish blue color. They also described the blue color as iridescence under natural daylight or daylight-equivalent lighting.

Iridescence is an optical phenomenon in which a surface appears to shift color as the viewing angle or angle of illumination changes (Nassau, 1983). Although most iridescence is caused by interference, Liu et al. (1999b) found that in pearls and shells it results from diffraction. Each layer of shell and pearl is optically heterogeneous. Light is strongly diffused as it passes through the layers, causing the milky white color observed. The diffused light cannot produce interference to cause the iridescence color. For this to happen, each layer would have to be optically uniform and have a thickness on the order of visible-light wavelengths.

UV fluorescence is also known to cause significant visible color change in some diamonds. Strong UV fluorescence under daylight caused such an effect in the 56.07 ct Tavernier diamond (Liu et al., 1998).

See end of article for About the Authors and Acknowledgments.

GEMS & GEMOLOGY, Vol. 50, No. 2, pp. 134–140,
<http://dx.doi.org/10.5741/GEMS.50.2.134>.

© 2014 Gemological Institute of America



Figure 1. Map of the Dominican amber mines visited by one of the authors in 2013.

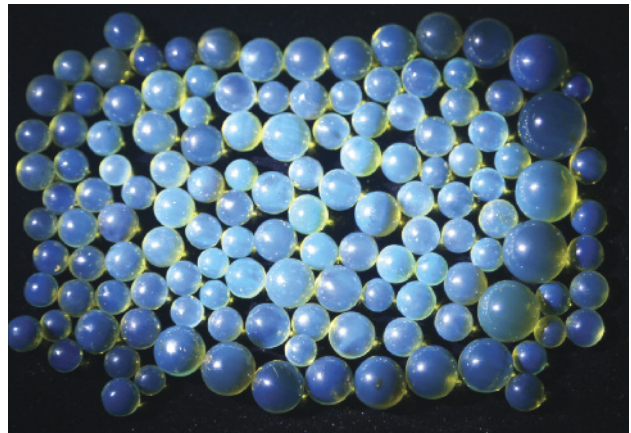


Figure 3. These blue amber beads from the Dominican Republic, 6.0–12 mm in diameter, are shown under daylight-equivalent flashlight. Their greenish blue color is evenly distributed. Photo by Guanghai Shi.

The UV fluorescence changed the entire diamond's bodycolor from light brown under incandescent light to light pink under daylight.

The phenomenon by which bodycolor varies with a gemstone's thickness is called the Usambara effect. Liu et al. (1999a) determined that this color variation is caused by the hue angle change corresponding with the path length of light through a gem material.

This article presents the color phenomena of blue amber from the Dominican Republic and Indonesia. Fluorescence and photoluminescence were measured at room temperature to show the characteristic features. As a result, we found that the amber's greenish blue color is only superficial. By calculating the colorimetric data at different depths within a sample,

we determined that the hue angle changed with depth, an indication of the Usambara effect in blue amber.

MATERIALS AND METHODS

In 2013, one of the authors visited amber deposits in the northern and eastern parts of the Dominican Republic (figure 1). Figure 2 shows a typical mining operation, while figure 3 shows blue amber beads acquired from the local miners.

In the northern area, the upper 300 meters of the La Toca Formation of 1,200-meter-thick clastic rocks contains the amber-bearing unit, composed of sandstone with occasional conglomerate that accumulated in a deltaic to deep-water environment. Amber

Figure 2. Left: Amber is mined by hand in the Dominican Republic. Right: After digging an open pit inside a hill, the miners typically dig a well more than 10 meters deep to look for an amber layer. Blue amber can occasionally be found with other varieties of amber. Photos by Guanghai Shi.



fragments in this deposit, which measure up to 40 cm in length, show few surface signs of transportation. Lignite occurs in the form of thin lamellae within the sandstones. These clastic rocks grade into flyschoid, with deeper-water deposits containing detrital amber.*

In the eastern area, the amber-bearing sediments in the approximately 100 m thick Yanigua Formation are composed of organically rich laminated sand, sandy clay, and some intercalated lignite layers up to 1.5 m thick. Amber pieces occur in the lignite and the sandy clay. In addition to indicative sedimentary features, the characteristics of the invertebrate and vertebrate fossils from these beds—crocodiles, sirenians, and turtles—imply that deposition occurred in a near-shore context, probably in coastal lagoons fronting low, densely forested hills (Brouwer and Brouwer, 1982).

Two blue amber samples were studied. Sample 1, a cabochon from the Dominican Republic, appeared to have a greenish blue surface color and a yellow bodycolor (figure 4). Sample 2, a rough Indonesian amber with one surface polished, showed blue color on the polished surface and a red bodycolor (figure 5). Both samples showed very strong greenish blue fluorescence under long-wave UV radiation at 365 nm, and weak fluorescence under short-wave UV at 254 nm. Both also showed greenish blue phosphorescence that lasted several seconds.

An MDIS-f8 multifunction dual integrating sphere spectrometer was used to measure the samples' spectral transmittance and UV fluorescence so

Figure 4. Sample 1 was a 1.25 ct blue amber cabochon from the Dominican Republic, measuring 10.98 × 7.57 × 4.68 mm. Photo by Yan Liu.

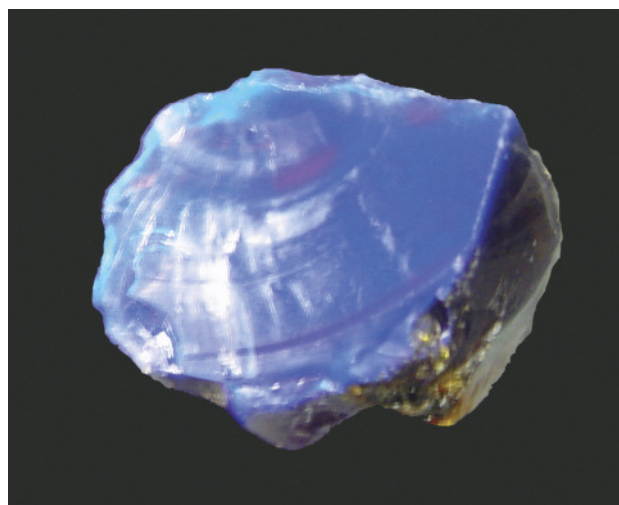


Figure 5. Sample 2, a rough amber from Indonesia, weighed 35.15 ct and measured 26.21 × 25.96 × 20.42 mm. Photo by Yan Liu.

that we could calculate hue and saturation. The optical arrangement for measuring the greenish blue fluorescence is shown in figure 6. The polished surface of sample 2 was held at a 45° angle to the sam-

In Brief

- Blue amber—amber that exhibits a greenish blue color under certain conditions—owes this color component to fluorescence.
- The greenish blue fluorescence color is essentially confined to the surface, as both the excitation and emission wavelengths are completely absorbed.
- Blue amber also displays the Usambara effect, whereby its bodycolor changes from yellow to red with increasing thickness.

ple stage. A 365 nm light-emitting diode (LED) was used to illuminate the polished surface at a 45° angle to excite blue fluorescence. A portion of the blue fluorescence passed through the aperture into the integrating sphere, where it was collected by a collimator and sent to the spectrometer for measurement. The spectrometer was calibrated by a radio-

*Clastic refers to a sedimentary rock composed of broken pieces of older rocks. Lignite, a brownish black coal, is considered the lowest grade of coal due to its relatively low heat content. Flyschoid formations consist of cyclic sedimentary deposits and formed under deep marine circumstances, in a low-energy depositional environment.

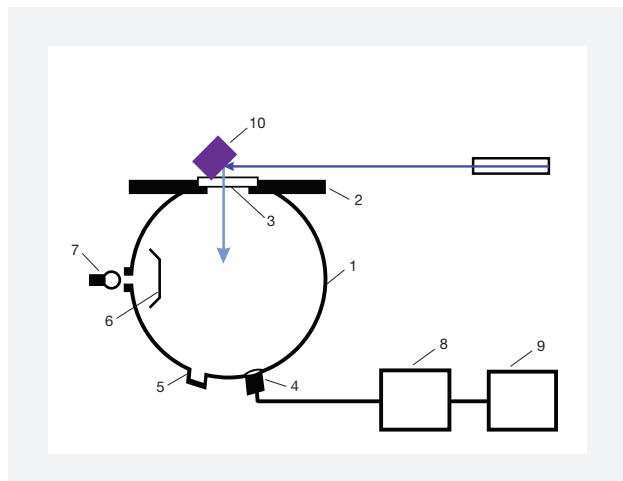


Figure 6. The optical arrangement for measuring the amber's blue fluorescence featured a multifunction spectrometer with a 365 nm LED. Components include: (1) light measurement integrating sphere, (2) sample stage, (3) aperture, (4) collimator, (5) light trap, (6) baffle, (7) light source, (8) spectrometer, (9) computer, (10) blue amber sample, and (11) 365 nm LED.

metric calibration lamp to measure the relative spectral power distribution of the blue fluorescence rather than the digital counts. Therefore, the measured blue fluorescence spectrum was true in spectral power distribution.

Figure 7 shows the optical arrangement for measuring spectral transmittance using the multifunction spectrometer with a xenon-filled tungsten lamp at the top of the integrating sphere. We placed an unpolished area chipped from sample 2 that was about 1 mm thick on the measurement stage, where the diameter of the aperture was 3 mm. The light from the lamp at the top of the measurement integrating sphere passed through both the slice and the aperture, into the measurement integrating sphere. The collimator collected the transmitted light from the amber slice and sent it to the spectrometer for measurement. To measure the percentage of spectral transmittance, the spectrometer is calibrated to 100% without the sample on the stage, and to 0% by turning off the tungsten lamp.

SURFACE COLOR

Figure 8 shows the unpolished slice taken from sample 2. Figure 9 shows the slice's spectral transmittance, which is essentially a typical long-pass transmittance spectrum with a half-pass wavelength at about 530 nm and a cutoff wavelength at about 450 nm. The slope is not steep at the short-wavelength end of the long-pass transmittance spectrum.

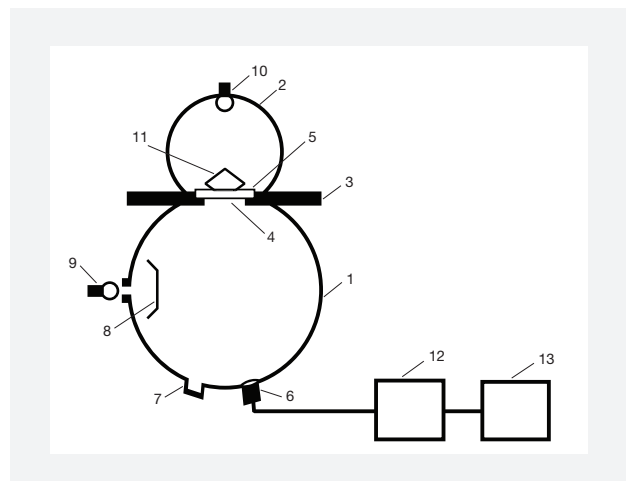
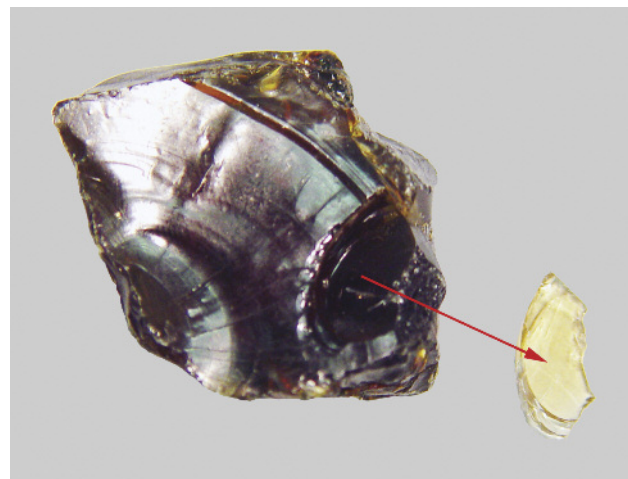


Figure 7. The optical arrangement for measuring transmittance uses a multifunction spectrometer, with a xenon-filled tungsten lamp at the top of the integrating sphere. Components include: (1) light measurement integrating sphere, (2) sample integrating sphere, (3) sample stage, (4) aperture, (5) disk, (6) collimator, (7) light trap, (8) baffle, (9) light source for reflectance measurement, (10) light source for transmittance measurement, (11) blue amber sample, (12) spectrometer, and (13) computer.

The blue light with a wavelength shorter than 450 nm is completely absorbed, and the transmittance of visible light from 450 to 760 nm increases gradually. Thus, the 1 mm slice appears yellow, and the body-color of the amber appears orangy yellow to brown in the thicker area.

Figure 8. This slice, taken from sample 2, is 1 mm thick at the center. This piece was used for measuring the spectral transmittance of blue amber. Photo by Yan Liu.



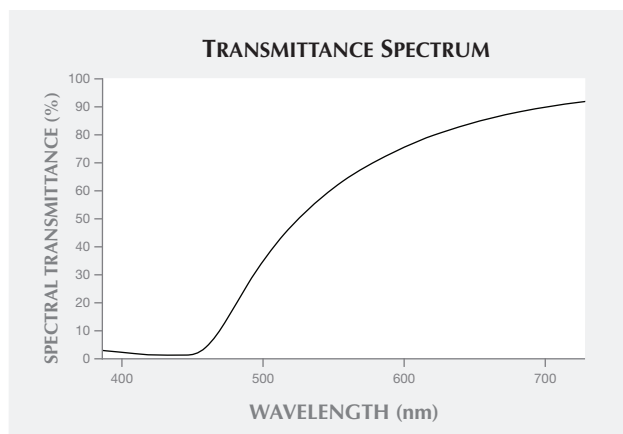
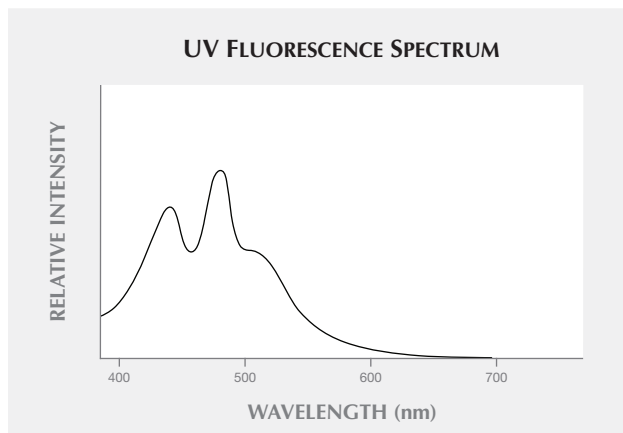


Figure 9. Spectral transmittance of the slice from sample 2. This is a long-wavelength pass spectrum with a cutoff wavelength at about 450 nm, and a half-pass wavelength at about 530 nm. Only light with wavelength longer than 450 nm can partially pass through the amber slice, and the transmittance increases gradually from 450 to 760 nm.

Figure 10 shows the UV fluorescence spectrum of sample 2, measured with a 365 nm UV light source. The UV light was incident to the surface of the sample, and the UV fluorescence was collected from the surface by the measurement integrating sphere component of the dual integrating sphere spectrometer. The UV fluorescence spectrum showed three peaks at around 450, 485, and 500 nm. This UV fluorescence spectrum was similar to the one recorded by Bellani et al. (2005). It is this short-wavelength fluorescence spectrum that causes the greenish blue surface color of blue amber.

Figure 10. The UV fluorescence spectrum of the bulk piece of sample 2, generated by 365 nm long-wave UV light.



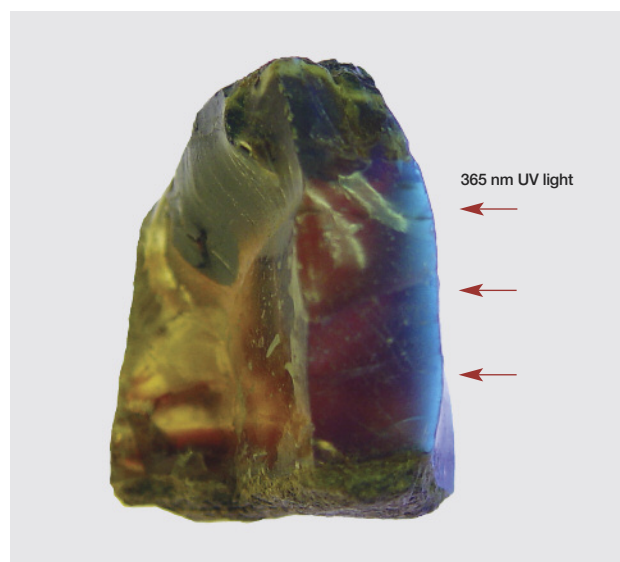
When UV light struck the blue amber, it excited the greenish blue fluorescence. Because of the total absorption of UV light, however, it cannot penetrate into the blue amber. It can only cause blue fluorescence at the surface.

With increasing depth below the surface, the cutoff wavelength shifts to a long wavelength, and the greenish blue fluorescence is eventually totally absorbed. As this depth is still very shallow, the fluorescent light penetration is confined near the surface, limiting the ability to change bodycolor.

Figure 11 shows a lateral view of the greenish blue fluorescence of sample 2. To emphasize the greenish blue surface UV fluorescence, the photo was taken with a 365 nm UV light source. The UV light illuminated the blue amber from the right side, while incandescent light illuminated the top and bottom to show the bodycolor. The observed fluorescence agreed with the theoretical fluorescence based on the fluorescence measurements in the short-wavelength visible range (see figure 10).

UV light cannot penetrate the amber's surface, but fluorescence can penetrate to a shallow depth;

Figure 11. Lateral view of the greenish blue fluorescence of sample 2. Long-wave UV illumination from the right produced the greenish blue fluorescence at the surface; incandescent illumination from above and below was used to show its bodycolor. Due to the short-wavelength cutoff, UV light can only excite the greenish blue fluorescence at the surface. The greenish blue fluorescence cannot penetrate deep into the blue amber. Photo by Yan Liu.



therefore, the very strong greenish blue fluorescence cannot cause the alexandrite effect of bodycolor unless the sample is very thin. This is different from the alexandrite effect previously mentioned in the Tavernier diamond, where the greenish blue fluorescence penetrated the stone and caused a change in its bodycolor. The greenish blue fluorescence color of our amber samples was superficial.

UV fluorescence is generally very weak compared to the reflected or transmitted light of a material's bodycolor under daylight or daylight-equivalent light, even if the UV fluorescence is very strong. This statement holds true for the greenish blue fluorescence of blue amber. Under daylight, the surface greenish blue fluorescence is difficult to observe, and only the yellow to brownish orangy red bodycolor is apparent. The surface fluorescence is usually observed when the blue amber is held against a black background. The black background limits light reflection, enhancing the fluorescence.

THE USAMBARA EFFECT

One surface of sample 2 was polished to form a wedge shape to show color change with different thicknesses. With increasing thickness, sample 2's cutoff wavelength moves to longer wavelengths, and its transmission color changes from yellow to red (figure 12). The hue is yellow where the sample is thin and changes to brownish orangy red with increasing thickness.

Table 1 shows the calculated relationship between the thickness and hue angle of sample 2 in the CIELAB color space under the CIE standard illuminant A at a color temperature of 2856 K, which represents the incandescent light used to observe the transmission color (Wyszecki and Stiles, 2000). Where the amber is 1 mm thick, its hue angle is 88.1° and its chroma is 33.4. The 88.1° hue angle represents a yellow hue, the 33.4 chroma a medium saturation. As the thickness increases, the hue angle becomes smaller and the chroma becomes higher. When the thickness reaches 7 mm, the hue angle is lowered to 76.7° and the chroma achieves its maximum saturation at 75.0. This hue angle and chroma represent an orange color with high saturation. When the thickness reaches 25 mm, the hue angle is reduced to 62.8°, observed as an orangy red hue, and the chroma becomes 55.1, representing a medium-high saturation.

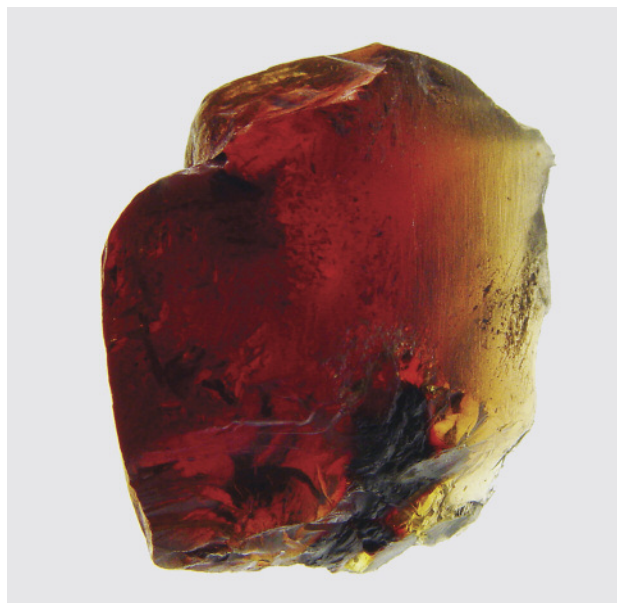
Figure 13 shows the hue angle change of the blue amber in the CIELAB color space under the CIE

TABLE 1. Calculated relationship between thickness and hue angle and chroma of a blue amber sample.

Thickness (mm)	Hue angle	Chroma
1	88.1°	33.4
2	85.6°	51.7
3	83.3°	62.0
4	81.4°	68.0
5	79.6°	71.6
7	76.7°	75.0
10	75.3°	73.1
15	70.2°	68.7
20	65.4°	62.9
25	62.8°	55.1

standard illuminant A at 2856 K. The locus of these hue angles is a closed curve, with a hue angle variation of more than 20° in CIELAB color space. This locus is typical of the Usambara effect, which describes color variation with material thickness. In fact, many red and reddish brown ambers we have observed, with or without the blue fluorescence, clearly displayed the Usambara effect. As sample thickness increased, their bodycolor went from yellow

Figure 12. The bodycolor of sample 2 changes from yellow to orangy red where the stone is thicker. Photo by Yan Liu.



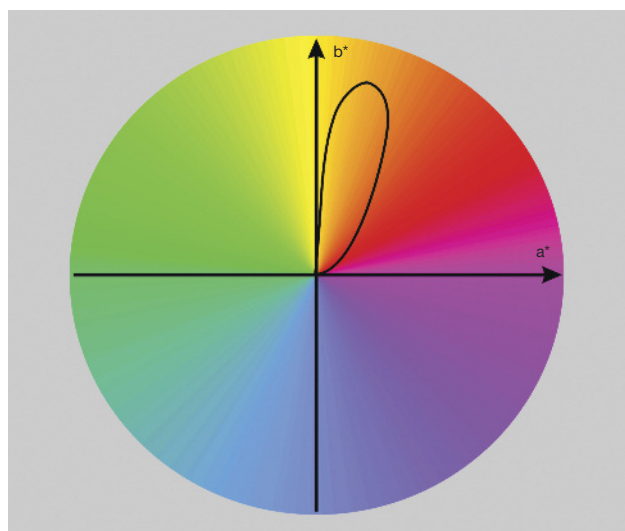


Figure 13. In CIELAB color space, the hue angle locus of sample 2 shows a variation of more than 20° , attributable to the Usambara effect.

low to brownish orange or orangy brown, brownish red, or even red.

CONCLUSION

The greenish blue color of blue amber from the Dominican Republic and Indonesia is caused by UV-stimulated fluorescence. The greenish blue fluorescence color is confined to the surface. There are two reasons for this: (1) UV light can only stimulate the greenish blue fluorescence on the surface of amber, and (2) amber strongly absorbs the greenish blue fluorescence light and does not allow it to penetrate much below the surface. Where a sample is thicker, the cut-off wavelength of the long-wavelength pass spectrum moves to a longer wavelength, and the greenish blue fluorescence can only penetrate a very thin layer of the amber. Thus, the blue fluorescence only appears on the surface.

Blue amber's bodycolor changes with increasing thickness: yellow in areas less than 3 mm thick, orangy yellow to yellowish orange at approximately 3–6 mm, orange at 6–8 mm, and reddish orange and orangy red where the stone is more than 8 mm thick.

ABOUT THE AUTHORS

Mr. Liu is president of Liu Research Laboratories in South El Monte, California. Dr. Shi is a professor at the School of Gemology, China University of Geosciences in Beijing. Mr. Wang is a student at Swarthmore College in Swarthmore, Pennsylvania.

ACKNOWLEDGMENTS

This research was partially supported by Grant No. 41373055 from the National Science Foundation of China.

REFERENCES

- Baroni-Urbani C., Saunders J.B. (1982) The fauna of the Dominican Republic amber: the present status of knowledge. In W. Snow et al., Eds., *Transactions of the 9th Caribbean Geology Conference*, Vol. 1, pp. 213–223.
- Bellani V., Giulotto E., Linati L., Sacchi D. (2005) Origin of the blue fluorescence in Dominican amber. *Journal of Applied Physics*, Vol. 97, No. 1, p. 016101, <http://dx.doi.org/10.1063/1.1829395>.
- Brouwer S.B., Brouwer P.A. (1982) Geologia de la region ambarifera oriental de la Republica Dominicana. In W. Snow et al., Eds., *Transactions of the 9th Caribbean Geology Conference*, Vol. 1, pp. 305–322.
- Burleigh R., Whalley P.J. (1983) On the relative geological ages of amber and copal. *Journal of Natural History*, Vol. 17, pp. 919–921.
- Grimaldi D.A. (1996) *Amber: Window to the Past*. Harry Abrams, New York.
- Iturralde-Vinent M.A., MacPhee R.D.E. (1996) Age and paleogeographical origin of Dominican amber. *Science*, Vol. 273, pp. 1850–1852, <http://dx.doi.org/10.1126/science.273.5283.1850>.
- Lambert J.B., Frye J.S., Poinar G.O. (1985) Amber from the Dominican Republic: Analysis by nuclear magnetic resonance spectroscopy. *Archaeometry*, Vol. 27, pp. 43–51.
- Liu Y., Shigley J., Moses T., Reinitz I. (1998) The alexandrite effect of the Tavernier diamond caused by the fluorescence under daylight. *Color Research & Application*, Vol. 23, No. 5, pp. 323–327, [http://dx.doi.org/10.1002/\(SICI\)1520-6378\(199810\)23:5<323::AID-COL8>3.0.CO;2-Y](http://dx.doi.org/10.1002/(SICI)1520-6378(199810)23:5<323::AID-COL8>3.0.CO;2-Y).
- Liu Y., Shigley J., Halvorsen A. (1999a) Color hue change of a gem tourmaline from the Umba Valley, Tanzania. *Journal of Gemology*, Vol. 26, No. 6, pp. 386–396.
- Liu Y., Shigley J., Hurwit K. (1999b) Iridescent color of a shell of the mollusk *Pinctada margaritifera* caused by diffraction. *Optics Express*, Vol. 4, No. 5, pp. 177–182.
- Nassau K. (1983) *The Physics and Chemistry of Color*. John Wiley and Sons, New York.
- Poinar G.O., Cannatella D.C. (1987) An Upper Eocene frog from the Dominican Republic and its implications for Caribbean biogeography. *Science*, Vol. 237, No. 4819, pp. 1215–1217, <http://dx.doi.org/10.1126/science.237.4819.1215>.
- Poinar G., Poinar R. (1999) *The Amber Forest: A Reconstruction of a Vanished World*. Princeton University Press, Princeton, New Jersey.
- Wyszecki G., Stiles W. (2000) *Color Science*, 2nd ed. John Wiley and Sons, New York.

EXPERIMENTAL STUDIES ON THE HEAT TREATMENT OF BALTIC AMBER

Yamei Wang, Mingxing Yang, and Yiping Yang

Amber samples were subjected to heat treatment experiments aimed at reproducing heated products found in the jewelry market today. Using a furnace and applying specific conditions, the authors produced four types of heated amber: golden, red, “flower,” and “beeswax.” This paper describes the procedures and parameters that influence the characteristics of heated amber.

Amber’s naturally soft color is appreciated by connoisseurs the world over. In China, the gem has been regarded as sacred since ancient times. It is one of China’s seven Buddhist treasures, along with gold, silver, pearl, coral, Tridacna clams, and *liuli* (glass). Huge quantities of amber are consumed each year, especially in the Chinese market, but high-quality natural material is rare and expensive. As a result, some dealers seek to improve its appearance and quality through heat treatment, which expands the variety available but poses identification challenges.

Numerous studies have dealt with the identification of heat-treated amber (e.g., Brody et al., 2001; Zhang, 2006; Feist et al., 2007; Abduriyim et al., 2009). Yet the methods of heat treatment are closely guarded and quite complex. Details surrounding enhancement mechanisms, the evolution of flow striations, and the reworking of inclusions, as well as changes in gemological properties under different treatment conditions, are not well understood.

In recent years, a few reports have focused on reproducing the heat treatment of amber (e.g., Zhang 2003; Abduriyim et al., 2009; Ross, 2010). In one

study, samples were placed in plant oil or fine-grained sands and heated, improving their transparency and generating “sun spark” inclusions. Such methods are not easily duplicated, however. This investigation adopts standard equipment and procedures for commercial-scale heat treatment and explores the mechanisms behind a series of changes resulting from the treatment.

To simulate the heat-treated varieties available in the Chinese market, the authors chose raw Baltic amber specimens from Kaliningrad, Russia, and performed a series of heating experiments at an anonymous processing facility. We succeeded in producing a full range of heated amber varieties, including golden, red, “flower,” and “beeswax” (figure 1). These

Figure 1. These photos show four types of heated Baltic amber found in the market. Clockwise from top left: a 21.34 g golden amber, a 42.80 g red amber, a 23.21 g “beeswax” amber, and a 11.95 g golden amber with flower inclusions. Photos by Yamei Wang, courtesy of Shengji Co.



See end of article for About the Authors and Acknowledgments.

GEMS & GEMOLOGY, Vol. 50, No. 2, pp. 142–150,
<http://dx.doi.org/10.5741/GEMS.50.2.142>.

© 2014 Gemological Institute of America

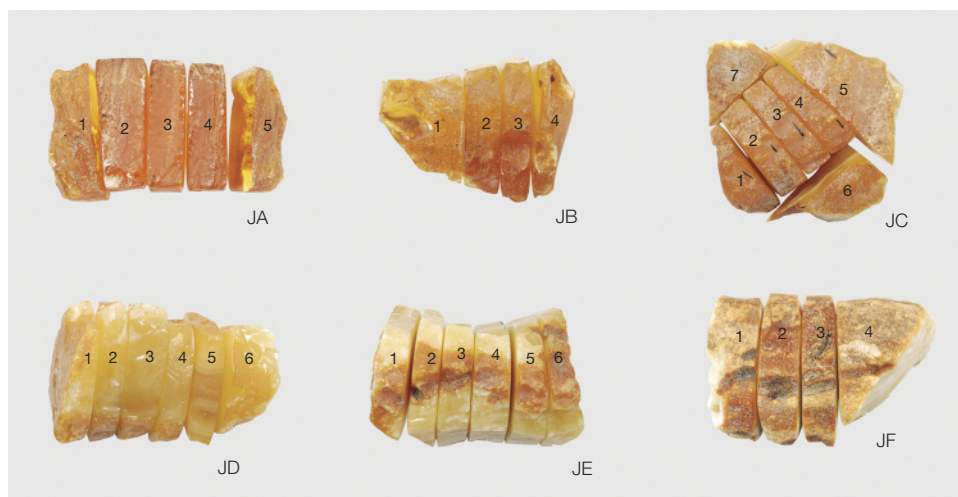


Figure 2. Raw amber specimens from Kaliningrad, Russia, were collected for heat treatment experiments. The whole specimens ranged from 27.23 g (sample JB) to 74.70 g (sample JE). Photo by Yamei Wang.

experiments yielded useful information about procedures, conditions, and influencing factors for heat treatment. The gemological parameters and inclusion characteristics may provide valuable references for the identification of heat-treated amber.

MATERIALS AND METHODS

Six good-quality Russian amber specimens were obtained from Beata Amber (Vilnius, Lithuania) for heat treatment. The raw samples weighed 380 g total and were labeled JA–JF. They ranged from orange-yellow to honey yellow in color and from transparent to opaque, with naturally weathered surfaces (table 1). For this study, each specimen was cut into several subsamples, designated as JA-1 through JA-5, etc. (figure 2). This enabled us to track and observe changes in structure and properties at different experimental stages.

For the heat treatment experiments, we used a Kapex AB/3/KAP furnace (figure 3). The automatic control and protection system can be connected to the pressure furnace through a stop valve, depending on the desired enhancement effect. Slowly charging inert gas (N_2) into the pressure furnace and heating it removes cloudy bubbles inside the amber, improving its transparency and hardness. By regulating the gas medium used for enhancement, the resulting color can also be adjusted.

RESULTS

The heat treatment of amber generally consists of four stages: preparation, dosing, enhancement, and blowing-out. Details of the stages are described in table 2. Table 3 shows the samples' appearance before and after treatment, as well as the treatment param-

eters and overall effectiveness. It should be noted that these parameters are given in averages or approximate values, as detailed data were not divulged by the processing facility.

Purification Process. Purification removes bubbles from amber in an inert gas medium, improving transparency. This process requires careful regulation of temperature and pressure inside the autoclave to avoid melting the amber. Thick specimens with poor transparency may need to undergo several rounds of purification, or one lengthy process at higher pressure and temperature. Purification is the primary method for producing golden and pearly beeswax amber, and it is commonly used as a pretreatment before oxidation or sun sparking.

Figure 3. A Kapex AB/3/KAP amber furnace was used in the heat treatment experiments. Photo by Yamei Wang.

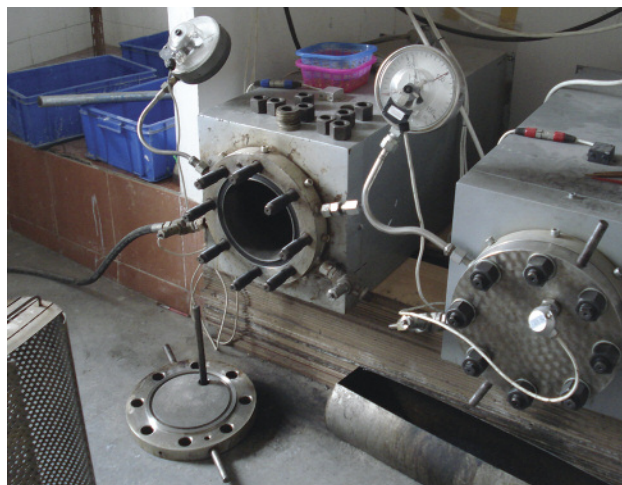








TABLE 1. Characteristics of the amber samples used in heat treatment experiments.

Sample code	Description	
JA	Golden specimen, rectangular and sub-angular in shape. Transparent, with a yellowish orange and fine-grained surface. The interior is clean, occasionally showing small silky and cloudy inclusions, a few tiny gas bubbles, and an apparent disc-shaped crack.	
JB	Beeswax-colored specimen, nearly trigonal to sub-triangular in shape, showing a color variation of golden yellow to milky white from the edge to the center. Transparent to opaque, exhibiting a brownish yellow and saccharoidal surface. The center shows smooth flow structure, gas bubbles, and a disc-shaped structure.	
JC	Beeswax-colored specimen. Slightly transparent to semitransparent, showing a brownish dendritic surface. The inside displays flow striations and clearly defined boundaries, with bubbles visible in cloudy inclusions.	
JD	Beeswax-colored specimen, nearly elliptical in shape. Slightly transparent to semitransparent, showing a brownish yellow dendritic surface. The inside displays smooth flow striations and bubbles.	
JE	Beeswax-colored specimen, nearly rectangular. Opaque, with a brownish yellow surface. The inside shows mottled or smooth distribution of light yellow and white veins with clearly defined boundaries.	
JF	Beeswax-colored specimen, nearly trigonal and sub-angular. Milky white, opaque, with a brownish yellow dendritic surface and flow structures inside.	

For the first test, we chose samples JA-3, JA-4, JA-5, and JC-7; the JA samples are transparent, naturally golden amber, and JC-7 has an opaque yellow beeswax color. We started with a gas pressure of 4.5 MPa and a room temperature of 27°C, which was increased over a three-hour period to 200°C. That temperature was maintained for about two hours, then cooled down to 35°C over a period of 14 hours, at which point the samples were removed. After purification, all the samples showed better transparency. Sample JC-7 exhibited the most dramatic improvement, changing from near opaque to transparent at the edges, with slight transparency at the center for a pearly beeswax effect. Its color did not change. Samples JA-3, JA-4, and JA-5 changed from golden yellow to brownish yellow. After purification, the JA samples were reserved for oxidation and sparking.

Theoretically, less-transparent amber can be purified in a single round by setting the proper conditions, but since the process is performed in a sealed


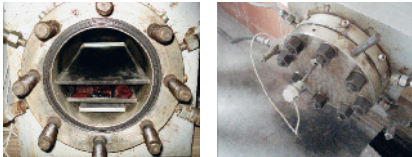

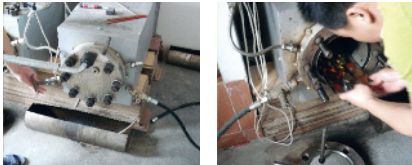
tank, the effects cannot be observed in real time. To prevent overheating and damaging the amber's physical-chemical properties, multiple purifications may

In Brief

- Portions of six raw amber specimens were subjected to heat treatment experiments to understand the conditions necessary to create specific effects in amber.
- Purification, oxidation, and sparking processes yielded four distinct types of heat-treated amber: golden, red, "flower," and "beeswax."
- The wide variety and quality of amber on the market depends on the material's inherent properties and the treatment parameters.

be used for transparency enhancement. For the second test, semitransparent to opaque sample JB-2 and

TABLE 2. General procedures for the heat treatment of amber.

Stage	Description	
1. Preparation	Check the autoclave operation system. Determine operating parameters such as temperature, pressure, and atmosphere for heat treatment, based on thickness, size, and transparency of semi-finished and finished amber products.	
2. Dosing	Arrange the samples on an iron tray and place inside the autoclave. Close and tighten the cover and insert the sensor.	
3. Enhancement	Set the pressure, fill the autoclave with an inert gas (or oxygen) until the initial pressure is reached, and shut off the gas valve. Turn on the autoclave power supply and set the temperature, heating rate, and duration. After heating, the system will automatically shut off.	
4. Blowing-out	When the autoclave naturally cools down to about 40°C, shut off the power supply. Remove the temperature sensor, release the gas inside the stove, open the cover, and retrieve the specimens.	

opaque beeswax samples JB-4, JC-1, JC-4, JD-3, JD-4, JD-5, JD-6, JE-2, JF-1, and JF-2 were selected for two purification cycles, using the procedure described for the first test. The initial pressure was set at 5 and 5.5 MPa, respectively; the temperature was set at 200–210°C, with heating times of five and six hours, respectively.

After two purification cycles, the cloudy inclusions disappeared, turning the samples transparent. Samples JB-2 and JD-3 became transparent brownish yellow golden amber, while the others turned brownish red. Polishing off the superficial red oxidized layers of samples JC-4, JD-4, JE-2, and JF-2 revealed a golden yellow color. After polishing, samples JD-4, JD-5, and JD-6 were set aside for sparking and oxidation. The red oxidation is thought to be related to remnants of air left inside the autoclave from incomplete purging or from the presence of oxygen impurity in the nitrogen gas, either of which would oxidize the amber's surface and turn it red during pu-

rification. Charging air into the autoclave to a pressure of 0.2 MPa and then releasing it would improve air exhaust and help prevent such oxidation. When the preset temperature is reached inside the autoclave, slowly releasing some air and exhaust vapor would help accurately regulate pressure for the purification test.

Oxidation Process. Oxidation at an elevated temperature is the main process used to create red amber. It produces a red to deep reddish brown oxidized layer on the surface. Purified samples JA-4, JA-5, JB-4, JC-2, JD-6, and JF-3 were selected for oxidation in a sealed autoclave. The process was somewhat different from the purification test, in that a small amount of oxygen was charged into the inert gas media, according to a strict volume ratio of the two gases. Too little oxygen would produce an insufficient oxidation effect on the amber surface, while too much oxygen would be dangerous to the test equipment and the material

due to carbonization. Pressure was set at 4.5 MPa and the temperature was raised to 210°C over three hours, with inert gas charged into the autoclave together with a small amount of oxygen.

After testing, all the samples had transformed into red to blackish red amber. A longer heating time generally means a deeper color of red amber. If one oxidation did not produce the expected effect, another could be performed. Only gas pressure needs to be increased (under the same temperature) by 0.5–1.0 MPa above the previous oxidation test; otherwise, the amber samples tend to show sparking inside.

“Sun Spark” Inclusions. To create small “sun spark” inclusions, the bubbles present in amber need to be “burst.” After heating the amber as in a purification step, the gas from the autoclave is released, causing a rapid decrease of interior pressure and breaking down the equilibrium between the inner and outer pressure of a bubble. This results in the expansion and sparking of bubbles and the formation of disc-shaped internal cracks, since the pressure inside the bubbles exceeds the pressure outside them. These disc-shaped cracks are termed “sun spark” inclusions. Amber with these inclusions is known as flower amber. Multiple rounds of sparking are needed to produce golden flower and red flower amber varieties.

Conventional sparking consists of deep-frying and baking in sand, and the sparking effect is visually regulated. Because these processes are time-consuming and quantities of amber containing the appropriate amount of gas/liquid inclusions are limited, most flower amber is manufactured by autoclave.

Golden Flower Amber. Sparking for golden flower amber starts with the same procedures used in purification but differs in the latter stages. After heating is complete, the power supply is immediately switched off, releasing gas inside the autoclave to cool down the pressure chamber. Samples JA-3, JD-5, and JE-5, which contain relatively abundant gas bubbles, were selected for this test. To prevent excessive sparking, which would result in cracking, all samples underwent purification treatment beforehand. For the first sparking test, the initial pressure was set at 2.0 MPa. The maximum temperature was set at 200°C, which was reached within two hours and maintained for one hour. Samples that failed to produce a flower effect after the first sparking test underwent a second and in some cases a third sparking test, at successively higher pressure and temperature conditions, until a golden flower effect was obtained.

In our testing, sample JE-5 achieved the best results, which came from two rounds of sparking.

Red Flower Amber. Red flower amber is produced by two different methods: (1) sparking red amber and (2) oxidizing golden flower amber. The first process involves manufacturing red amber, stopping the heating, and directly releasing the air. This results in an instantaneous pressure decrease that produces sparking inside the red amber; when the superficial red oxidized layer is polished off, red flower amber is revealed. In the second method, golden flower amber undergoes oxidation treatment and its oxidized skin is polished off. Although the first method is more efficient, both yield identical results.

To produce red flower amber, we chose samples JC-3, JD-4, JE-3, and JE-4. The parameters for the sparking were an initial pressure of 3.0 MPa and a maximum temperature of 200°C after three hours of heating. Sample JC-3 was successful, while the other three failed. Sample JA-5 underwent oxidation, followed by sparking, after which the dark red layer was partially polished off to expose the golden yellow bodycolor. In this manner, golden and red bicolored flower amber was generated.

“Beeswax” Amber. The method for manufacturing “beeswax” amber is relatively simple but consumes considerable time and energy. The process requires prolonged heating and slow oxidation under constant pressure and low temperature. First, samples are arranged in an iron tray that is spread with a layer of fine-grained sand and placed in the furnace. The temperature is set at approximately 50–60°C, for a heating period of 60–100 days. During the baking process, the temperature must be controlled within a certain range. Samples JD-2 and JE-6 were chosen to produce beeswax samples. The specimens were heated at about 60°C for 60 and 90 days, respectively. After heating, the samples had a dull yellow color like ancient beeswax.

DISCUSSION

Heat treatment of amber is aimed at altering or improving color, enhancing transparency, or producing inclusions with special effects. Different results were targeted, including purification, oxidation, “sun spark,” and “beeswax” effects. Based on these tests, several conclusions can be drawn.

Beeswax-colored amber can be purified as transparent golden material using an initial pressure of 4.5–5.0 MPa and a maximum temperature of 200–210°C

TABLE 3. Enhancement parameters and characteristics of amber samples.
































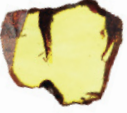

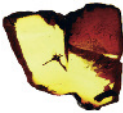









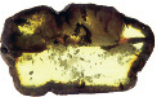


Sample	Before test	After test	Enhancement method(s) and parameters	Assessment
JA-3 (9.44 g)	Golden yellow 	Bicolored golden and red flower 	Purification, sparking Temperature: 200°C Time: 2.5 hours Pressure: 3.0 MPa Ambient medium: inert gas	The “sun spark” was small and only slightly visible.
JA-4 (8.94 g)	Golden yellow 	Red 	Purification, oxidation Temperature: 210°C Time: 3.0 hours Pressure: 4.5 MPa Ambient medium: inert gas + oxygen	The expected effect was achieved.
JA-5 (6.90 g)	Golden yellow 	Bicolored red and golden flower 	Purification, oxidation, sparking Temperature: 210°C Time: 3.0 hours Pressure: 4.5 MPa Ambient medium: inert gas + oxygen	The expected effect was achieved.
JB-2 (6.82 g)	White and golden yellow pearly beeswax 	Brownish yellow golden 	Purification Temperature: 200°C Time: 5.0 hours Pressure: 5.0 MPa Ambient medium: inert gas	The expected effect was largely achieved; only the right lower corner part was not completely transparent.
JB-4 (5.42 g)	White and golden yellow beeswax 	Blackish red 	Purification, oxidation Temperature: 210°C Time: 3.0 hours Pressure: 4.5 MPa Ambient medium: inert gas + oxygen	The expected effect was achieved.
JC-1 (6.58 g)	White and honey yellow beeswax 	Dark red 	Purification Temperature: 210°C Time: 6.0 hours Pressure: 5.5 MPa Ambient medium: inert gas	Ideal color was produced, but transparency was not ideal.
JC-2 (7.82 g)	White and honey yellow beeswax 	Red 	Purification, oxidation Temperature: 210°C Time: 3.0 hours Pressure: 4.5 MPa Ambient medium: inert gas + oxygen	The expected effect was achieved.
JC-3 (8.71 g)	White and honey yellow beeswax 	Golden with red flower 	Purification, sparking, oxidation Temperature: 200°C Time: 3.0 hours Pressure: 3.0 MPa Ambient medium: inert gas + oxygen	The expected effect was achieved, with the middle part showing attractive “sun spark” inclusions.

TABLE 3 (continued). Enhancement parameters and characteristics of amber samples.

Sample	Before test	After test	Enhancement method(s) and parameters	Assessment
JC-4 (8.78 g)	White and honey yellow beeswax 	Bright yellow golden 	Purification Temperature: 210°C Time: 6.0 hours Pressure: 5.5 MPa Ambient medium: inert gas	The expected effect was achieved, due to oxidation of the polished surface after three rounds of purification.
JC-7 (25.64 g)	White and honey yellow beeswax 	Pearly beeswax 	Purification Temperature: 200°C Time: 5.0 hours Pressure: 4.5 MPa Ambient medium: inert gas	The expected effect was achieved.
JD-2 (5.66 g)	Honey yellow beeswax 	Beeswax 	Beeswax baking Temperature: 60°C Time: 60 days Pressure: constant Ambient medium: air	The expected effect was achieved.
JD-3 (8.36 g)	Honey yellow beeswax 	Brownish yellow golden 	Purification Temperature: 210°C Time: 5.5 hours Pressure: 5.5 MPa Ambient medium: inert gas	The expected effect was achieved after three rounds of purification.
JD-4 (6.18 g)	Honey yellow beeswax 	Bright yellow golden 	Purification, sparking Temperature: 200°C Time: 3.0 hours Pressure: 3.0 MPa Ambient medium: inert gas	After three rounds of purification, the expected effect was achieved. The sparking test failed, as no "sun spark" inclusions were produced.
JD-5 (5.26 g)	Honey yellow beeswax 	Golden flower 	Purification, sparking Temperature: 200°C Time: 2.5 hours Pressure: 3.0 MPa Ambient medium: inert gas	The expected effect was achieved.
JD-6 (6.82 g)	Honey yellow beeswax 	Red 	Purification, oxidation Temperature: 210°C Time: 3.0 hours Pressure: 4.5 MPa Ambient medium: inert gas + oxygen	The expected effect was achieved.
JE-2 (11.50 g)	White and yellow beeswax 	Bright golden 	Purification Temperature: 210°C Time: 6.0 hours Pressure: 5.5 MPa Ambient medium: inert gas	After three rounds of purification and polishing of the oxidized surface, the expected effect was largely achieved, though cracks formed inside the amber.

Sample	Before test	After test	Enhancement method(s) and parameters	Assessment
JE-3 (11.25 g)	White and yellow beeswax 	Golden and red 	Purification, sparking, oxidation Temperature: 200°C Time: 3.0 hours Pressure: 4.0 MPa Ambient medium: inert gas + oxygen	The test failed, as no “sun spark” inclusions were produced.
JE-4 (13.87 g)	White and yellow beeswax 	Red flower 	Purification, sparking, oxidation Temperature: 200°C Time: 3.0 hours Pressure: 4.0 MPa Ambient medium: inert gas + oxygen	The test failed, as no “sun spark” inclusions were produced.
JE-5 (12.53 g)	White and yellow beeswax 	Golden flower 	Purification, sparking Temperature: about 200°C Time: 2.5 hours Pressure: Approx. 3.0 MPa Ambient medium: inert gas	Ideal “sun spark” inclusions were created after three rounds of purification.
JE-6 (12.00 g)	White and yellow beeswax 	Dull yellow beeswax 	Beeswax baking Temperature: 60°C Time: 90 days Pressure: constant Ambient medium: indoor open environment	The expected effect was achieved.
JF-1 (11.78 g)	Milky white beeswax 	Dark red 	Purification, oxidation Temperature: 210°C Time: 6.0 hours Pressure: 5.5 MPa Ambient medium: inert gas	After three rounds of purification, red color resulted from slow oxidation, but the transparency was not ideal.
JF-2 (9.76 g)	Milky white beeswax 	Golden 	Purification Temperature: 200°C Time: 5.0 hours Pressure: 5.0 MPa Ambient medium: inert gas	After three cycles of purification, the transparency was not noticeably improved.
JF-3 (7.45 g)	Milky white beeswax 	Red 	Purification, oxidation Temperature: 210°C Time: 3.0 hours Pressure: 4.5 MPa Ambient medium: inert gas + oxygen	The expected effect was largely achieved.

(reached in three to six hours and maintained for two hours), followed by 14 hours of cooling. Achieving the desired effect, such as pearly beeswax, may require multiple rounds of purification. Purification is also the pretreatment for other enhancement processes.

Well-controlled oxidation generates red amber by producing a red to dark red surface layer. The parameters are an initial pressure of 4.5 MPa (involving a specific volume ratio of inert gas and oxygen) and a maximum temperature of 210°C, to be reached in approximately three hours. The key parameter for oxidation is the amount of oxygen added: Too little oxygen produces a very light color, while too much increases the likelihood of carbonizing the test materials and damaging the equipment.

Samples containing certain levels of gas/liquid inclusions that undergo purification followed by a rapid pressure release acquire internal "sun spark" inclusions, converting them to flower amber. The parameters are: initial pressure of 2.0 MPa and a maximum temperature of 200°C, reached over a period of two hours. Sparking generally requires several rounds of treatment before the effect can be considered satisfactory, with higher pressure and temperature with each additional treatment. Red flower amber can be manufactured by two methods: the sparking of red amber, or the oxidation and polishing of golden flower amber.

Beeswax-colored amber is created by prolonged oxidation (color darkening) on the surface at constant pressure and low temperature, which involves a tem-

perature of about 50–60°C and a baking time of two to three months.

Amber heat treatment is affected by several factors, including:

1. Material properties: sample color, transparency, and bulk size, which determine the initial heat treatment parameters.
2. Temperature and pressure conditions: the time allowed for heating, maintaining temperature, and cooling, as well as the pressure and the rate of pressure decreases. These are the key parameters for achieving satisfactory amber products.
3. Atmospheric inert gas and oxygen, and the ratio between the two, which can determine the color of heat-treated amber.

CONCLUSION

This paper reports on methods of amber heat treatment and discusses several influencing factors. The study suggests that the variety and quality of heated ambers are influenced by the inherent properties (color, transparency, and bulk size) of the natural material, as well as the heat treatment parameters, including temperature, pressure, and atmosphere. Using a furnace and various parameters, four types of heated amber were produced: golden, red, "flower," and "beeswax." The study documented the various procedures for amber heat treatment, yielding valuable data on how different effects are achieved.

ABOUT THE AUTHORS

Ms. Wang is vice professor at the Gemological Institute, China University of Geosciences in Wuhan, and the director of the university's gem testing center in Guangzhou. Dr. Yang (yangc@edu.cn) is dean of the Gemological Institute. Ms. Yang, formerly a postgraduate at the Gemological Institute, works in the amber trade in Guangzhou.

ACKNOWLEDGMENTS

This work was financially supported by the Gemological Institute, China University of Geosciences in Wuhan. We are grateful to the peer reviewers and technical editors for constructive feedback. The authors would like to thank Beata Amber for providing the samples used in this study.

REFERENCES

- Abduriyim A, Kimura H, Yokoyama Y., Nakazono H., Wakatsuki M., Shimizu T., Tansho M., Ohki S. (2009) Characterization of "green amber" with infrared and nuclear magnetic resonance spectroscopy. *G&G*, Vol. 45, No. 3, pp. 159–171, <http://dx.doi.org/10.5741/GEMS.45.3.159>.
- Brody R.H.E., Howell G.M., Pollard A.M. (2001) A study of amber and copal samples using FT-Raman spectroscopy. *Spectrochimica Acta Part A*, Vol. 57, No. 6, pp. 1325–1338, [http://dx.doi.org/10.1016/S1386-1425\(01\)00387-0](http://dx.doi.org/10.1016/S1386-1425(01)00387-0).
- Feist M., Lamprecht I., Müller F. (2007) Thermal investigations of amber and copal. *Thermochimica Acta*, Vol. 458, No. 1-2, pp. 162–170, <http://dx.doi.org/10.1016/j.tca.2007.01.029>.
- Ross A. (2010) *Amber: The Natural Time Capsule*. Firefly Books Ltd., Ontario, Canada.
- Zhang P.L. (2006) *Systematic Gemology*, 2nd ed. Geology Press, Beijing (in Chinese).
- Zhang S.H. (2003) Can heat treatment change refractive index? *Journal of Gems and Gemmology*, Vol. 5, No. 2, p. 14–15 (in Chinese with English abstract).

Editors

Thomas M. Moses | Shane F. McClure

DIAMOND

Chameleon, with Nickel Absorption Band

The Carlsbad laboratory recently examined a 0.31 ct Light greenish yellow marquise-cut diamond. The stone displayed the strong yellow fluorescence, persistent yellow phosphorescence, and green color component of a chameleon diamond. A chameleon diamond has a green or greenish color component under normal conditions. When heated or left in the dark for long periods of time, the green component temporarily disappears, giving way to an orange component. Figure 1 shows the diamond before and immediately after heating, in which the removal of the green component leads to an orange-dominant hue, demonstrating that the stone was in fact a chameleon diamond. Unfortunately, the stone's low saturation makes the effect less noticeable.

Examination of the visible-NIR spectrum revealed a noticeable nickel-related absorption band at 685 nm (figure 2). DiamondView images were taken to prove the stone was not synthetic, as nickel is a common catalyst in HPHT synthetics (figure 3). While nickel has long been known to occur as a trace element in chameleon diamonds (T. Hain-schwang et al., "A gemological study

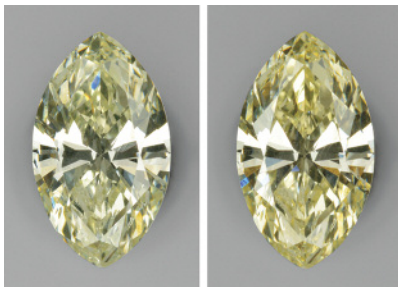


Figure 1. The chameleon diamond is shown before and after heating (left and right).

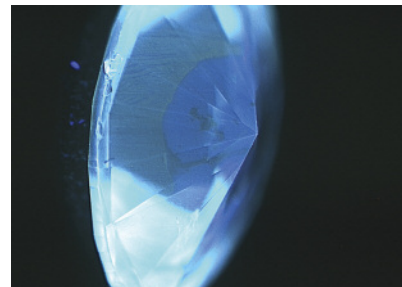
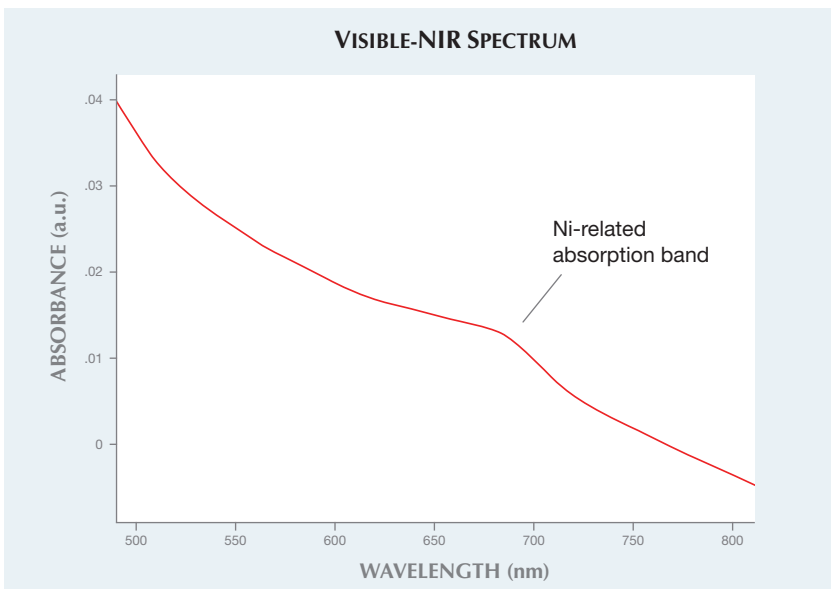


Figure 3. DiamondView imaging showed uneven blue and green fluorescent zones, proving the stone's natural origin.

of a collection of chameleon diamonds," Spring 2005 *G&G*, pp. 20–34), its role in the color-change effect is unknown. Nickel has also been re-

ported as a cause of green coloration in certain diamonds (W. Wang et al., "Natural type Ia diamond with green-yellow color due to Ni-related de-

Figure 2. The absorption spectrum of the chameleon diamond shows a nickel-related band at 685 nm.



Editors' note: All items were written by staff members of GIA laboratories.

GEMS & GEMOLOGY, Vol. 50, No. 2, pp. 151–157, <http://dx.doi.org/10.5741/GEMS.50.2.151>.

© 2014 Gemological Institute of America

fects," Fall 2007 *G&G*, pp. 240–243), but this may be the first time it has been identified as the major cause of a green component in a chameleon. The rarity of chameleon diamond, combined with the rarity of Ni-related natural green diamonds, makes this a truly unique specimen.

Troy Ardon

Long-Term Durability of CVD Synthetic Film on Natural Diamond

In 2005, a thin film (< 10 μm) of synthetic diamond grown by chemical vapor deposition was deposited on the pavilion of a 0.27 ct natural diamond. The CVD layer was deliberately doped with boron to create a bluish color. No subsequent polishing was performed. Rather than blue, the resulting color was a less desirable gray. This natural diamond with CVD overgrowth was then reset in a ring and worn daily by the author for the next eight years. Recently, this hybrid diamond was removed from its setting for gemological and spectroscopic characterization and to assess the current state of the CVD film.

Well-controlled durability studies have examined non-diamond coatings on diamond (e.g., A.H. Shen et al., "Serenity coated colored diamonds: Detection and durability," Spring 2007 *G&G*, pp. 16–34) and nanocrystalline diamond coatings on non-diamond materials (J.E. Shigley et al., "Characterization of colorless coated cubic zirconia [Diamantine]," Spring 2012 *G&G*, pp. 18–30). To our knowledge, however, none have been performed on CVD diamond films grown on natural diamond. The assessment of this one sample, given the exposure a ring is usually subjected to, can indicate the long-term stability of such coatings on diamond. The expectation was that such films would remain stable, as there is no lattice mismatch in the crystal structure between the CVD synthetic film and the natural diamond. Lattice mismatch and the resulting low cohesion at the diamond/non-diamond interface typically result in moderate to very poor durability.

It was difficult to find evidence of the CVD layer using spectroscopic techniques. FTIR absorption (which generally provides data from the bulk of the diamond) revealed no CVD-specific features, only that the underlying diamond was type Ia. Using PL spectroscopy, which collects data from a limited area, it was difficult to find spectroscopic evidence of the CVD film, even when the PL data were collected in confocal mode. No CVD-related 3123 cm^{-1} peak was detected in IR absorption, and the silicon peak at 737 nm was not observed in PL. The best evidence of the CVD layer's continued existence on the diamond was from its unusual appearance in visual observation (figure 4) and microscopic analysis (figure 5). The pavilion also showed electrical conductivity, which provides another indication of the boron doping.

By examining the pavilion of the diamond at high magnification, we could assess the condition of the CVD layer after eight years of daily wear. The film was still largely intact, covering the entire pavilion and containing only a few sporadic pinholes. There was no noticeable degradation at the facet junctions. The obvious color zoning in figure 4 that appears to divide the diamond into quadrants

Figure 4. This 0.27 ct diamond with a boron-doped CVD synthetic diamond film on the pavilion received a color grade of Fancy Dark brownish yellowish gray. The distinct color zoning seen in this photo makes it apparent that the diamond has been treated in some way and is not a natural stone.

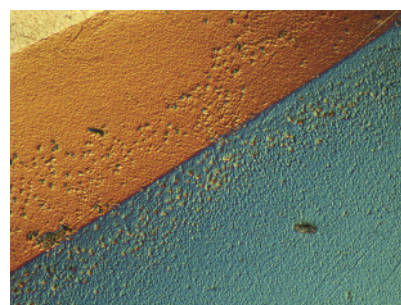


Figure 5. This differential interference contrast image shows the irregular texture of the CVD overgrowth film on the pavilion facets of the 0.27 ct natural diamond. Each facet is a different color, and the boundaries between colors are facet junctions. Field of view 246 microns.

is likely due to differences in deposition and boron incorporation rates on the various facets. Recently, the diamond was annealed twice, at 600°C and 700°C for one hour each in a reducing atmosphere, in an effort to make it appear bluer. This treatment changed the color from Fancy Dark brownish yellowish gray to Fancy Dark gray.

As treatments become more sophisticated and move from the laboratory into the trade, the need for accurate detection only intensifies. Nevertheless, such semipermanent films are identifiable and reiterate the need to use both spectroscopic and traditional methods for gemological characterization.

Sally Eaton-Magaña

Star OPAL

Opal is best known for displaying play-of-color. It may also display asterism, though star opal has only been reported from Idaho, and a perfect six-rayed star is exceptionally rare (J.V. Sanders, "The structure of star opals," *Acta Crystallographica*, Vol. A32, 1976, pp. 334–338). The Bangkok laboratory recently had the opportunity to examine a transparent star opal (figure 6). The 2.39 ct light brownish yellow cabochon displayed a distinct six-rayed star.

Standard gemological testing gave a spot RI reading of 1.43 and a hydro-

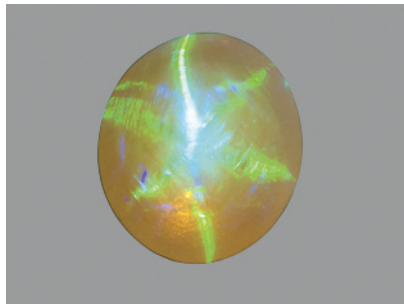


Figure 6. This 2.39 ct transparent opal with a light brownish yellow bodycolor possessed a six-rayed star.

static SG of 2.10. When exposed to ultraviolet radiation, the stone fluoresced strong bluish white under long-wave and weak bluish white under short-wave UV. It phosphoresced green after exposure to long-wave UV. Advanced gemological testing by energy-dispersive X-ray fluorescence (EDXRF) confirmed a silica-rich material with some additional trace elements, including aluminum and iron. All of these properties were consistent with opal.

Microscopic examination revealed large parallel planes with play-of-color intersecting to form a hexagonal pattern (figure 7). This is responsible for

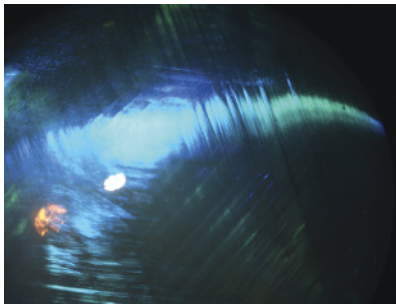


Figure 7. This photomicrograph of the opal shows the intersection of large parallel planes with play-of-color, producing asterism. Magnified 15 \times .

producing the six-rayed star. This unusual stone serves as a reminder that, unlike asterism in other gem materials, the star in opal is caused by diffraction of light from faults or imperfections in the packing arrangement of silica spheres.

Wasura Soonthornantikul

Shell PEARL as a Pearl Imitation

Imitation pearls made of shell, or “shell pearls,” have a long history in the jewelry market and have been reported in previous Lab Notes columns (Fall 1984, p. 170; Winter 1986, p. 239; Summer 2001, pp. 135–136; Summer 2004, p.

Figure 8. These shell pearls range from 10 to 12 mm and display black, white, and golden colors.



178). The shell beads are often coated with artificial materials to simulate a wide variety of natural and cultured pearls in the market. Recent submissions of such imitations to GIA prompted researchers in the lab to obtain several samples from a commercial website. Labeled as shell pearls (figure 8), they resembled Tahitian black, white, and yellow/golden South Sea cultured pearls.

Although the samples were similar in appearance and heft to cultured pearls, routine gemological tests revealed unnatural surface characteristics. The black shell pearl necklace also exhibited multicolored but rather oily orient. Magnification showed numerous minute particles with a glittering effect (figure 9, top), as well as a lack of the obvious overlapping nacre platelets commonly found in nacreous pearls. These features suggested that an artificial coating had been applied to the bead. Inspection

Figure 9. Top: The surface of the imitation pearls contained a glittery coating rather than overlapping nacre platelet structures (magnified 112.5 \times). Bottom: White bead-like shell material was exposed at a damaged area near the drill hole (magnified 10 \times).

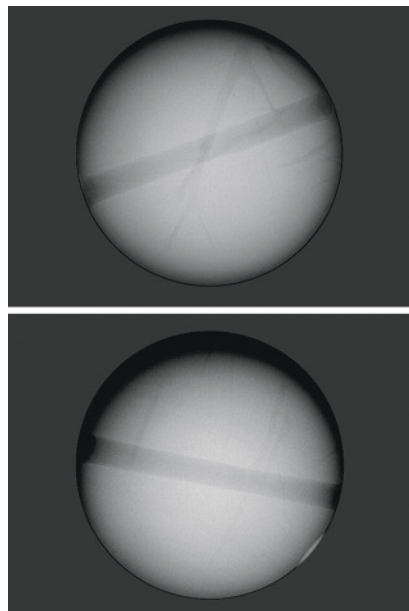


near the drill holes of some samples revealed chipping and peeling of this very thin coating, exposing white bead-like shell material underneath (figure 9, bottom).

X-radiography showed only the inner bead, with occasional parallel banding and cracks—similar to the banding and trematode “tunnels” common in some saltwater shell beads—while the outer coating remained transparent (figure 10). EDXRF analysis detected a high concentration of bismuth, which usually does not occur in pearls but had been reported previously in coated natural and cultured pearls (Fall 2005 Gem News International, pp. 272–273; Winter 2011 Lab Notes, pp. 313–314). Finally, Raman spectroscopic analysis of the exposed white bead identified it as aragonite. These results, coupled with the bead’s inert reaction under X-ray fluorescence, confirmed it was made of saltwater shell.

We have noted the use of the terms *shell pearl* or just *pearl* for such imitations in product descriptions on numerous commercial websites. Such inappropriate nomenclature could be

Figure 10. X-radiography revealed banding and cracks in the inner shell beads.



misleading to inexperienced buyers. According to the CIBJO Blue Book on pearls, “Imitations or simulants of natural pearls and cultured pearls ... shall be immediately preceded by the word ‘imitation’ or ‘simulated’, with equal emphasis and prominence ... as those of the name itself.” *Imitation pearl* would be the proper name of this material, and consumers need to be aware of its true identity.

Jessie (Yixin) Zhou and
Chunhui Zhou

Yellow CVD SYNTHETIC DIAMOND

Gem-quality CVD-grown synthetic diamonds are usually type IIa and occasionally type IaA. In addition, a faceted type Ib yellow CVD synthetic of 3 mm in diameter was reported more than a decade ago (J.E. Butler, “Chemical vapor deposited diamond: Maturity and diversity,” *Interface*, Spring 2003, pp. 22–26). To the best of our knowledge, no other type Ib examples have been documented in the gem industry since then. The New York laboratory

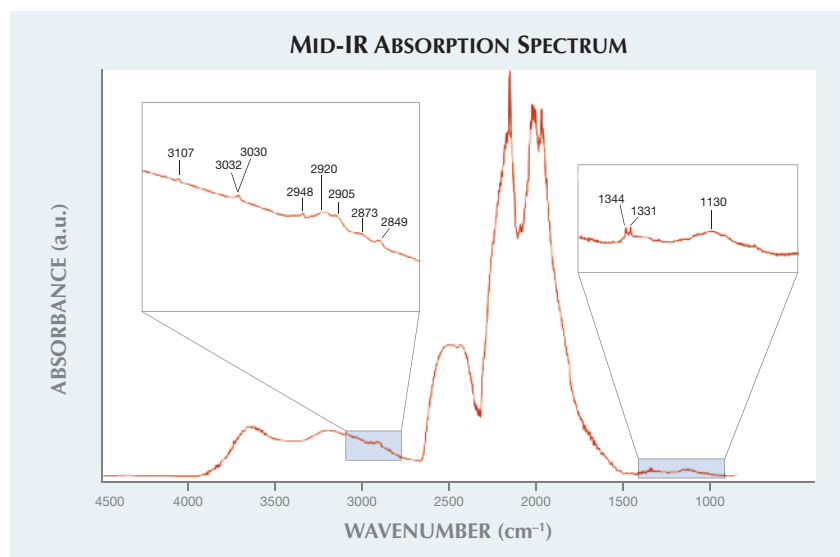


Figure 11. This 0.40 ct square-shaped type Ib CVD synthetic diamond was color graded as Fancy yellow.

recently examined a gem-quality type Ib CVD-grown synthetic diamond. This Fancy yellow square weighed 0.40 ct and measured $4.20 \times 4.12 \times 2.55$ mm (figure 11).

As is typical for CVD synthetics, the strong silicon-vacancy ([Si-V] center) was detected as a doublet at 736.5 and 736.9 nm in the 633 nm PL spectrum. The mid-IR spectrum showed a single substitutional nitrogen atom (N_s^0) at 1130 and 1344 cm^{-1} (figure 12). The nitrogen content, which contributed to the yellow color, was calculated from absorption bands in the

Figure 12. The yellow CVD synthetic’s mid-IR spectrum revealed single substitutional nitrogen atoms (N_s^0) at 1130 and 1344 cm^{-1} . The diamond Raman band was detected at 1331 cm^{-1} . A hydrogen-related defect was detected at 3107 cm^{-1} , and C-H defects could be observed at 2948, 2920, 2905, 2873, and 2849 cm^{-1} . An unknown doublet was also observed at 3030 and 3032 cm^{-1} .



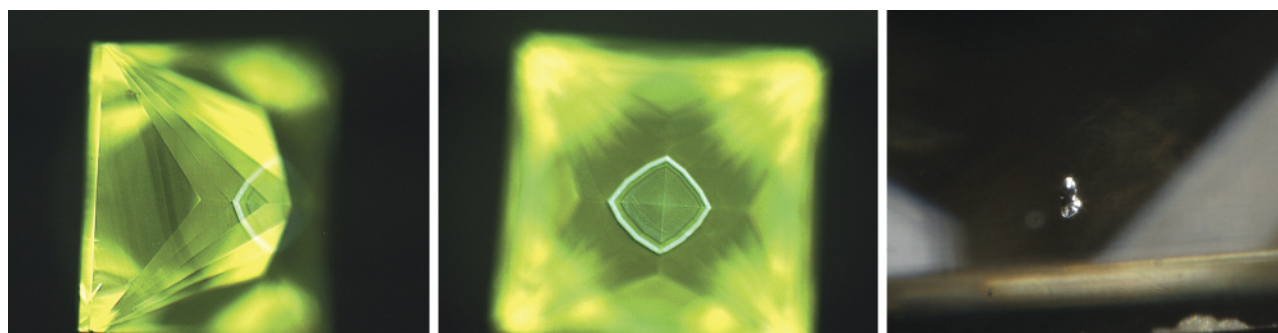


Figure 13. DiamondView imaging revealed curved green lines, reflecting changes in growth conditions (left). Pronounced growth events were also observed in green and bluish green regions near the culet (middle). Microscopic examination revealed a graphitized stress halo (right, magnified 112.5 \times), along with small feathers on the girdle (not shown).

1000–1400 cm^{-1} mid-IR spectral region as 4.5 ppm. Nitrogen can be unintentionally introduced during the growth process; it can also be added deliberately to control the growth rate of single-crystal CVD synthetic diamond. DiamondView images showed curved green lines, indicating changes in conditions during growth (figure 13, left). The DiamondView also revealed green and greenish blue regions of pronounced growth events near the culet, as in the middle image of figure 13. A graphitized stress halo (figure 13, right) and small feathers on the girdle were observed under the microscope. Typical CVD strain—a localized tatami-like structure with low-strain interference colors—was visible under cross-polarized light.

Post-growth treatment was detected: a hydrogen-related defect at 3107 cm^{-1} and C-H defects at 2948, 2920, 2905, 2873, and 2849 cm^{-1} (again, see figure 12). We did not observe the neutral charge state of the nitrogen vacancy–hydrogen complex ($[\text{N-V-H}]^0$) at 3123 cm^{-1} . These results suggested that the sample was HPHT-treated. An unknown doublet at 3030–3032 cm^{-1} was also found. Strong N-V (nitrogen-vacancy) defects at 575 (NV^0) and 637 (NV^-) nm were detected in PL spectrum using a 514 nm laser. The negatively charged nitrogen vacancy–hydrogen complex ($[\text{N-V-H}]^-$) is usually contained in as-grown nitrogen-doped single-crystal CVD synthetic diamond, but it is unstable. After HPHT treatment, the hydrogen atoms were dissociated,

causing C-H and N-V defects to form. Additional defects, such as H3 and H2, were also detected. Both centers could be introduced in as-grown CVD synthetic diamonds by HPHT annealing. The H3 centers were responsible for the observed green dislocations in the DiamondView image. As-grown CVD synthetic diamonds usually possess an unattractive brown color component. This can be removed by HPHT treatment to achieve an attractive yellow color, as observed in this sample.

Type Ib CVD synthetics are also of interest for technological applications, especially for quantum computing (see E. Gibney, “Flawed to perfection: Ultra-pure synthetic diamonds offer advances in fields from quantum computing to cancer diagnostics,” *Nature*, Vol. 505, 2014, pp. 472–474). The N-V electron spin could be used as a basic unit of quantum computing, known as a quantum bit or “qubit.” Qubits are not limited to the binary “0” or “1” states of bits in traditional computers, but can simultaneously exist in both binary states and any state in between—a difficult concept to grasp but one that will lead to vastly enhanced computational capacity. Type Ib yellow CVD diamonds of micrometer size were grown and subsequently electron beam-irradiated and annealed by P. Neumann to create NV centers, as noted in his 2012 PhD thesis, “Towards a room temperature solid state quantum processor: The nitrogen-vacancy center in diamond.” After irra-

diation, the color changed from the as-grown yellow to green, then to purplish pink after annealing.

*Kyaw Soe Moe, Wuyi Wang, and
Ulrika D’Haenens-Johansson*

Flux-Grown SYNTHETIC RUBY with Hydrothermal Synthetic Seed Crystal

The Carlsbad laboratory recently received a 1.18 ct transparent red octagonal step-cut stone for ruby report service. Standard gemological testing established the following properties: RI—1.762 to 1.770; birefringence—0.008; optic sign—uniaxial negative; pleochroism—orangy red to purplish red; specific gravity—4.01; fluorescence reaction—strong red to long-wave, weak red to short-wave UV radiation. Examination with a desk-model spectroscope revealed a typical ruby spectrum. All of these properties were consistent with natural or synthetic ruby.

Under magnification, the most distinctive internal characteristic in the crown was the presence of strong irregular growth features: zigzag- or mosaic-like striated patterns (figure 14), typical of a hydrothermal synthetic. Other areas of the ruby lacking these irregular growth features contained hexagonal metallic platelets and high-relief, whitish flux inclusions (figure 15), typical of a flux-grown synthetic. Flux and hydrothermal inclusions have not been previously documented in the same specimen.

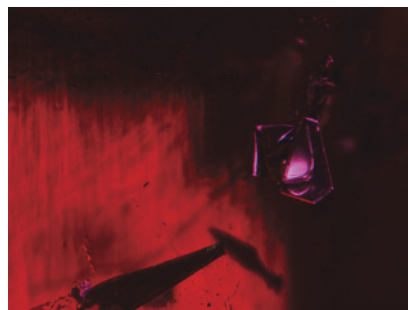


Figure 14. The zigzag-like growth structure observed in this 1.18 ct synthetic ruby is characteristic of hydrothermal growth. Field of view 1.42 mm.

Laser ablation–inductively coupled plasma–mass spectrometry (LA-ICP-MS) analysis revealed traces of Ca, Ti, Cr, Fe, Mo, Rh, Sn, W, and Pt. The low amount of Fe and Ti, the absence of V and Ga, and the presence of Pt were consistent with flux-grown corundum.

Both natural and flame-fusion synthetic ruby have been used as seed crystals in the flux growth of ruby (J.I. Koivula, “Induced fingerprints,” Winter 1983 *G&G*, pp. 220–227; Summer 1991 Lab Notes, p. 112). The seed crystals are generally removed during the cutting process but may, on rare occasions, be detected in finished specimens. Upon close microscopic examination, we noted that several of

Figure 15. When the synthetic ruby was examined under diffused fiber-optic lighting and darkfield illumination, hexagonal platinum platelets and trapped flux residue became apparent. Field of view 1.42 mm.



the flux-filled healed fractures (wispy veils) extended into the areas showing hydrothermal graining. These observations led us to conclude that the hydrothermal material was a seed crystal and that the flux healing was a secondary process to the hydrothermal growth. There was an irregular separation between the materials under brightfield illumination.

This unusual combination of a hydrothermal ruby seed with flux ruby overgrowth is the first of its kind examined by GIA.

Ziyin Sun and Dino DeGhionno

Rare Faceted WURTZITE

Recently the Carlsbad laboratory examined a 3.97 ct transparent brownish red pear-shaped modified brilliant for identification service (figure 16). Standard gemological testing revealed a refractive index that was over the limit of the RI liquid and a specific gravity (obtained hydrostatically) of 3.96. There was no fluorescence observed with exposure to long- and short-wave UV light. The stone also displayed an adamantine luster and a uniaxial optic figure when examined with polarized light. Microscopic examination with a fiber-optic light source showed fine needles and a large reflective decrepitation halo surrounding a negative crystal. Examination also revealed that the decrepitation halo was perpendicular to the optic-axis direction, suggesting the stone had basal cleavage (figure 17).

Figure 16. This 3.97 ct faceted wurtzite has an adamantine luster and brownish red bodycolor.

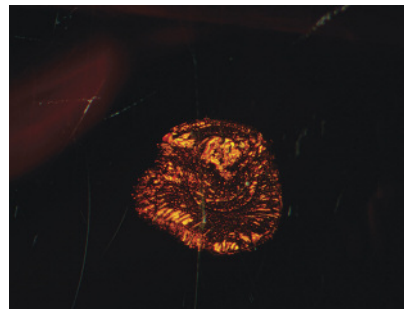


Figure 17. A decrepitation halo surrounds a negative crystal in the faceted wurtzite. Field of view 2.15 mm.

Raman spectroscopy and X-ray powder diffraction conclusively identified the stone as wurtzite. EDXRF analysis detected zinc and sulfur, which further supported this identification.

Wurtzite, a polymorph of sphalerite, commonly occurs in hydrothermal vein deposits associated with barite and sphalerite. Facet-grade wurtzite has been reported to occur in Merelani, Tanzania (Winter 2013 *GNI*, p. 261). This is the first wurtzite examined by the GIA laboratory.

Amy Cooper and Nathan Renfro

Tenebrescent ZIRCON

The Bangkok laboratory recently received for identification a 13.16 ct reddish orange stone, submitted as tenebrescent zircon (figure 18, left). Standard gemological testing indicated typical properties for the stable form of zircon: RI was over the detection limit of the standard refractometer, SG was approximately 4.50, and the sample was inert to both long- and short-wave UV. After exposure to short-wave UV for approximately 30 minutes, however, its tone became darker. Chemical analysis using EDXRF showed significant amounts of zirconium and silicon, as well as a trace amount of hafnium.

Tenebrescence, the phenomenon of reversible photochromism, is common in gemstones such as hackmanite (a variety of sodalite) but unusual in zircon. In September 2011, GIA examined two zircons from central Australia that

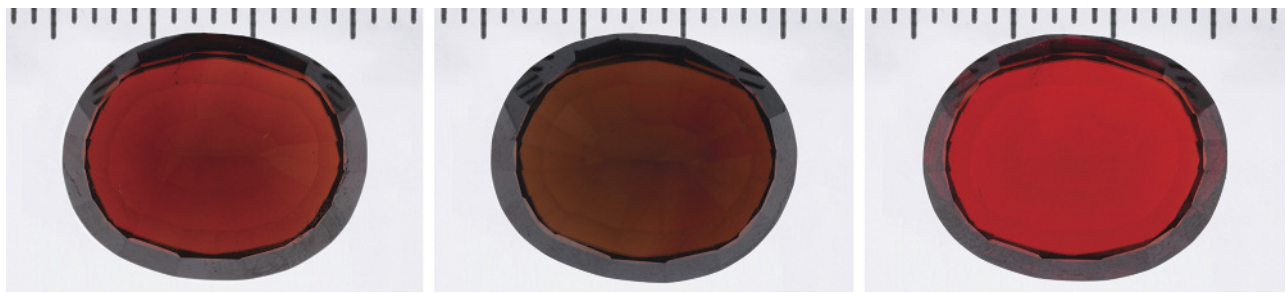


Figure 18. This 13.16 ct zircon is shown before (left) and just after 30 minutes of short-wave UV exposure (center). The SWUV lighting darkened the stone, while darkness restored the orange color. The image on the right shows the color of the stone after it was left in the dark for three weeks.

turned orange in darkness and faded to near colorless when exposed to light (S.F. McClure, "Tenebrescent zircon," Winter 2011 *G&G*, pp. 314–315). This zircon displayed a different phenomenon: Its reddish orange color did not fade under fluorescent lighting or fiber-optic light. Exposure to short-wave UV (SWUV) caused it to darken. The reddish orange component gradually di-

minished, and the stone appeared brown (figure 18, center). There was no further change after 30 minutes.

The UV-visible spectrum after SWUV exposure showed a significant increase in absorption in the 590–750 nm range, reducing transmission of the orange to red color and making the stone darker (figure 19).

As noted above, the reaction is re-

versible. The reddish orange color returned when the stone was stored in the dark at room temperature (see figure 18, right). The color change was obvious in the first 10 to 20 hours. After that, no further color change was observed.

To determine whether the process was repeatable, the stone was again subjected to SWUV. Once again the reddish orange color darkened in tone.

In summary, the reddish orange zircon was darkened by short-wave UV exposure, and the color returned when the stone was stored in the dark. The darkening reaction was much faster than the recovery. Further studies incorporating other conditions that might affect the rate of color modification in tenebrescent zircon are being conducted.

Ratima Suthiyuth

Figure 19. After 30 minutes of SWUV exposure, the zircon's absorption spectrum revealed more absorption in the 590–750 nm range, which relates to an orange to red color.

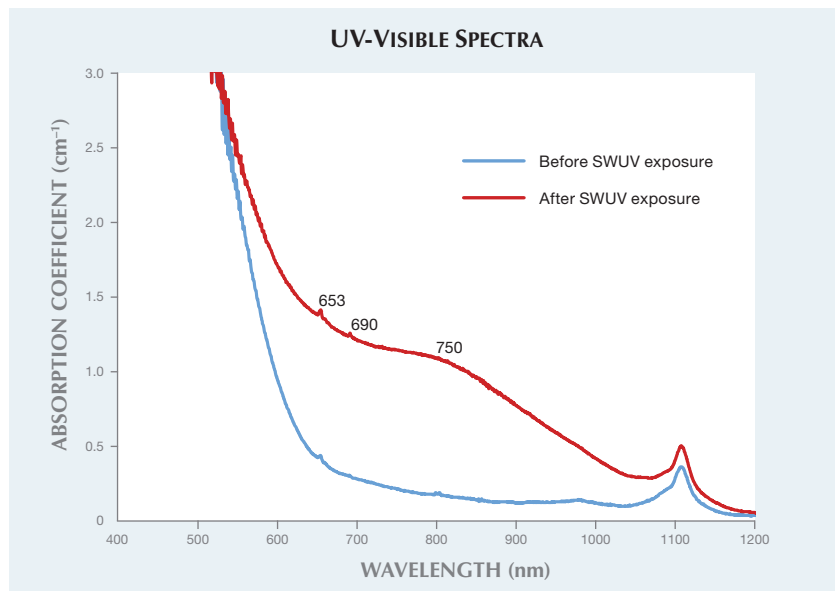


PHOTO CREDITS:

Robison McMurtry—1, 4; Troy Ardon—3; Lhapsin Nillapat—6; Charuwan Khawpong—7; Jian Xin (Jae) Liao—8; Chunhui Zhou—9, top; Jessie (Yixin) Zhou—9, bottom; Nathan Renfro—5, 14, 15, and 17; Sood Oil (Judy) Chia—11; Kyaw Soe Moe—13; Don Mengason—16; Sasithorn Engniwat—18.

Contributing Editors

Emmanuel Fritsch, *CNRS, Team 6502, Institut des Matériaux Jean Rouxel (IMN), University of Nantes, France* (fritsch@cnsr-immn.fr)

Kenneth Scarratt, *GIA, Bangkok* (ken.scarratt@gia.edu)

COLORED STONES AND ORGANIC MATERIALS**Jadeite bangle with the appearance of polymer treatment.**

Jadeite jade always comes under close scrutiny in the market because it is so frequently treated. The treatment options for jadeite jade are numerous: bleaching, dyeing, polymer impregnation, or a combination of these. Polymer impregnation is a particular favorite, a process that is not always easy to observe by magnification. A 244.29 ct translucent light to deep green and brownish yellow bangle measuring approximately 70 × 14 mm was recently submitted to the Lai Tai-An Gem Lab in Taipei. The client was concerned about a more transparent light-colored area (figure 1) that appeared to be possible evidence of impregnation.

Standard gemological testing indicated a spot RI reading of 1.54 at the more transparent light-colored area and 1.66 elsewhere on the bangle, an SG of approximately 3.32, and a characteristic jadeite spectrum exhibiting a band at

Figure 1. This 244.29 ct translucent light to deep green and brownish yellow bangle measures approximately 70 × 14 mm. It contained a transparent, light-colored area that suggested the possibility of a polymer impregnation process. Photo courtesy of Lai Tai-An Gem Lab.



Figure 2. Microscopic examination of the suspect area revealed natural inclusions and a crystalline form. Neither would be found in an impregnated specimen. Photo courtesy of Lai Tai-An Gem Lab.

about 437 nm. FTIR and Raman spectroscopy were also applied, producing spectral features that confirmed the bangle's identity as jadeite jade. Microscopic examination revealed natural inclusions within the transparent area that appeared to be polycrystalline (figure 2). Neither would be seen in an impregnated specimen, ruling out this treatment. Further analysis with Raman microscopy was conducted to identify its true nature.

Sharp absorption peaks at around 207, 347, 400, 465, and 990 cm^{-1} were a match for nepheline (figure 3), a min-

Editors' note: Interested contributors should send information and illustrations to Justin Hunter at justin.hunter@gia.edu or GIA, The Robert Mouawad Campus, 5345 Armada Drive, Carlsbad, CA 92008.

GEMS & GEMOLOGY, VOL. 50, No. 2, pp. 158–169,
<http://dx.doi.org/10.5741/GEMS.50.2.158>.

© 2014 Gemological Institute of America

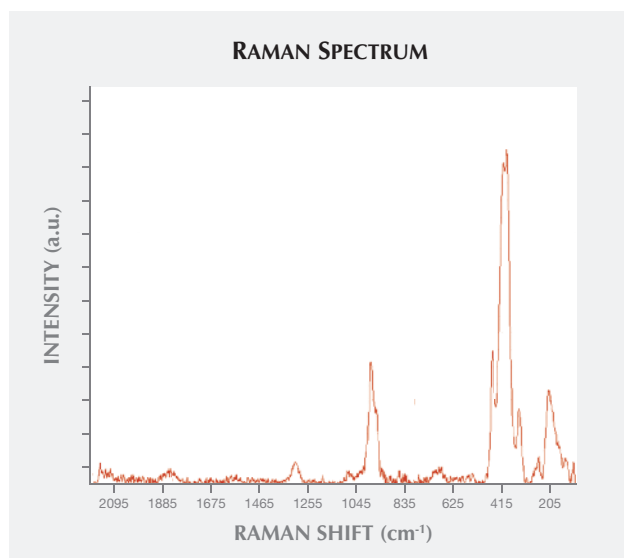


Figure 3. Sharp absorption peaks around 207, 347, 400, 465, and 990 cm^{-1} were consistent with nepheline, a mineral sometimes associated with albite in jadeite.

eral sometimes associated with albite in jadeite. The nepheline crystal remained intact during the fashioning process, and its presence led to confusion over whether the bangle had been treated.

Larry Tai-An Lai (service@laitaian.com.tw)
Lai Tai-An Gem Laboratory, Taipei

Prasiolite with inclusion influenced by Brazil-law twinning. The Indian Gemological Institute Gem Testing Laboratory recently examined a 6.43 ct transparent grayish yellowish green oval mixed-cut specimen. Standard gemological examination gave an RI of 1.545–1.553 with a uniaxial positive optic sign and a birefringence of 0.008, and a hydrostatic SG of 2.65. These readings readily identified the stone as prasiolite, a green variety of quartz.

The prasiolite displayed prominent Brazil-law twinning, with very sharp twinning planes when the sample was observed parallel to the optic axis between crossed polarizing filters, though only two sections of twinning were clearly visible in the stone (figure 4). The presence of such sharp and prominent Brazil-law twinning confirmed the sample's natural origin. When synthetics do exhibit such patterns, it has a flame-like or irregular shape (J.I. Koivula and E. Fritsch, "The growth of Brazil-twinned synthetic quartz and the potential for synthetic amethyst twinned on the Brazil law," Fall 1989 *G&G*, pp. 159–164).

Magnification showed no inclusions, but illumination from the side using a fiber-optic light source revealed minute white particles that scattered the light (figure 5). These pinpoint inclusions followed the pattern of the Brazil-law twinning, which was apparent without the aid of polarized filters (E.J. Gübelin and J.I. Koivula, *Photoatlas*

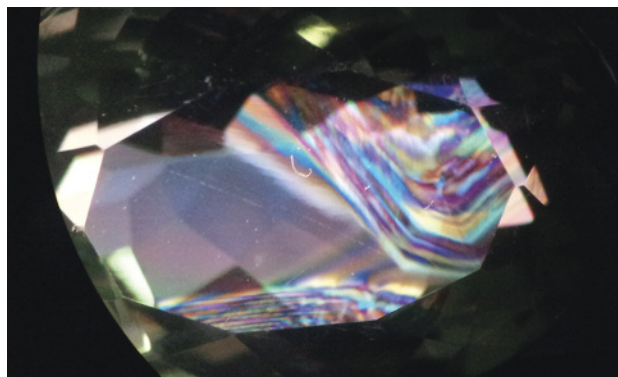


Figure 4. Between crossed polarizers, the prasiolite showed two sections of Brazil-law twinning in the optic-axis direction. Photo by Meenakshi Chauhan, magnified 15 \times .

of *Inclusions in Gemstones Volume 2*, Opinio Verlag, Basel, Switzerland, 2005, p. 573).

Minor rhombohedron faces that did not feature Brazil-law twinning were filled with these minute light-scattering particles. These inclusions were visible on the faces with some tilting of the fiber-optic light source but did not show any pattern (figure 6). The minute particles were not visible in both zones simultaneously.

In diffused transmitted light, the minor rhombohedron faces displayed a slightly darker shade of the grayish yellowish green color seen in prasiolite. These faces also showed a wavy internal growth structure between crossed polarizers. The major rhombohedron faces were even lighter in color. No color bands were observed in the stone.

Although the owner claimed the stone's color was natural, the presence of Brazil-law twinning raised suspicion, since this twinning has only been associated with the

Figure 5. Fine dotted inclusions demonstrated a Brazil-law twinning pattern along the optic axis, exactly where this twinning was visible under polarized filters. Photo by Meenakshi Chauhan, magnified 10 \times .

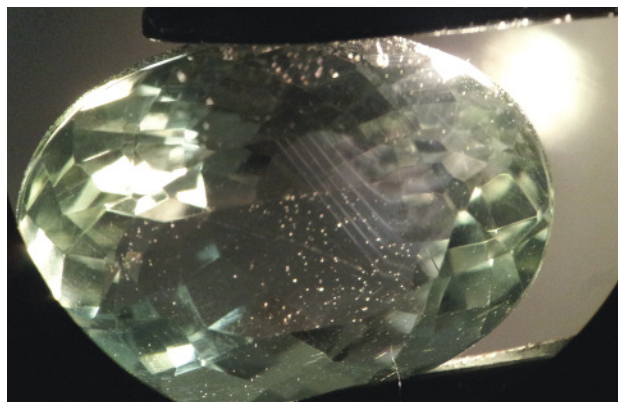




Figure 6. Fine dotted inclusions were visible in this minor rhombohedral face where Brazil-law twinning was absent. Photo by Meenakshi Chauhan, magnified 10x.

amethyst variety of quartz. There is still no way to separate naturally heated from heat-treated prasiolite.

Meenakshi Chauhan
 Indian Gemological Institute
 Gem Testing Laboratory, GJEPC, New Delhi

Record-size natural moissanite crystals discovered in Israel.

Synthetic silicon carbide (SiC) is well known in the gem and jewelry market as synthetic moissanite. Natural SiC is very rare and has been found as tiny crystals (usually less than 1.5 mm) in only a few deposits worldwide (Y. Bauer et al., "Moissanite from middle mountains of Czechoslovakia," *International Geology Review*, Vol. 7, No. 7, 1965, pp. 1194–1206; A.A. Shiryayev et al., "Moissanite (SiC) from kimberlites: Polytypes, trace elements, inclusions and speculations on origin," *Lithos*, Vol. 122, No. 3-4, 2011, pp. 152–164, and references therein).

Over the past 14 years, however, more than 2,500 crystals of natural moissanite have been discovered by Shefa Yamim, an Israeli exploration and mining company. The crystals come from primary and alluvial deposits along the Kishon River, near Haifa in northern Israel. Shefa Yamim began prospecting in this area following the 1988 prophetic statement of the Lubavitcher Rebbe that "precious stones and gems" would be discovered in the valley next to Haifa (see video at http://youtu.be/_uzY5mV8rdY). In 2000, the company unearthed moissanite crystals ranging from 0.1 to 1 mm in size; two years later, 2.2 mm crystals were found. In 2009, a 3.5 mm moissanite discovery set a world record, only to be surpassed in August 2012 by a crystal measuring 4.1 mm—the largest specimen to date (figure 7 and <http://goo.gl/JZFiwe>).

There is evidence of even larger crystals, as many broken crystals were discovered. Some crystals have also been found *in situ* in the volcanic rock of the Rakefet magmatic



Figure 7. The largest known natural moissanite crystal, found along the Kishon River in northeastern Israel, measures 4.1 mm in its longest dimension. Photo by Vered Toledo.

complex, one of the magmatic bodies of Mount Carmel, just southeast of Haifa, which is drained by a small tributary to the Kishon River.

We studied 30 Israeli crystals ranging from less than 1 mm to 3.5 mm. All were identified as moissanite (SiC 6H) by Raman spectroscopy. Their morphology was hexagonal,

Figure 8. These natural moissanite crystals are hexagonal to pyramidal, showing rounded areas that may result from either growth or dissolution. The crystals range up to 2.5 mm (not to scale). Composite photo by Aurélien Delaunay.

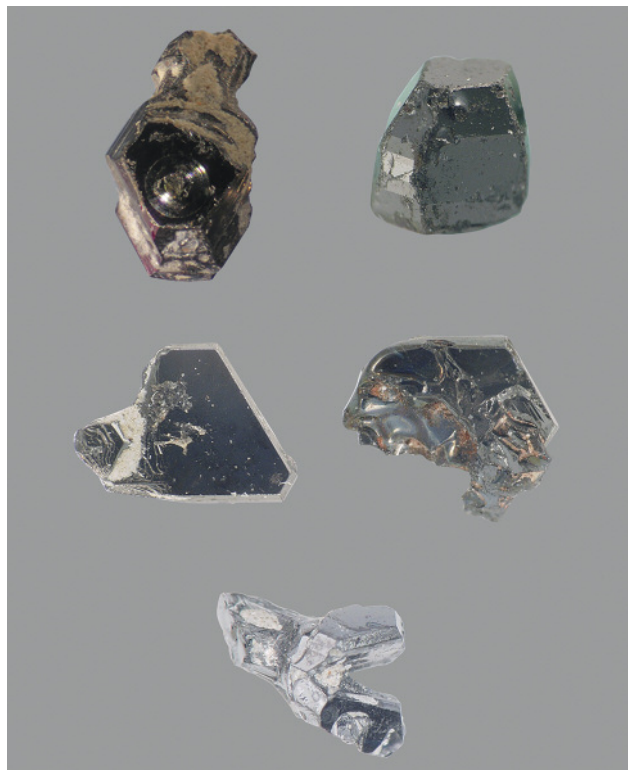




Figure 9. The colors seen in moissanite from the Mount Carmel area of northern Israel range from dark blue to light green. Note the broken or rounded morphology. Composite photo by Aurélien Delaunay.

bipyramidal to platy, with the pinacoid generally present (figures 8 and 9). The crystals were often broken, particularly the larger ones with rounded, shiny surfaces (again, see figure 7). As shown in figure 9, the crystals were transparent and ranged from deep blue (the most common color) to light green. Except for size, these characteristics are similar to those of other natural moissanites documented in the literature. The crystals are often associated with small bits of creamy white or red complex matrix.

The crystals we examined were inert under long- and short-wave UV radiation, with the exception of five small green to light green samples. In these five specimens, medium to strong orange luminescence was seen under either long- or short-wave UV. These were found to be magnetic when placed next to a powerful permanent alnico magnet. All of the samples contained small metallic inclusions, the largest approximately 30 microns in size, which could be the source of magnetism. We will continue to follow moissanite exploration in this area, and a more in-depth research paper is forthcoming.

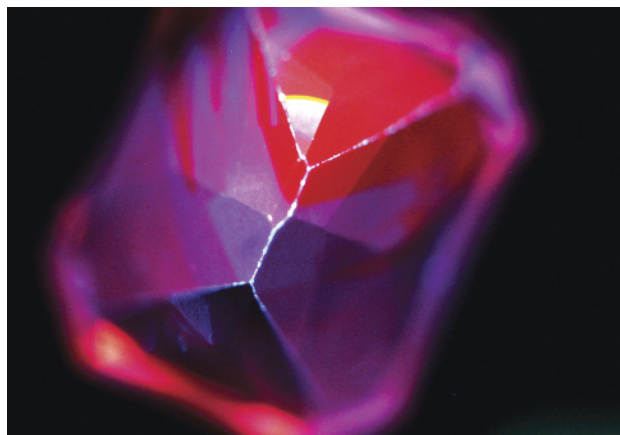
Emmanuel Fritsch
 Vered Toledo
 Shefa Yamim
 Akko, Israel
 Antoinette Matlins
 Antoinette Matlins, LLC
 Woodstock, Vermont



Figure 10. This 1.36 ct light bluish violet sapphire displayed an interesting color shift when exposed to the UV radiation of the DiamondView. Photo by Igor Iemelianov; magnified 15x.

Unusual optical effect in blue sapphire. A 1.36 ct light bluish violet sapphire (figure 10) was presented to the laboratory of the State Gemological Centre of Ukraine for examination. The stone exhibited an RI of 1.762–1.770, with a birefringence of 0.008, and a hydrostatic SG of 3.97. The samples displayed typical pleochroism and a very weak pinkish orange fluorescence to long-wave UV. Qualitative analysis using EDXRF spectroscopy showed major amounts of Fe, Cr, and Mg, and minor amounts of Ti and Ga. Microscopic examination revealed dot-like dissolved rutile, proof of heat treatment. The sapphire showed a small color shift from bluish violet in the daylight to pale blue in incandescent light. A band with pink luminescence (apparently due to Cr³⁺ impurity) was identified using the DiamondView (figure 11). When removed from the DiamondView,

Figure 11. The DiamondView recorded this band with pink luminescence in the light bluish violet sapphire. Image by Igor Iemelianov.



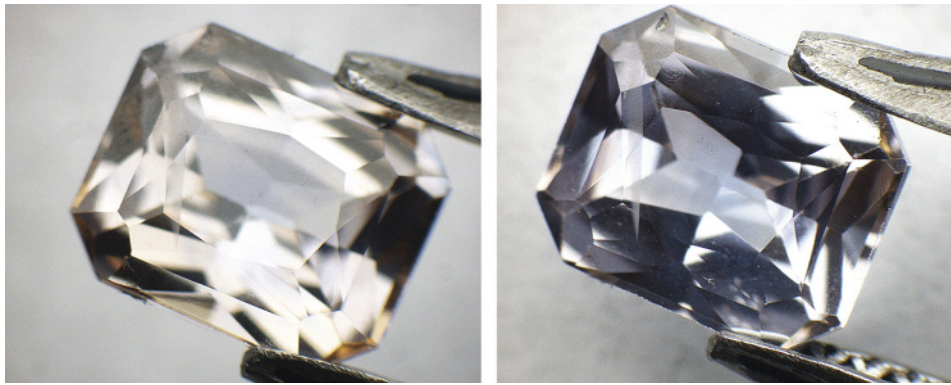


Figure 12. When removed from the DiamondView, the sapphire had completely turned brown (left). After about 12 hours, the stone reverted to its original light bluish violet color (right). Photos by Igor Iemelianov, magnified 15 \times .

the stone had completely changed color to brown (figure 12, left). After about 15 minutes in natural daylight, the light bluish violet hue began to return (figure 12, right). About 12 hours later, its original blue-violet color was restored. Such color instability is extremely unusual in blue sapphires.

It should be noted that the UV lamp in the DiamondView has a wavelength less than 225 nm (according to the user's manual). The energy of UV radiation is considered too weak for the color treatment of corundum (see K. Nassau, *Gemstone Enhancement*, Butterworth-Heinemann, 1984, p. 221). In this sapphire, the DiamondView apparently caused the color change. Such a reversible change of color with exposure to light is called photochromism.

*Iurii Gaievskiy (gaevsky@hotmail.com),
Igor Iemelianov, and Elena Belichenko
State Gemological Centre of Ukraine, Kiev*

SYNTHETICS AND SIMULANTS

Assemblage of synthetic ruby in calcite matrix. Recently, the Dubai Central Laboratory received a white and cream-

Figure 13. This synthetic ruby was fixed in a white and cream-colored matrix and represented as natural ruby. Photo by Sutas Singbamroong, Dubai Central Laboratory.



colored rough sample for identification (figure 13). The 124.4 \times 107.7 \times 65.8 mm, 5917.35 ct specimen had two openings, the larger one about 25 mm long and 10 mm wide. A hexagonal red stone embedded in the matrix could be seen through these openings (figure 14). Only the prism side was visible, and the rough concealed both terminations.

The red stone's refractive index and specific gravity were impossible to determine, and only a very small portion was visible for obtaining other information. A spectroscope was the only option, and the stone clearly showed a ruby spectrum. It also displayed strong and medium red reactions to long- and short-wave UV radiation, respectively. Microscopic examination with fiber-optic light revealed a group of round gas bubbles and tiny fractures, but curved striae were not seen. These properties indicated a flame-fusion synthetic ruby cleverly embedded in matrix to imitate natural ruby.

Raman spectroscopy identified the matrix as calcite. Close examination indicated that the cream-colored side of the stone had been drilled to make a hole for inserting the synthetic ruby. After the drilled area was sealed with a mixture of glue and calcite powder, two openings were cut

Figure 14. The synthetic ruby was embedded in a calcite matrix, seen here under incandescent light. Photo by Nazar Ahmed, Dubai Central Laboratory.



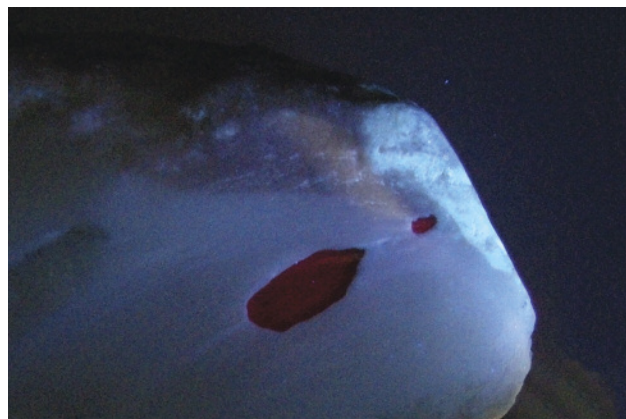


Figure 15. Under long-wave UV radiation, the drilled area showed strong greenish blue fluorescence. Photo by Nazar Ahmed, Dubai Central Laboratory.

to reveal the synthetic ruby inside. Under long-wave UV radiation, the drilled area showed strong greenish blue fluorescence, while the rest of the stone was inert or exhibited a light greenish blue reaction (figure 15).

These types of artificial assemblages should alert traders to exercise caution when purchasing rough stones, especially in newer, less established markets.

*Nazar Ahmed (nanezar@dm.gov.ae) and
Sutas Singbamroong
Gemstone Unit, Dubai Central Laboratory
United Arab Emirates*

Composite coral veneer glued to artificial matrix. Red coral, one of the most precious organic gems, has become increasingly popular in the Chinese jewelry market. With natural coral resources being depleted, ornaments of large size and high quality are becoming even more valuable. As a result, the market for treated red coral and imitation products is rapidly growing.

Composite red coral normally consists of coral fragments glued together with cement compounds. In 2010,



Figure 16. These 14 ornaments, represented as red coral products, consisted of a coral veneer glued to a matrix. The ten bangles (top) weigh 37.34–57.43 g, and the four snuff bottles (bottom) range from 121.95 to 145.07 g. Photo by Haibo Li.

the National Gemstone Testing Center Gem Laboratory in Beijing tested one bangle that was represented as red coral (Summer 2010 GNI, pp. 158–159). Because the client did not allow the lab to take a powder sample, further testing was restricted. There was some concern about whether the bangle had an artificial matrix, but this could not be determined without destructive tests.

Recently, the NGTC received 10 bangles and four snuff bottles (figure 16) presented as red coral. The bangles resembled the one tested in 2010. Each of the 14 pieces was covered with a very thin surface layer of red coral. The composition of the material below this coral veneer was analyzed.

Magnification revealed the boundaries between the coral fragments and the cement compounds, which tended to be recessed (figures 17 and 18). This clearly demonstrated that the veneer was composite red coral. The coral



Figure 17. Left: A close-up of a bangle with coral veneer. Right: The bangle's inner surface is covered with rectangular coral slices, but gaps filled with cement compounds are still visible. Photos by Haibo Li; magnified 6.5×.

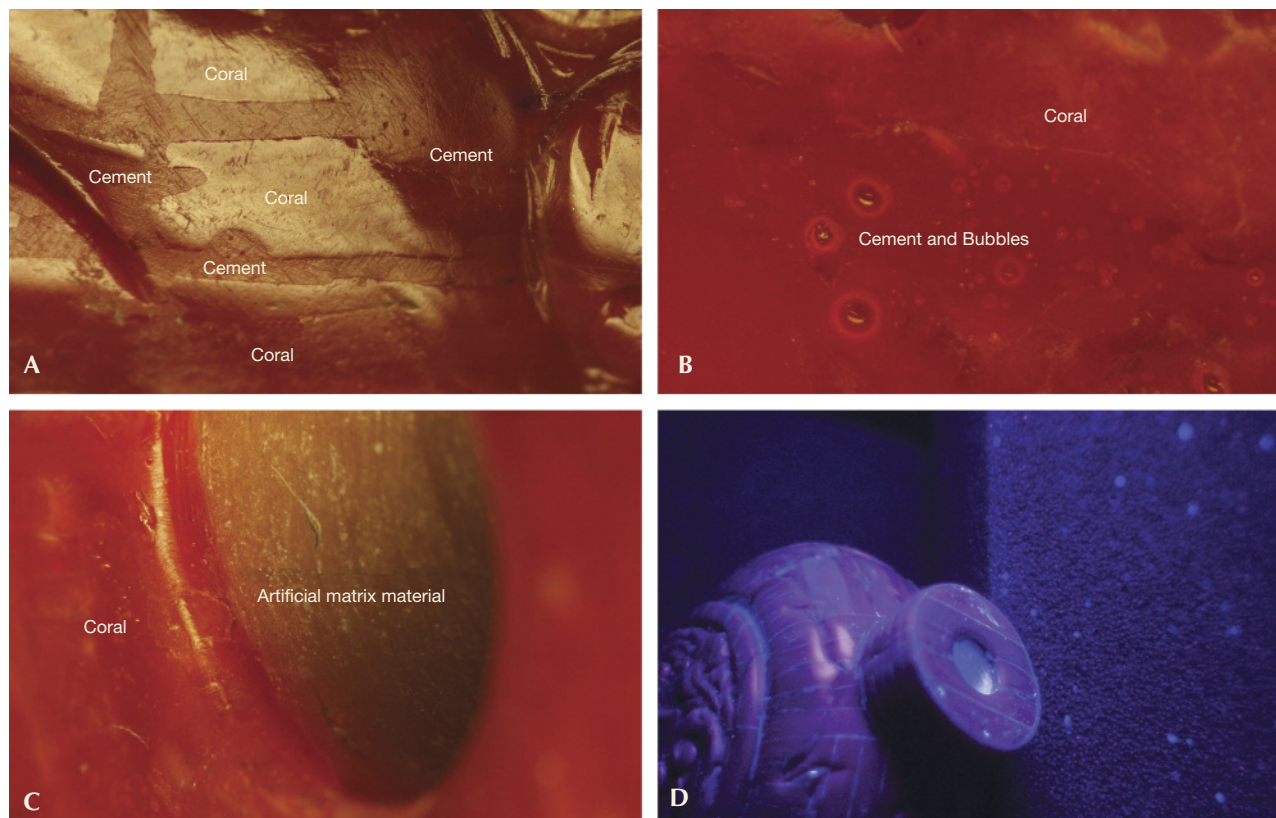


Figure 18. A: Reflected light showed the difference in luster between the cement compounds and the coral fragments; magnified 10 \times . B: Under transmitted light, air bubbles can be found in the cement compounds; magnified 20 \times . C: The boundary between the matrix and the composite coral veneer is very clear and sharp; magnified 10 \times . D: The fluorescence reaction of the same sample under short-wave UV. Photomicrographs by Haibo Li.

fragments had a vitreous luster and showed wavy growth patterns typical of natural coral. No growth patterns were seen in the cement compounds except for air bubbles.

Whitish material seen inside the neck of the bottles was identified as an artificial matrix. The composite red coral veneer, which was only about 1–2 mm thick, had been glued to the surface of the whitish matrix. Under a short-wave UV lamp, strong blue-white fluorescence from the cement compounds and the matrix was visible (figure 18).

Micro-infrared spectrometry (with 4.0 cm^{-1} resolution and 64 scans in the 675–4000 cm^{-1} range) identified the cement compounds as epoxy resin (figure 19A). Two different kinds of artificial matrix material were detected: ethyl cyanoacrylate (figure 19B) and alkyd synthetic resin mixed with carbonates. The main component of the carbonates was established as calcite by subtracting the spectra (figure 19C). The calcite could have come from the manufacturing process of the composite red coral.

The SG of the synthetic resin was about 1–2 g/cm^3 , much lower than that of red coral (2.65 g/cm^3). Carbonates could have been added to the matrix to make it heavier and

approximate the heft of coral. The snuff bottles all had similar size but different weights. The three that contained alkyd resin mixed with calcite, which has a relatively high SG, weighed 140–145 g. The matrix in the fourth snuff bottle was ethyl cyanoacrylate, which has a lower SG than calcite. As a result, it only weighed 121 g.

In today's market, oversized red coral products are often constructed from an artificial matrix. After the matrix is shaped, a veneer of red coral fragments is glued to its surface. This makes it easier to manufacture larger ornaments while preserving natural coral reefs. Combining magnification and UV fluorescence observation with infrared spectrometry, we can identify composite coral assemblages quickly and effectively.

Haibo Li (1978lihb@163.com), Zhoujing Yue, Jie Liang,
Taijin Lu, Jun Zhang, and Jun Zhou
National Gemstone Testing Center Gem Laboratory,
Beijing

Dyed bone as a red coral imitation. Numerous materials have been widely used to imitate red coral: glass, plastic,

ceramics, composites, and dyed shells. Recently, the Gem Testing Laboratory in Jaipur examined an 8.86 ct orange-red cabochon measuring $16.56 \times 12.19 \times 7.34$ mm (figure

Figure 19. A: The IR spectrum of the cement compound in one of the bangles identified it as epoxy resin. B: The IR spectrum of the artificial matrix material in one of the snuff bottles indicated ethyl cyanoacrylate. C: The artificial matrix material in the other three snuff bottles was identified, by subtracting IR spectra, as alkyd resin mixed with carbonates.

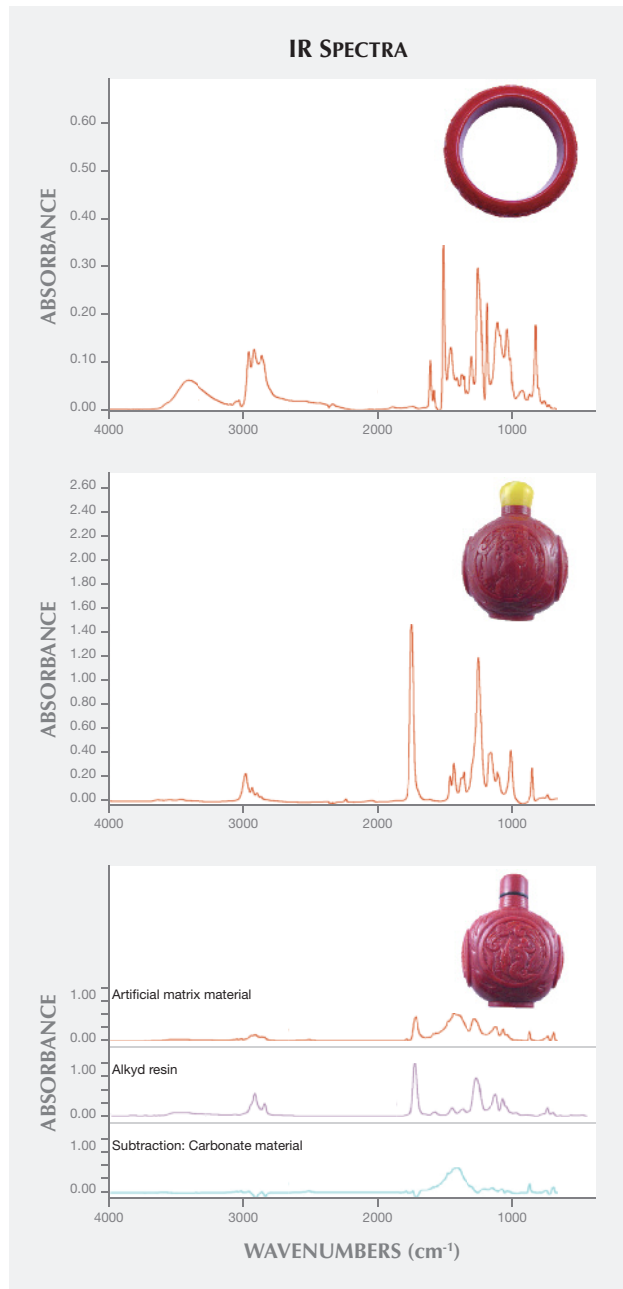


Figure 20. This 8.86 ct orange-red cabochon, submitted as coral, was identified as dyed bone. Photo by Gagan Choudhary.

20) that was presented as red coral but proved to be dyed bone, an unusual imitation.

Initial observation showed a strong resemblance to red coral, but careful microscopic observation proved otherwise. The sample lacked the typical “tree ring” or striated growth structure seen in corals, though it did display a network of fine veins throughout. Viewed from above, these veins appeared subparallel and were oriented along the length of the cabochon (figure 21). The veins also displayed orange-red color concentrations against the cabochon’s whitish bodycolor (again, see figure 21), suggesting that the

Figure 21. The dyed bone illustrated in figure 20 displayed subparallel veins oriented along the length of the cabochon; also note the orange-red color concentrations against the sample’s whitish bodycolor. Photomicrograph by Gagan Choudhary; magnified 48 \times .



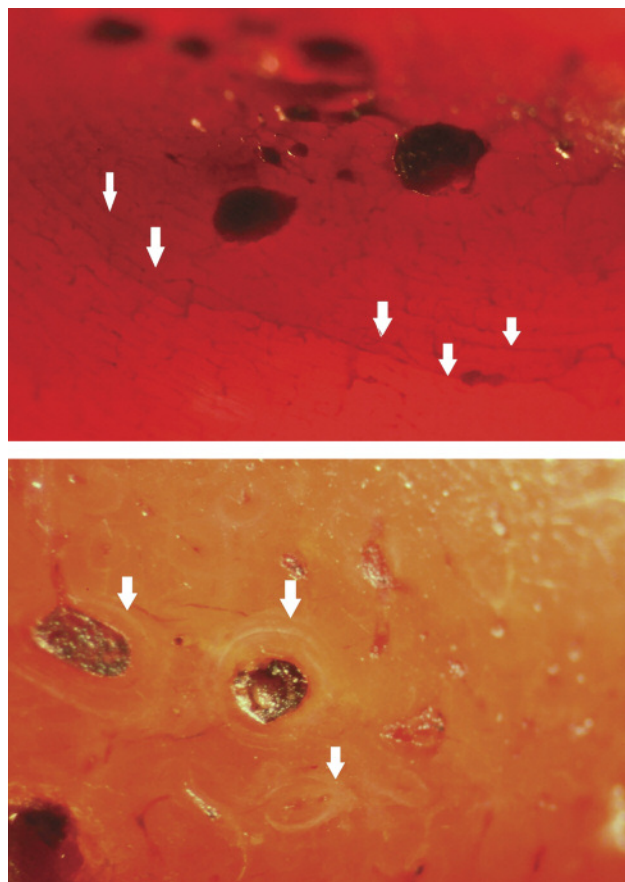


Figure 22. Subparallel veins were confined to circular concentric planes oriented along the length of the cabochon (top), while the individual veins were surrounded by concentric whitish rings (bottom). Photomicrographs by Gagan Choudhary; magnified 40× (top) and 56× (bottom).

material was both dyed and organic. Detailed observations of the sample from all sides revealed that the subparallel veins were confined to circular concentric planes oriented along the length of the cabochon (figure 22, top); the individual veins were further surrounded by concentric whitish rings (figure 22, bottom). These structural features ruled out the possibility of coral, but the identity had yet to be established.

The sample's spot RI was approximately 1.56, without any noticeable birefringence blink, while its hydrostatic SG was 2.01. Under a UV lamp, it displayed pinkish orange patchy fluorescence (which was stronger under long-wave UV). This characteristic is typically associated with dyes. Qualitative EDXRF analysis revealed the presence of phosphorus and calcium. Chemical, gemological, and observational features indicated bone, which was further confirmed by Raman spectroscopy. Raman spectra (figure 23) obtained using a 785 nm laser in the 200–2000 cm^{-1} region displayed

a strong peak at approximately 960 cm^{-1} , with weaker peaks at approximately 430, 586, and 1072 cm^{-1} . Also present were a few indistinct features in the 1200–1700 cm^{-1} region. The peaks at approximately 960, 586, and 430 cm^{-1} were attributed to PO_4^{3-} bending and stretching, and the one at 1072 cm^{-1} to CO_4^{3-} stretching. The indistinct features between 1200 and 1700 cm^{-1} were due to collagen—the essential component of bone tissue (C. Kontoyannis et al., "Analysis of bone composition with Raman spectroscopy," *Proceedings of the 13th Panhellenic Pharmaceutical Congress*, 2012, <http://nemertes.lis.upatras.gr/jspui/bitstream/10889/5187/1/PMO031.pdf>).

Bones have been used as jewelry since ancient times, and some specimens are dyed or stained to make them appear older (Summer 2006 Lab Notes, p. 160). Bone is used to imitate ivory, but this is the first time we have seen a bone dyed red and presented as coral, an interesting and unusual imitation. Although the market penetration of this material is unknown, we cannot rule out the possibility of it being mixed in packets of red coral, and this separation would pose a challenge for jewelers and gemologists.

Gagan Choudhary (gagan@gjepcindia.com)
Gem Testing Laboratory, Jaipur, India

MORE FROM TUCSON 2014

Bumble Bee "jasper" from Indonesia. At the Tucson Gem and Mineral Show, All in Vein (Quartzsite, Arizona) exhibited slabs and pairs of Bumble Bee "jasper," which was sold elsewhere at the show as Eclipse "jasper." The term *jasper* is a misnomer, as this vibrantly colored orange, yellow, and

Figure 23. The bone's Raman spectrum showed major PO_4^{3-} peaks at about 960, 586, and 430 cm^{-1} ; a CO_4^{3-} peak at 1072 cm^{-1} ; and collagen-related peaks in the 1200–1700 cm^{-1} region.

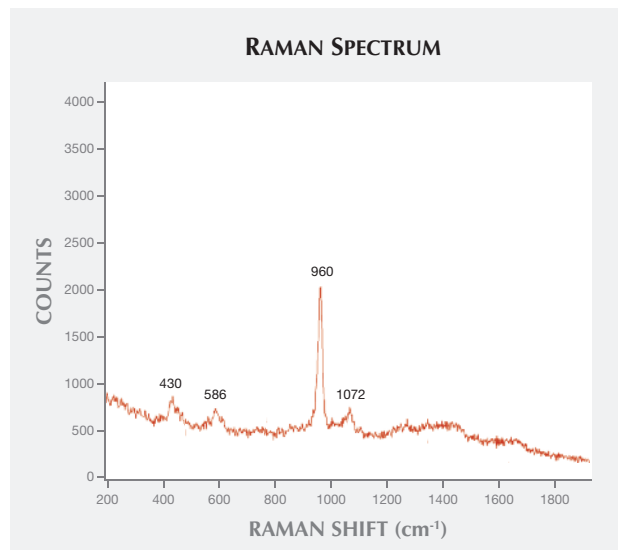




Figure 24. This Bumble Bee “jasper,” measuring 32 × 54 mm, is a mixture of volcanic lava and sediment. Photo by Robert Weldon/GIA; courtesy of Robert E. Kane.

black material (figure 24) actually formed from a mixture of Indonesian volcano lava and sediment. A carbonate-rich rock first discovered on the island of Java during the 1990s, the material is soft, with a Mohs hardness of 5 or below. The porous rock is easily cut and polished, and most specimens are filled with Opticon (H. Serras-Herman, “Bumble Bee ‘jasper’: A colorful volcanic lapidary material,” *Rock & Gem*, Vol. 43, No. 8, pp. 26–29).

Stuart Overlin

Pyrex bracelets. At the Pueblo Gem & Mineral Show, Kevin O’Grady (Scottsdale, Arizona) exhibited a line of glass bracelets and other jewelry (figures 25 and 26). O’Grady has worked with borosilicate glass, better known by the brand name Pyrex, since the late 1980s. He touted the durability and versatility of this medium, which lends itself to a variety

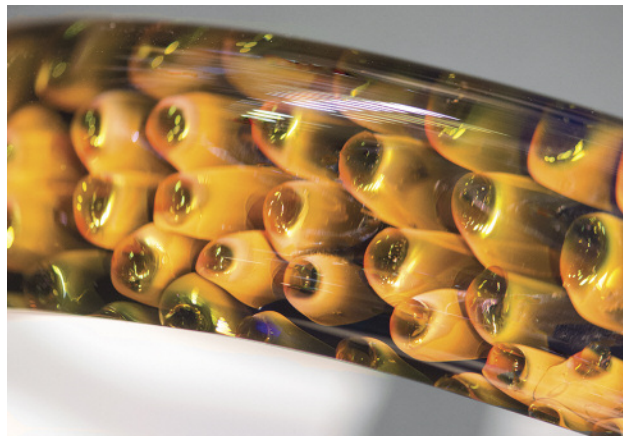


Figure 26. This Pyrex bracelet displays a striking orbicular pattern that appears three-dimensional. Photo by Eric Welch; courtesy of Kevin O’Grady.

of dramatic effects. He crafts each piece freehand using a torch, adding elements such as cobalt to achieve colors and embedding flower mosaics and other patterns that appear three-dimensional. O’Grady’s signature bracelets contain gold, silver, or a combination of both.

Stuart Overlin

Shattuckite from the DRC. At the Tucson Gem and Mineral Show, Brett Kosnar of Mineral Classics (Black Hawk, Colorado) exhibited rare specimens of shattuckite from the Democratic Republic of Congo. A new find of this intense medium to dark blue copper silicate (figure 27) occurred in the Kambove District in October 2013. The mineral has a Mohs hardness of 3.5 and is used for cabochons and carvings. Shattuckite has been reported from various African and European sources, as well as copper mines in the



Figure 25. Pyrex bracelets with attractive colors and patterns were on display at the Tucson show. Photo by Eric Welch; courtesy of Kevin O’Grady.

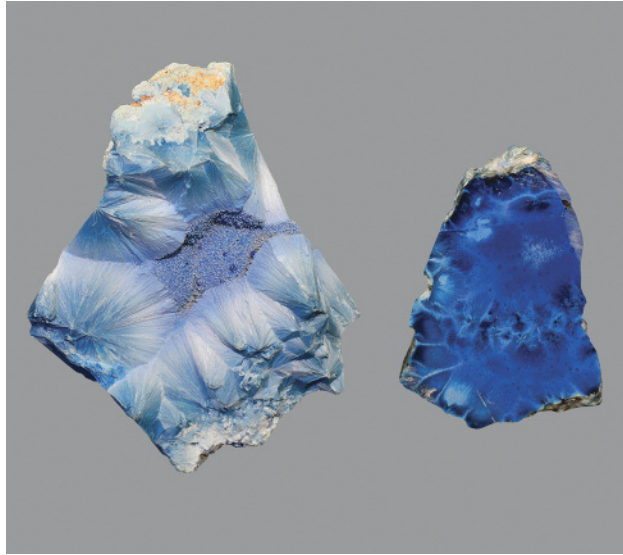


Figure 27. These intense blue shattuckite specimens are from a recent find in the Democratic Republic of Congo. Photo by Brett Kosnar; courtesy of Brett Kosnar, Kosnar Gem Co.

American West. The type locality is the Shattuck-Denn mine in Bisbee, Arizona (R. Bowell and R. Cook, "Connoisseur's Choice: Shattuckite: Kunene District, Kaokoveld, Namibia," *Rocks & Minerals*, Vol. 84, November/December 2009, pp. 544–550).

Kosnar's Congolese shattuckite is being stabilized prior to jewelry manufacturing. He plans to debut cabochons of this very limited material at Tucson in 2015.

Stuart Overlin

Figure 28. Top-quality stones, including purple and green jade, were offered at Jewelry Shanghai 2014. Photo by Jennifer Stone-Sundberg.



Figure 29. This clear quartz carving seen at the Shanghai show demonstrates the exceptional craftsmanship sought by Chinese collectors. Photo by Jennifer Stone-Sundberg.

CONFERENCE REPORT

Jewelry Shanghai 2014. Organized by the Gems & Jewelry Association of China, Jewelry Shanghai 2014 took place May 8–12 at the Shanghai World Expo Exhibition & Convention Center. The two exposition halls held over 1,000 vendors representing more than 22 countries in 4,200 square meters of exhibitor space. A wide variety was offered, including exceptional examples of tourmaline, jade (figure 28), and ruby, as well as phenomenal stones such as cat's-eye chrysoberyl and star sapphire. Additionally, superb craftsmanship was on display in the form of fine jade and quartz carvings (figure 29), gold work, and cloisonné enameling. This year saw the addition of top-level fossil, mineral, and gem collector specimens. Other popular items for sale were amber, turquoise, and moonstone.

The show featured lectures on topics such as Chinese jade carving, diamond, and Burmese rubies. As Shanghai is



Figure 30. “Fantastic Cross,” an 18K gold brooch featuring turquoise, variscite, chrysocolla, cultured pearl, and enamel, is part of the museum display at GIA’s New York laboratory and campus. Photo by Orasa Weldon/GIA, courtesy of the Anthony and Elizabeth Duquette Foundation for the Living Arts.

China’s diamond import center, the Shanghai Diamond Exchange (which handles every diamond imported into the country) and the Hoge Raad voor Diamant (HRD) were present. Several other gem- and jewelry-related agencies, including the Shanghai Gold Exchange and the International Gemological Institute (IGI), also attended. Mainland China posted jewelry retail sales of 295.9 billion yuan (approximately US\$47 billion) in 2013 (http://www.stats.gov.cn/tjsj/zxfb/201401/t20140120_502082.html), and this show certainly indicated the quality and diversity of items the Chinese gem and jewelry market demands today.

Jennifer Stone-Sundberg
Crystal Solutions, LLC
Portland, Oregon

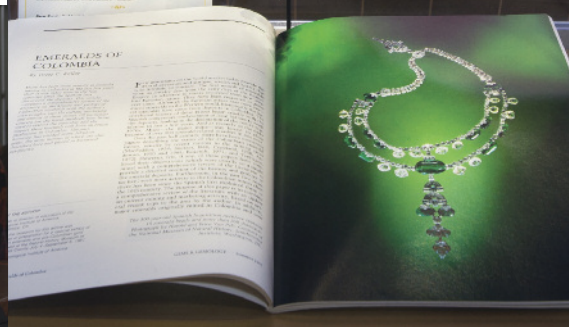
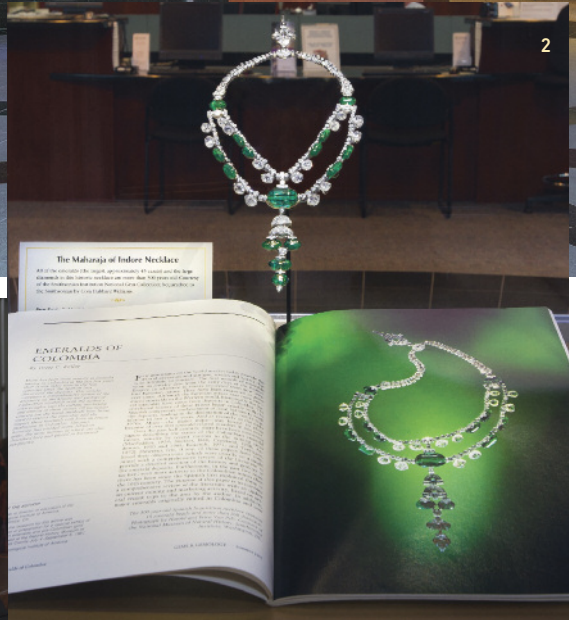
Ren Lu
China University of Geoscience
Wuhan

MISCELLANEOUS

GIA Museum exhibits in New York. GIA’s recently opened laboratory and campus at the International Gem Tower in New York’s Diamond District features a permanent museum exhibit of gems, jewelry, and mineral sculptures. Fourteen display cases highlight nearly 100 items from the GIA collection, ranging from large aquamarine crystals to a diminutive *objet d’art* golden cactus and a necklace featuring akoya, Tahitian, and South Sea cultured pearls (figure 30). The exhibit showcases the wonder of gems to visitors and students.

ERRATUM

In the Gem News International section of the Spring 2014 issue, the photographer of the large oolitic opal block should have been listed as Don Mengason.



1: The exhibit's location at the GIA library entrance. 2: Colombian emerald necklace, Summer 1981 issue. 3: Kathryn Kimmel (left) with Harold and Erica Van Pelt. 4: 80th anniversary decor. 5: Rubellite necklace and ring, Winter 1988 cover. 6: Bill Larson, Susan Jacques, and Eloise Gaillou. 7: Tom Overton, Brendan Laurs, Alice Keller, and John King.

Celebrating *G&G's* 80th Year and the Artistry of Harold and Erica Van Pelt

On June 11, *G&G* contributors, supporters, and staff toasted the opening of the new GIA Museum exhibit, "The Beauty of Science: *Gems & Gemology* Celebrates 80 Years, Featuring the Artistry of Harold and Erica Van Pelt." The exhibit spotlights gems and jewelry featured on selected *G&G* covers since 1981. The cover photos are the work of the Van Pelt, the husband-and-wife team who contributed nearly three decades of photography to the journal's pages. In addition to gathering treasures from the Smithsonian and other sources, the collection offers intriguing examples of cutting-edge research, locality reports, and industry coverage over the years. The exhibit runs through December 14.



1



8



9



10



11



12



13



14



15

8: Kathryn Kimmel, Janine Castro, Laila Sharif, Susan Jacques, Tess Lecklitner, and Amanda Bilberry. 9: Pat Syvrud, Jeff Post, and Terri Ottaway. 10: John King. 11: Qing dynasty jade vase, Spring 1986 cover. 12: The Van Pelt, and Stan and Leslie Weinberg. 13: Kate Donovan and Gabriel Mattice. 14: Jeff Post and Zee Allred. 15: Marcelo Souza, Diane Caldwell, Dona Dirlam, and Charlie Carmona.

Photos by Kevin Schumacher and Matt Hatch/GIA.



RESEARCH AND NEWS

Visit G&G online to explore free multimedia content. Scan the QR codes with your smartphone or tablet, or enter the links below.

Gemological Field Expeditions: GIA's Andy Lucas and Vincent Pardieu discuss the challenges and rewards of gemology fieldwork. Contains slideshows from local mines and markets. www.gia.edu/gia-news-research-behind-scenes-gemological-field-expedition.



Mogok Expedition Three-Part Series: Our resident field gemologists reminisce about the sights, the people, and the gem markets in Myanmar's famed "Valley of Rubies." Contains slideshows showing local sites, miners, and gem markets. www.gia.edu/gia-news-research-expedition-to-the-valley-of-rubies-part-1.



Chinese Gem and Jewelry Industry: The authors explore the development, impact, and future of China's domestic and international gemstone and jewelry market. Includes artisan video interviews, on-site slideshows, and a Chinese language PDF. www.gia.edu/gems-gemology/spring-2014-lucas-chinese-gem-industry.



Understanding the Geology of Diamonds: Delves into the relationship between natural diamond formation and the geological formation of Earth. Includes a diamond geology glossary, slideshows, and author interviews. www.gia.edu/gems-gemology/WN13-diamond-geology-shirey.



The Museum of London's Cheapside Hoard: An inside look at this extraordinary jewelry and gemstone collection dating from the 17th century. Contains slideshows of the exhibit and video interviews with museum curators. www.gia.edu/gems-gemology/FA13-cheapside-hoard-weldon.



Occurrences of Oregon Sunstone: GIA visits three major sources of Oregon sunstone to collect samples for research and provide background into the geological relevance of this material. Includes video interviews and slideshows from the sites. www.gia.edu/gems-gemology/FA13-oregon-sunstone-pay.



A Look at Tucson 2014: Industry insight, creative innovations, and unusual finds from this year's gem and mineral shows. Includes video interviews. www.gia.edu/gems-gemology/spring-2014-gemnews-tucson-2014-overview.

